A STUDY OF
RUBRENE ELECTROGENERATED CHEMILUMINESCENCE
AND
RELATED SYSTEMS

by

Albert Pighin

A thesis submitted to the School of Graduate Studies in partial fulfillment of the requirements for the degree of Master of Science in the Department of Chemistry, University of Ottawa

Ottawa, Canada

May, 1974

PREFACE

This work is a study of rubrene electrogenerated chemiluminescence (EGCL). In particular, it is an investigation of the redox processes and quantum efficiency of rubrene EGCL. The information contained herein is both of fundamental interest in regard to energy transfer mechanisms and of practical concern to those investigating the phenomenon as a potential transducer for visual devices.

Some of the present work has been reported to the academic community:

(1) A. Pighin, Can. J. Chem., 51, 3467 (1973). "Effects of Solvents on the Quantum Efficiency of Rubrene Electrogenerated Chemiluminescence."

(2) A. Pighin and B.E. Conway. Paper presented at the Meeting of the Electrochemical Society of America, San Francisco, May 12-17, 1974. "A Correlation Between the Quantum Efficiency of Electrogenerated Chemiluminescence and the Redox Potentials of Rubrene in Various Solvents."

(3) Item (2) has been submitted to the J. Electrochem, Soc. for publication.

ACKNOWLEDGEMENTS

The experimental work reported here was carried out at Bell-Northern Research (BNR) while I was investigating EGCL for display applications. I am indebted to BNR for having allowed me to use their facilities for the present study. The research on EGCL at BNR was supported, in part, by the National Research Council of Canada through its Industrial Research Assistance Program.

R.M. van Dyk assisted in the design of the electronic circuitry for the quantum efficiency measurements and D.P. Malanka helped purify some of the chemicals employed in this investigation of rubrene EGCL.

I was fortunate in having had Professor B.E. Conway for thesis supervisor. His personal interest and thoughtful guidance helped shape this work.

Finally, I wish to thank my wife, Brenda, for allowing me the time and giving me the moral support to achieve this thesis.

TABLE OF CONTENTS

LIST OF FIGURES

LIST OF TABLES

ABSTRACT

From a review of the literature on electrogenerated chemiluminescence (EGCL), it was concluded that the present state of knowledge of the phenomenon was limited by the extent to which the redox processes and the quantum efficiency of the EGCL were understood. Rubrene was selected as a model electrochemiluminescent compound for study. The choice of methods for study of the problems were critically examined and optimum processes selected. The stabilities of the ion-radicals were determined by means of cyclic voltammetry, chronoamperometry and electron spin resonance spectroscopy while the kinetics of the redox processes were studied by small-amplitude a.c. polarography. The quantitative applicability of the a.c. polarographic technique was proven by applying it to a known system, the ferro-ferricyanide couple. The radical-ions generated from rubrene were found to be stable under the conditions of the present work. The heterogeneous rate constants for the redox reactions of rubrene were found to be several orders of magnitude less than those predicted from theoretical considerations. A unique method for measuring the electrochemical quantum efficiency ϕ_{coul} of EGCL was devised which offered superior precision and accuracy for evaluation of ϕ_{coul}. The quantum efficiency of rubrene EGCL was found (a) to increase with increasing solvation of the neutral rubrene, (b) to decrease with increasing fluorescor concentration and frequency of the a.c. voltage used to generate the EGCL, and (c) to be independent of the electrolyte concentration. It was established that the mechanism for the production of rubrene EGCL was exclusively via the "triplet route".

1. TECHNOLOGICAL BACKGROUND

In electrogenerated chemiluminescence, a compound is electrolyzed during which process light is produced. The process thus converts electrical energy into visible light. Therefore, the phenomenon can be utilized as a transducer. Presently available transducers for converting electrical energy into light, e.g. by means of gas discharge, light emitting diodes or incandescent filaments, have limited applications in instrument technology and the need exists in industry for a more widely useful and more economical means of producing light from electricity. Consequently, electrogenerated chemiluminescence has been investigated as a potential transducer for visual devices. The present fundamental work described in this Thesis has resulted from, and complemented, the applied research on electrogenerated chemiluminescence carried out at Bell-Northern Research, Ottawa.

2. INTRODUCTION

A variety of organic luminescent compounds can be made to emit light by allowing their oppositely charged ion-radicals to react with each other. When the ion-radicals are electrochemically generated, the process is termed "electrogenerated chemiluminescence" and is abbreviated as ECL. In this work, preference was given to the term EGCL as an abbreviation for the name of the phenomenon because ECL is also employed as the short form for Emitter-Coupled Logic.

Hercules was the first to report EGCL, in 1964[1]. He electrolyzed a large number of aromatic hydrocarbons in conducting aprotic solutions with an alternating potential. In each case, the emission was visually identical to the fluorescence of the compound being electrolyzed.

Since the light from EGCL characterized the products of the homogeneous electron transfer reaction, Hercules' work quickly attracted the interest of those studying such reactions. Their work revealed that EGCL was not limited to the polyacenes. Bard's school showed that EGCL could be obtained from metal chelates[2], porphyrins[3] and mixed systems[4], while Zweig, Metzler, Maurer and Roberts[5] obtained EGCL from a large number of isobenzofurans and isoindoles.

The more recent investigations of EGCL have shown that the emission can be other than fluorescence. The metal chelates, for example, produce phosphorescent EGCL, while the EGCL from some aromatic hydrocarbons contains excimer emission[6].

Not all of the interest in EGCL has been academic. The phenomenon has been the subject of industrial research aimed at developing a transducer for visual devices[7]. This thesis originates from fundamental evaluation work on EGCL at Bell-Northern Research, Ottawa, with development of display applications as the technological aim.

3. OBJECTIVES

1. To devise selected techniques for studying the phenomenon. A critical review of published methods for studying the phenomenon was made and where inadequacies seemed to be apparent, improved methods were established.
2. To find a stable EGCL system. The known luminescors, e.g. rubrene, 9,10-diphenylanthracene, all have unstable ion-radicals, especially their cation-radicals. Consequently, their EGCL fades to extinction within minutes of continuous generation. If such unstable systems were to be studied, it would be easy to be misled by the effects of secondary reactions on the results. Therefore, the best of the reported EGCL systems was chosen as the model system. The components of the model system were further purified in the hope of improving their performance. If the more pure system still exhibited unacceptable instability, then the cause was sought in order to diminish it.
3. To establish the mechanism whereby the model system produces light. Some EGCL systems produce luminescence which is more energetic than the change in enthalpy of the ion-radical charge neutralization reaction. The thermodynamics of the model system must hence be evaluated before its light-producing mechanism can be established.
4. To investigate the kinetics of the various reactions in the EGCL mechanism. Only those reactions about which insufficient information was known were studied. The purpose of this work

was to determine the limiting reactions in the EGCL mechanism.

5. To study the effect of each component of the EGCL system on the quantum efficiency of the EGCL. An EGCL system consists of: (a) luminescor, (b) solvent, (c) electrolyte, (d) electrodes and (e) external stimulus (voltage).

4. REVIEW OF THEORETICAL ASPECTS OF EGCL

This review of EGCL will be limited to those systems for which the emmision strictly corresponds to the fluorescence of the compound being electrolyzed. For information on phosphorescent EGCL or EGCL with excimer emission, the reader is referred to Tokel and Bard[2] or Grabner and Brauer[6], respectively.

4.1 Reaction Mechanism

The first step in the production of EGCL involves the electrolysis of the fluorescor. The electrolysis reactions are the only reactions in the EGCL mechanism which require an external stimulus; all other reactions are spontaneous. In order to observe EGCL, the positive and negative ion-radicals of the fluorescor must be generated within access of each other. The simplest way of achieving this is by employing an alternating potential, the voltage limits of which correspond to the oxidation and reduction of the fluorescor. A square-wave potential is the most efficient a.c. stimulus because it can cause electrolysis of the fluorescor for the highest fraction of the cycle time and with the minimum amount of neutralization of the ion-radicals during reversal of polarity.

The a.c. electrolysis of the fluorescor results in alternating generation of both positively and negatively charged ion-radicals at each electrode. The ion-radicals which are produced in a given half-cycle diffuse away from the electrode while those oppositely charged,

produced in the previous half-cycle, tend to diffuse towards the electrode in the diffusion boundary layer. The encounter between the anion- and cation-radicals in the interphase allows homogeneous electron transfer reactions to take place between the ion-radicals.

Each homogeneous electron transfer reaction produces on the average 3/4 triplets together with 1/4 singlets, all in their lowest excited state, and one neutral molecule (see Equation (3) in Table 1). The fractions are given by spin statistics assuming that the solvent does not preferentially enhance either the formation of triplets or singlets[8]. This seems probable for simple aromatic hydrocarbons[9]. It has been assumed that the change in enthalpy of the charge neutralization reaction is sufficient to directly promote some of the products to their lowest excited singlet state. The thermodynamics of EGCL will be examined in Section 4.3.

The excited triplets produced by the charge neutralization reaction can engage in triplet-triplet annihilation reactions to produce excited quintets, triplets and singlets. The quintet state is, however, usually energy forbidden. The excited triplet state resulting from the triplet-triplet annihilation reaction will, directly or indirectly, be in the lowest excited state (i.e. the same as the reactant; see Equation (4) in Table 1). With the foregoing assumptions, spin statistics then predict an average of 3/4 triplets and 1/4 singlets, all in the lowest excited state, and one neutral molecule for each triplet-triplet annihilation.

The products from the homogeneous electron transfer and triplet-triplet annihilation reactions which have attained their lowest excited singlet state will promptly return to their ground state with the emission of light. The electronic transition from the lowest excited singlet state to the ground state produces light emission by fluorescence.

In general, then, the EGCL mechanism may be represented as shown in Table 1.

TABLE 1
General EGCL Mechanism for Systems Emitting Fluorescent Light Only

$R \rightarrow \dot{R}^+ + e$	oxidation of fluorescor at electrode	(1)
$R + e \rightarrow \dot{R}^-$	reduction of fluorescor at electrode	(2)
$\dot{R}^+ + \dot{R}^- \rightarrow 3/4\ {}^3R^* + 1/4\ {}^1R^* + R$	homogeneous electron transfer	(3)
${}^3R^* + {}^3R^* \rightarrow 3/4\ {}^3R^* + 1/4\ {}^1R^* + R$	triplet-triplet annihilation	(4)
${}^1R^* \rightarrow R + h\nu$	radiative decay of excited singlet	(5)

where

R = fluorescor

${}^3R^*$ = lowest excited triplet state

${}^1R^*$ = lowest excited singlet state

4.2 Reaction Kinetics

The interest here was to establish the rate-determining reaction in the EGCL mechanism and thus to provide a basis for the interpretation of the experimental results.

4.2.1 Heterogeneous Electron Transfer

The oxidation and reduction of the fluorescor at the electrode by an applied potential are examples of heterogeneous electron transfer reactions. A theory on this type of electron transfer has been formulated by Marcus[10] based on the activated complex theory of reaction rates[11]. The rate constant is given by the following well-known equation in which the symbols have their usual significance:

$$k = A \exp - \frac{\Delta G^*}{RT} \qquad (6)$$

Marcus developed a treatment for the free energy of activation which contained terms for electrolyte, solvent and electrode material effects. In a subsequent paper[12], he successfully tested his theory in relation to some experimental results.

Aten, Dieleman and Hoytink, in discussing heterogeneous electron transfer to or from aromatic hydrocarbons, assumed that the activation entropy factor $T\Delta S^*$ dominated the free energy of activation[13]. Their argument was based on an analogy with homogeneous electron transfer reactions involving the same compounds. They estimated the activation entropy to be *ca.* -4.5 cal mole^{-1} °K^{-1}. According to Marcus[10], the pre-exponential term in Equation (6) is of the

order of 5×10^4 cm sec^{-1}. Thus, theory predicts a heterogeneous rate constant of the order of 5×10^4 cm sec^{-1}.

There are only a few reports in the literature of actual, measured rates of heterogeneous electron transfer to or from electrochemiluminescent compounds. Dietz and Peover[14] measured the apparent rate constant k_{app} for the reduction of tetracene and other compounds at mercury in a conducting, aprotic solution. They used the Faradaic impedance method[15] for determining k_{app} and obtained k_{app} of *ca.* 2 cm sec^{-1}. The measured rate constants increased with increasing electrolyte concentration (tetra-*n*-butylammonium iodide). When they corrected their k_{app} for double-layer effects, they obtained k_{corr} of *ca.* 20 cm sec^{-1}. Aten, Büthker and Hoytink[16], using the same electrode material and solution as Dietz and Peover but a different experimental method (small-amplitude a.c., see Section 5.4), obtained k_{app} of *ca.* 0.1 cm sec^{-1} for tetracene and other aromatic hydrocarbons. However, Aten, Dieleman and Hoytink[13] later reported that these rate constants were too high to be measured and must be in excess of 5 cm sec^{-1}.

It is obvious that further experiments are required in this area.

4.2.2 Homogeneous Electron Transfer

The charge neutralization reaction between oppositely charged fluorescor ion-radicals is an example of a homogeneous electron transfer reaction. Marcus[10] also formulated a general theory for

this type of electron transfer while Hoytink[8] focussed his approach on the behaviour of simple aromatic hydrocarbons. Both authors noted the basic similarity between heterogeneous and homogeneous electron transfer reactions. The essence of Hoytink's treatment was that the coulombic forces of the reactants extend out to *ca.* 80 Å so that when they attract each other to within 10 Å there must exist almost unit probability that the anion-radical will transfer its surplus electron to the cation-radical.

A large number of homogeneous electron transfer rates have been measured. The method commonly employed is ESR[17,18] but internal reflection spectroelectrochemistry has also been successfully used[19]. The rate constants range from 10^7-10^9 1 mole^{-1}sec^{-1}. These values are close to the diffusion controlled limit which is given[20] by:

$$k_{dc} = \frac{8RT}{3000\eta} \qquad (7)$$

where η is the solution viscosity in Poises and the remaining symbols have their usual significance. Typically, at 298 °K, the viscosity of EGCL solutions is 0.9 cp so that

$$k_{dc} = \frac{8(8.31\times10^7)(298)}{3000(0.009)} = 7\times10^9 \text{ 1 mole}^{-1}\text{sec}^{-1}$$

For a cation- and anion-radical concentration of, say, 1 mM, the half-life of the diffusion-controlled charge neutralization reaction would be

$$t_{1/2} = \frac{1}{k_{dc}C} = \frac{1}{7\times10^9(10^{-3})} = 1.4\times10^{-7} \text{ sec} \qquad (8)$$

Kowert, Marcoux and Bard[17] measured the homogeneous electron transfer rate constants of aromatic hydrocarbons in several solvents. When they used their results to test Marcus' theory in terms of the dielectric constant parameter, the agreement was very poor but could be improved by treating the frequency-factor as a solvent-dependent variable.

4.2.3 Triplet-Triplet Annihilation

The excited triplets resulting from the homogeneous electron transfer reaction are produced in a compact reaction zone - the diffusion boundary layer near the electrode surface. The probability of a triplet-triplet encounter will, therefore, be very high. Actual kinetic information on this type of reaction is virtually non-existent. However, it seems reasonable to assume that the process is diffusion controlled[20]. The rate constant for the triplet-triplet annihilation reaction is consequently given by Equation (7). Competing with this reaction will be, of course, the radiationless decay of the excited triplet and its quenching. A triplet state usually lasts for more than[20] 10^{-4} sec.

4.2.4 Decay of the Excited Singlet State

An excited singlet state normally returns to its ground state within[20] 10^{-8} sec. The fraction of energy dissipated as light is defined as the fluorescence efficiency of the compound. This reaction is clearly the fastest in the EGCL mechanism.

4.3 Thermodynamics

The change in free energy accompanying an electrochemical redox process is given by the following well-known equation in which ΔG° and nF have their usual significance and E° is the standard redox potential:

$$\Delta G^\circ = -nFE^\circ \tag{9}$$

In EGCL, both the anion- and cation-radicals are neutralized simultaneously. The free energy liberated in this type of reaction will be the sum of the free energies of the two electrochemical half-reactions:

$$\dot{R}^+ + e \rightleftarrows R \text{ and} \tag{1}$$

$$\dot{R}^- \rightleftarrows R + e, \text{ i.e.} \tag{2}$$

$$\Delta G^\circ = -nF(E^\circ_{R/\dot{R}^+} - E^\circ_{R/\dot{R}^-}) \tag{10}$$

The free energy can be expanded into its enthalpy and entropy components, i.e.

$$\Delta H^\circ - T\Delta S^\circ = -nF(E^\circ_{R/\dot{R}^+} - E^\circ_{R/\dot{R}^-}) \tag{11}$$

The energy released by the charge neutralization reaction is only the change in enthalpy of the reaction. There is also an entropy change but this is not available for external work, since a non-electrochemical reaction step is involved here. Equation (11) can be re-arranged into a more useful form:

$$-\Delta H_T = nF(E^\circ_{R/\dot{R}^+} - E^\circ_{R/\dot{R}^-})_T - T\Delta S^\circ \qquad (11a)$$

The change in entropy of the reaction can be calculated from the temperature coefficient of the free energy change, i.e.

$$\Delta S^\circ = \partial(E^\circ_{R/\dot{R}^+} - E^\circ_{R/\dot{R}^-})_p/\partial T \qquad (12)$$

Visco and Chandross[21] estimated the change in entropy of the rubrene anion-cation-radical annihilation reaction to be approximately 8 cal $mole^{-1}{}^\circ K^{-1}$. An upper limit for this value was estimated to be *ca.* 15 cal $mole^{-1}{}^\circ K^{-1}$ by Hoytink[8]. Although the change in entropy is relatively small when compared to the change in free energy, its magnitude is important in determining the EGCL reaction mechanism, as will be seen by the following examples.

When the rubrene anion-radical is reacted with Wurster's blue (the cation-radical of N,N,N',N'-tetramethyl-*p*-phenylenediamine), the resultant EGCL is spectrally identical with the fluorescence of rubrene[4]. The standard reduction potential of rubrene is -1.28 V *vs* SCE and the standard oxidation potential of Wurster's blue is +0.24 V *vs* SCE. It will be assumed approximately that the standard change in entropy of this anion-cation-radical reaction is 10 cal $mole^{-1}{}^\circ K^{-1}$. Therefore, the standard change in enthalpy of this reaction is (expressing the terms in the appropriate units):

$$-\Delta H^\circ = (1)\left(96{,}500 \frac{\text{amp sec}}{\text{mole}}\right)(+0.24 - (-1.28)\text{V})\left(\frac{1\text{cal}}{4.19\text{V amp sec}}\right) - 298^\circ\text{K}\,\frac{10\text{cal}}{\text{mole }^\circ\text{K}}$$

$$= 37.6 \text{ Kcal mole}^{-1}$$

The energy of the lowest excited singlet state of rubrene is 52.9 Kcal $mole^{-1}$. It is thus seen that a change in enthalpy of 37.6 Kcal $mole^{-1}$ actually leads to a 52.9 Kcal $mole^{-1}$ electronic transition. In this EGCL system, the singlet state is evidently not directly accessible from the anion-cation-radical annihilation reaction; it must be produced exclusively via triplet-triplet annihilation. Such cases are known as "energy deficient" EGCL processes.

The fluorescor 9,10-diphenylanthracene (DPA) has standard oxidation and reduction potentials of +1.35 and -1.89 V *vs* SCE, respectively, and its lowest excited singlet state is 69.0 Kcal $mole^{-1}$ above ground state[4]. The standard change in enthalpy of this reaction is slightly greater than the energy of the emission, *viz.* 71.6 Kcal $mole^{-1}$ compared with 69.0 Kcal $mole^{-1}$ (again assuming that ΔS° = 10 cal $mole^{-1}$ $^\circ K^{-1}$) . The EGCL from DPA is thus referred to as "energy sufficient".

Felderberg[22] has proposed a non-thermodynamic method for determining whether the EGCL system is energy deficient or sufficient. His method involves plotting the intensity of the EGCL *vs* time using pulse electrolysis of the fluorescor. He calculated that the EGCL of an energy sufficient system would decay twice as fast as the EGCL of an energy deficient system.

Faulkner, Tachikawa and Bard[23] have reported that the application of an external magnetic field enhanced the intensity of energy deficient EGCL but had no effect on the intensity of energy sufficient EGCL. They accounted for this observation by suggesting that the

magnetic field inhibited the quenching of triplets by radical-ions. Thus, the magnetic field effect of the intensity of EGCL could also be used to determine whether an EGCL system is energy deficient or sufficient.

4.4 Quantum Efficiency of EGCL

Bard, Keszthelyi, Tachikawa and Tokel have recently reviewed this topic[24]. They define the various ways of expressing this efficiency and list all of the published results. The reported efficiencies vary for 0.1 to 20 %. These results are for different types of systems and were measured by different methods with different kinds of corrections applied. Unfortunately, there is no agreement in values for the same system (rubrene in tetra-*n*-butylammonium perchlorate-benzonitrile). In fact, most of the original results have been revised upwards. Bard *et al* attribute the scatter in the results to the experimental difficulties (see Section 5.5) in making these measurements.

From the efficiency results in the review of Bard *et al*[24], it is nevertheless possible to conclude that the quantum efficiency of EGCL is solvent-dependent and, in some cases, also a function of electrolyte concentration, a factor that may originate from ion-pairing effects.

Some of the efficiency results reported in this thesis have already been published[25]. It will be seen that the method for measuring the EGCL efficiency developed in the present work is simple and precise. This, together with use of a stable EGCL system, has

allowed reliable efficiency values to be obtained. Consequently, the present results permitted further details concerning the EGCL mechanism to be elucidated.

It will be of interest here to calculate the maximum, theoretically possible quantum efficiencies of EGCL. This will allow comparisons to be made between the present experimental results and the theoretical values. The EGCL mechanism for an energy-sufficient system has been given in Table 1 but it is useful here to examine the consequences of the mechanism. In this scheme, each homogeneous electron transfer reaction (two electrons, one to produce the cation- and one to produce the anion-radical) produces on the average 1/4 excited singlets and 3/4 excited triplets. The excited triplets react via triplet-triplet annihilation to produce an average of 1/4 excited singlets and 3/4 excited triplets per triplet-triplet annihilation. It is important to note that the triplets produced from the triplet-triplet annihilation reaction are actually in the same state as the reactants so that they will participate in further triplet-triplet annihilations. This increases the excited singlet yield per triplet-triplet annihilation from 1/4 to 2/5. The total excited singlet yield per homogeneous electron transfer is, therefore, 1/4 directly produced together with $1/2 \times 3/4 \times 2/5 = 6/40$ via triplet-triplet annihilation. Thus, two electrons produce "2/5" of a photon. Hence, the quantum efficiency of an energy-sufficient EGCL system has a maximum theoretical value of 20 %. In an energy-deficient system, the excited singlets can only

be produced via the triplet route. Consequently, the maximum theoretical quantum efficiency of an energy deficient EGCL system is only $6/40 \div 2 \equiv 7.5$ %.

5. CHOICE OF METHODS OF STUDY

Some of the methods were already established (e.g. electrochemical techniques) while an improved method for measuring the quantum efficiency had to be devised.

5.1 Cyclic Voltammetry (CV)

A cyclic voltammogram[26] is the current-voltage trace resulting from the application of a time-dependent ramp potential that is varied or cycled between two limits (i.e. a triangular wave) and applied to an electrode immersed in the solution to be studied. Fig. 1 illustrates schematically the experimental arrangement for a CV experiment. In this circuit, the potentiostat maintains the ramp potential on the working electrode, WE, by controlling the input voltage signal to the cell between the counter and working electrodes, CE and WE, respectively.

The WE is preferentially fabricated to maintain linear diffusion. The solution is kept "quiet" to avoid mass transport by agitation. By performing the CV at a constant temperature, mass transport by convection is largely eliminated. An excess of supporting (unreactive) electrolyte in the solution prevents electrostatic migration of the species being electrolyzed. Under the preceding conditions, the sole remaining mode of mass transport is via diffusion.

A cyclic voltammogram is illustrated in Fig. 2. The voltammogram has the following characteristics if the heterogeneous electron

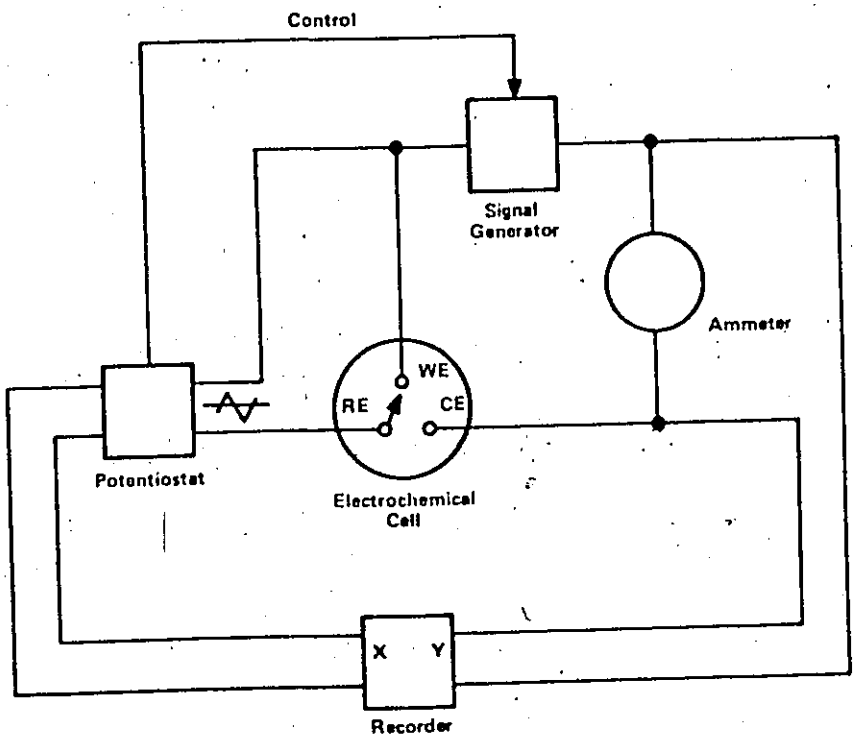

Fig. 1. Circuit for cyclic voltammetry.

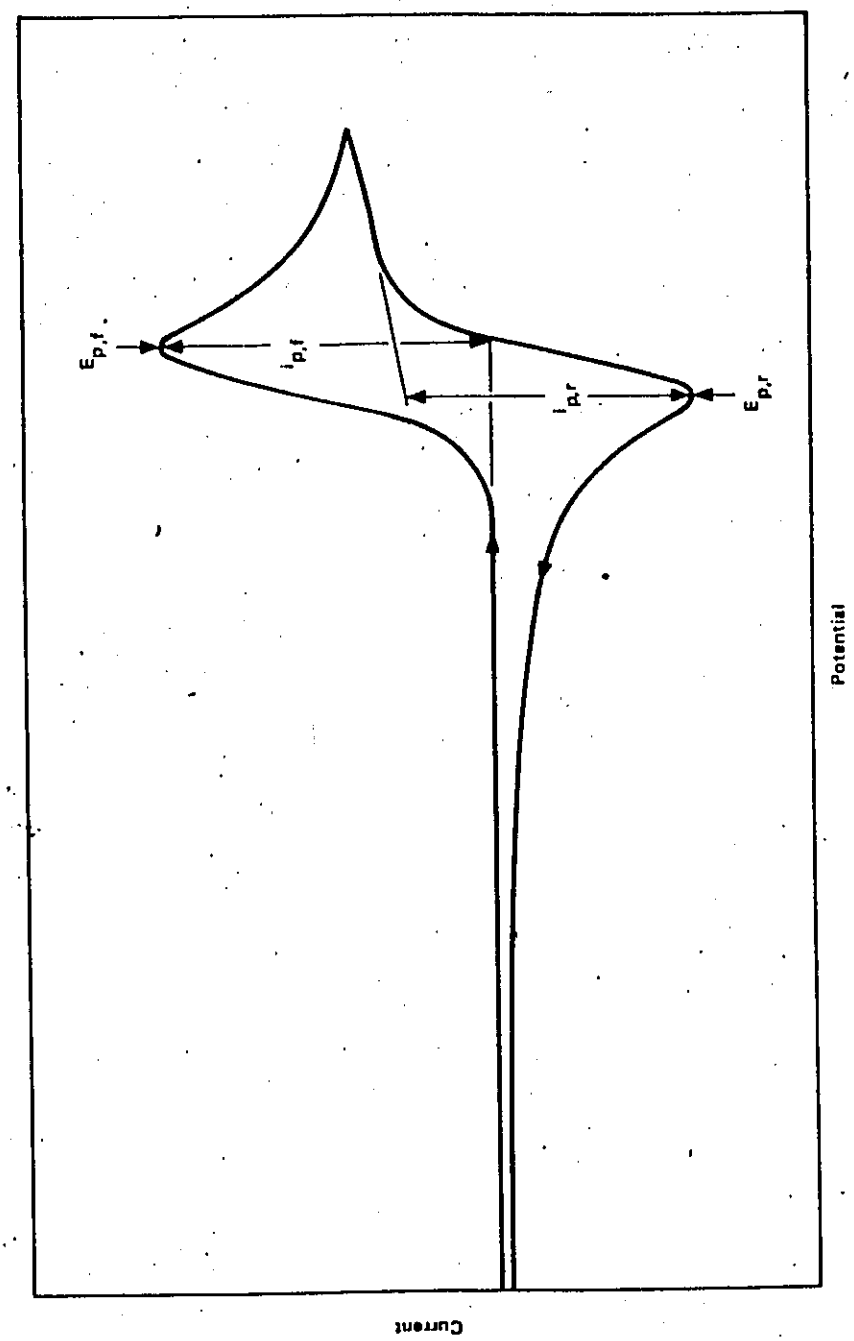

Fig. 2. Characteristics of cyclic voltammogram.

transfer is diffusion-controlled and the ion-radicals are stable:

i) The peak forward current, $i_{p,f}$, is equal to the peak reverse current, $i_{p,r}$ (provided both species have the same diffusion coefficient) or, more precisely, the net charge over the complete cycle is zero.

ii) The potential difference between the peak currents ($E_{p,f}$-$E_{p,r}$) is 58 mV at 25 °C for a one electron process. The separation increases inversely as the number of electrons involved in the redox reaction.

iii) The peak current varies according to the Randles-Sevčik equation:

$$i_p = kn^{3/2}AC_bD^{1/2}S^{1/2} \qquad (13)$$

where i_p = peak current in amperes

k = a constant (theoretical value = 269)

n = number of electrons involved in the redox reaction for one molecule

A = area of the electrode in cm^2

C_b = bulk concentration of substance being electrolyzed in moles cm^{-3}

D = diffusion coefficient of species undergoing electrolysis in cm^2 sec^{-1}

S = scan rate of ramp potential in V sec^{-1}

The first scan in CV is normally recorded. Subsequent scans exhibit smaller Faradaic currents because of the establishment of a time-dependent concentration gradient at the electrode.

A slow heterogeneous electron transfer reaction tends to increase the potential difference between the peaks of the voltammogram[27]. This separation increases with increasing scan rate. It is therefore possible to calculate the rate constant for the redox process from the dependence of $(E_{p,f}-E_{p,r})$ on scan rate. A slow charge-transfer process also yields less current than that predicted by the Randles-Sevčik equation. For slow reactions, $i_{p,f}/S^{1/2}$ will decrease with increasing scan rate. It must be recognized that cell and measuring circuit resistance and weak instrument compliance will lead to effects similar to those generated by a slow reaction, so that instrumental and circuit conditions must be chosen carefully.

When the primary product of the electrolysis is unstable, the reverse current will be less than the forward current since both currents are directly proportional to the concentration and square root of the diffusion coefficient of their respective reactants.

The Randles-Sevčik equation predicts that for a fast charge-transfer process limited by linear diffusion and in the absence of secondary reaction, the peak current is directly proportional to $S^{1/2}$ or $i_{p,f}/S^{1/2}$ is independent of S. By reducing S, more time is allowed for follow-up reactions to occur so that greater irreversibility can arise. For aromatic hydrocarbons, the products of side reactions are often electroactive at the prevailing potential[28]. Therefore, if the ion-radicals do participate in side reactions, this would be manifested by an increasing $i_{p,f}/S^{1/2}$ with decreasing scan rate.

5.2 Chronoamperometfy

When a constant potential sufficient to either reduce or oxidize the electroactive species is applied to an electrode that maintains linear diffusion, a decrease in current with time is observed. The decrease is caused by the fanning out of the diffusion layer and can be derived from Fick's second law[26]. It can be shown that under these conditions

$$i_t = \frac{nFAC_b D^{1/2}}{\pi^{1/2} t^{1/2}} \tag{14}$$

where i_t is the instantaneous current at time t and the remaining symbols have already been defined. This equation stipulates that diffusion controlled current-time curves obtained at constant voltage (chronoamperograms) are characterized by constancy of $it^{1/2}$. The potential should be rested at least 100 mV beyond the peak potential. If linear diffusion does indeed prevail at the electrode and a positive deviation in $it^{1/2}$ is obtained, this may indicate instability in the electrogenerated ion-radical with respect to further oxidation or reduction. The form of the i-t curve is a very sensitive indicator of follow-up reactions because a considerable quantity of ion-radicals is produced during its recording. The by-products will diffuse to the electrode and undergo further electrolysis and be indicated by excess current.

If an electrode of known area is employed in taking the chronoamperogram, it will be possible to calculate the diffusion coefficient

of the species being electrolyzed from the i-t plot. The surface area can be determined by electrolyzing a compound of known diffusion coefficient. The oxidation of 4 mM ferrocyanide in 1 M aqueous KCl is a useful standard for this purpose. Its diffusion coefficient at 25 °C is[26] 6.32×10^{-6} cm^2 sec^{-1}.

5.3 Electron Spin Resonance (ESR)*

The products from the electrolysis of the fluorescor each contain one unpaired electron. This free electron can have a spin of either +1/2 or -1/2. Thus, the ion-radicals are paramagnetic. When the ion-radicals are subjected to the influence of a magnetic field, this can result in spin transitions from one state to another. Normally, a spectrum of transitions is obtained with varying field strength because of intramolecular interactions between the unpaired electron and the nuclei.

The intensity of the ESR signal is, under normal conditions, directly proportional to the ion-radical concentration. Consequently, ESR can be used to study ion-radical stabilities and rates of electron transfer. In this investigation, ESR was only used to study the former because the latter has already been amply investigated (see Section 4.2.2). To determine the stability of the ion-radicals, the fluorescor was electrolyzed until a strong ESR signal was

---

* NOTE: ESR is also commonly known by another name, electron paramagnetic resonance (EPR).

developed. Then, the electrolysis was stopped and the strength of the ESR signal was recorded *vs* time. From the decay of the ESR signal with time, the half-life of the ion-radicals was calculated.

For further background information on ESR, the reader is referred to Pastro and Johnson[29].

5.4 Small-Amplitude A.C. Polarography

Small-amplitude a.c. polarography is a very useful technique for measuring the kinetic parameters of heterogeneous electron transfer reactions. The technique involves the measurement of the alternating current produced by a small a.c. potential superimposed on the ramp potential[30]. The alternating potential must vary considerably faster than the ramp potential. However, since high frequencies tend to create too much capacitive current, double-layer charging can become limited by the RC constant of the cell at such frequencies; hence, the frequency should be limited to 10-1000Hz. The lower limit is also determined by the curvature of the spherical working electrode. At low frequencies with a small diameter electrode, significant departure from linear diffusion can arise. The working electrode in a.c. polarography is purposely made small and beaded to minimize the cell impedance. Appreciable cell resistance has, of course, the same effect as slowness in the electron transfer process.

Alternating current can only flow when both the oxidized and reduced species of the compound undergoing electrolysis are present together. The alternating current will then exhibit a peak at the half-wave potential, $E_{1/2}$. The shape of a reversible a.c. polarographic wave (Fig. 3) is such that a plot of E_{dc} *vs* log $[(i_p/i)^{1/2} - (i_p-i)/i^{1/2}]$ has a slope of 120/n mV at 25 °C where i is the value of the current at E_{dc} (the ramp potential).

The electrochemical process can be represented by an electrical impedance with a potential-dependent conductance. The impedance is termed a Faradaic impedance. The Faradaic impedance can, in turn, be represented by a series combination of a Faradaic resistance, R_F, and a Faradaic capacitive reactance, $X_{c,F}$. Randles[31] has derived mathematical expressions for both R_F and $X_{c,F}$ but the equations are restricted to the potential at which the concentration of the reduced and oxidized species are equal, i.e. at the half-wave potential. The two equations are:

$$R_F = \frac{RT}{n^2F^2AC_o}\left[\left(\frac{2}{\omega D}\right)^{1/2} + \frac{1}{k}\right] \qquad (15)$$

and

$$X_{c,F} = \frac{1}{\omega C_F} = \frac{RT}{n^2F^2AC_o}\left(\frac{2}{\omega D}\right)^{1/2} \qquad (16)$$

where ω = angular frequency in radians sec^{-1}, C_o is the concentration of R and R^+ or R^- at the electrode surface and the other symbols

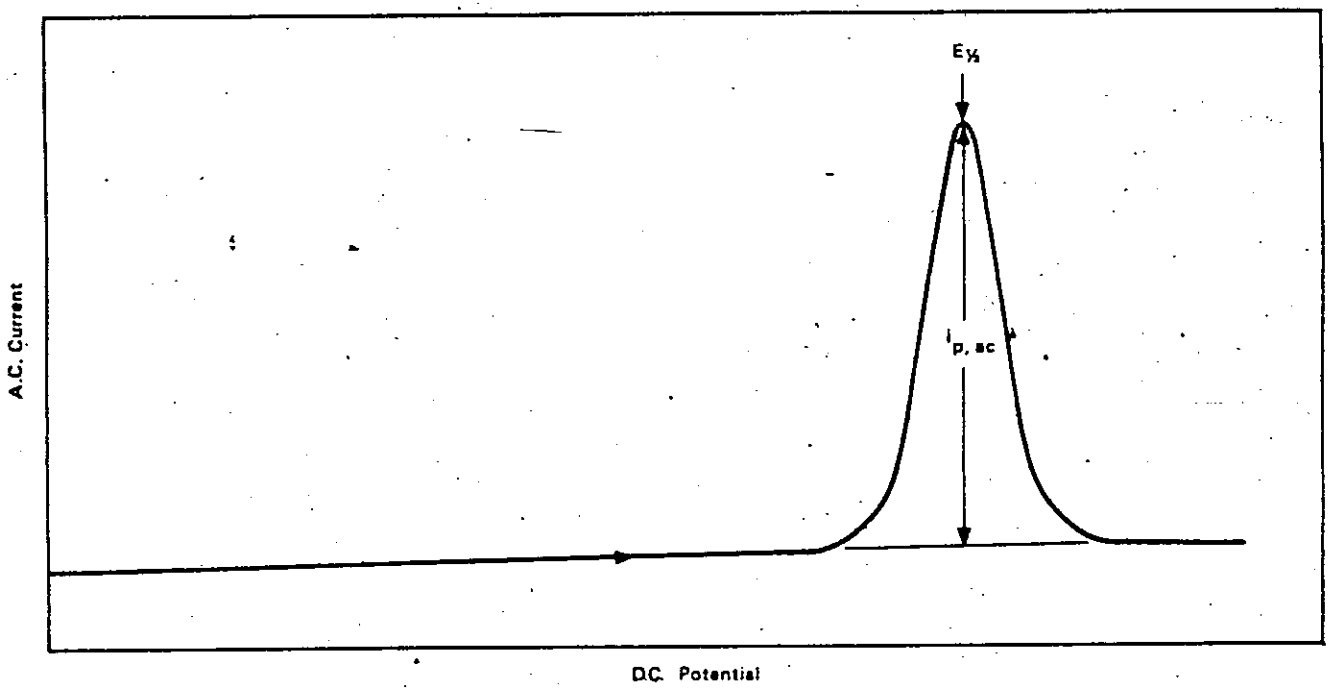

Fig. 3. Characteristics of small-amplitude a.c. polarogram.

have their usual significance.

From Equation 15 and 16 and the equation for the a.c. current through an impedance in the form of Equation 17 below,

$$I = \frac{V}{X_c} \sin \theta, \tag{17}$$

it is possible to derive an expression for the peak Faradaic current of an a.c. polarogram (see Appendix I. This derivation is not given in the literature.) The equation is:

$$i_{p,ac} = \frac{V_{ac} n^2 F^2 A C_b (\omega D)^{1/2}}{4RT} \left[1 - \frac{1}{2k} \left(\frac{\omega D}{2} \right)^{1/2} \right] \tag{18}$$

where V_{ac} = amplitude of the alternating potential superimposed on top of the ramp potential, volts (peak) and C_b is the bulk concentration of the electroactive species.

Application of Equation 18 may be refined by using a phase-sensitive current detector. Since R_F approximately equals $X_{c,F}$, then the Faradaic current peaks at slightly less than 45° out of phase with the voltage. By measuring the current at 45° with respect to the voltage, the detection of the Faradaic current is optimized and the effect of the capacitive current which charges the electrode double-layer is reduced. The ideal phase-angle for detection decreases with decreasing rate constant and increasing frequency. However, since the alternating current exhibits a broad maximum with phase angle and if k is large relative to ωD, then a phase angle of 35-45° will generally suffice.

Equation 18 indicates that a plot of $i_{p,ac}/\omega^{1/2}$ *vs* $\omega^{1/2}$ should be linear with a slope equal to $K(D/2)^{1/2}/2k$ where $K = \left(\frac{V_{ac} n^2 F^2 A C_b D^{1/2}}{4RT}\right)_{\omega=0}$ from which k can be calculated if D is known. By determining k at several temperatures, the energy of activation of the redox process can be derived from a plot of log k *vs* 1/T (Arrhenius plot).

5.5 Quantum Efficiency

Although "quantum efficiency" is, simple to define, e.g.

$$\text{quantum efficiency} = \frac{\text{no. of photons of EGCL generated sec}^{-1}}{\text{electrolytic current (in electrons sec}^{-1}\text{) transferred}} \quad (19)$$

its actual measurement is not trivial. The most difficult problem in this measurement is the low light intensities which originate from EGCL. Other obstacles to be overcome with the light measurements are the uncertainties inherent in such factors as reflection losses at the electrode, absorption losses in the solution, collection efficiency of the detector and spectral response of the detector.

The electrolytic current consists of Faradaic and capacitive components. Only the Faradaic component of the total current produces light; the capacitive component is used to charge the double-layer. Consequently, in order to obtain true quantum efficiency data, it is necessary to separate the electrolytic current into its Faradaic and capacitive components. Of the ion-radicals produced, some will diffuse away from the reaction zone without being neutralized while others can be lost to side reactions. The

Faradaic current should not include these losses since they do not contribute to the generation of light.

The presence of all of these factors limits the accuracy with which the quantum efficiency of EGCL can be determined.

The light from EGCL has been measured using calibrated photon detectors[32], actinometry[24] and integrating spheres[33] while the current was always assumed to be entirely Faradaic. Previous results in the literature for the quantum efficiency of the same system (rubrene in tetra-*n*-butylammonium perchlorate-benzonitrile) range from a low value of 0.1 % (corrected for photon and current losses) to a high one of 8.7 % (without any correction)[24]. The various measuring techniques give inconsistent results mainly because of the various forms of stimuli (d.c., voltage steps, a.c., etc.) that have been used to generate the EGCL. The ion-radicals are always, in some measure, unstable. Their degree of instability is dependent on the mode by which they are generated. For example, with an a.c. stimulus, the magnitude of ion-radical instability increases with decreasing frequency because at the low frequencies the ion-radicals have more time to participate in secondary reactions. From these observations, it is to be concluded that whatever method is devised and/or employed for measuring the quantum efficiency of EGCL, the EGCL should be generated with moderate or high frequency a.c. stimulus.

When a potential is applied across two equal-area electrodes immersed in a conducting solution, each electrode will establish the same voltage drop across the polarized interphase provided the

double-layer capacity is constant with potential. For large, simple aromatic hydrocarbons, it is to be expected that the values of the ionization potential and electron affinity are almost the same. Therefore, by applying a potential across two equal-area electrodes immersed in a conducting solution of the fluorescor, when the potential is sufficient to electrolyze the fluorescor, the same quantity of oppositely charged ion-radicals will be generated at each electrode. With a.c. stimulation, the same amounts of cation- and anion-radicals would alternately be produced at each electrode.

The non-steady electrolysis current consists of a capacitive and a Faradaic component. The capacitive component is directly proportional to the magnitude of the applied voltage and its frequency. However, the Faradaic current is only produced beyond a certain decomposition potential and then it is voltage and time dependent. It is these fundamental differences between the two components of the total a.c. current which makes it possible to devise a way to resolve each component.

A square-wave potential was applied to the equal-area, 2-electrode cell (Fig. 10) and the average rectified a.c. current was measured as a function of the applied voltage; the average photon current was also simultaneously recorded. The electrolysis current was converted to a voltage and amplified by a factor of 1000, rectified with a linear rectifier and finally read with an integrating digital voltmeter. This indicated the average rectified a.c. current.

Specifically, 1 V d.c. was equivalent to 1 mA average rectified a.c.

The average rectified a.c. current increases linearly with increasing voltage (provided that the double layer capacity is constant with voltage) up to the potential where the fluorescor begins to be electrolyzed. Beyond this, the total current is the sum of the capacitive and Faradaic currents. By extrapolating the capacitive current line into the potential range for the electrolysis of the fluorescor, it is possible to estimate the capacitive component of the total current. Any current above the capacitive current line is Faradaic (assuming that the Faradaic processes do no affect the capacitive current line). Fig. 4. illustrates this technique for measuring the Faradaic current when electrolyzing the fluorescor with an alternating square-wave potential. The frequency of the applied voltage can be increased until the EGCL exhibits complete stability, i.e. constant intensity on continuous generation. Any EGCL system can normally be made sufficiently stable by increasing the electrolysis frequency.

For the quantum efficiency measurement, the electrolysis cell was stood inside an open box, the sides and bottom of which were made of 1 cm^2 silicon solar cells (Fig. 10). The working electrodes in the electrolysis cell were positioned in the middle of the solar cell box. In this position, the solar cells collected 5/6 of the total light emitted from the electrolysis cell. The solar cells were connected in parallel and their total current was measured with an average-reading picoammeter. From the spectrum of the EGCL and the spectral

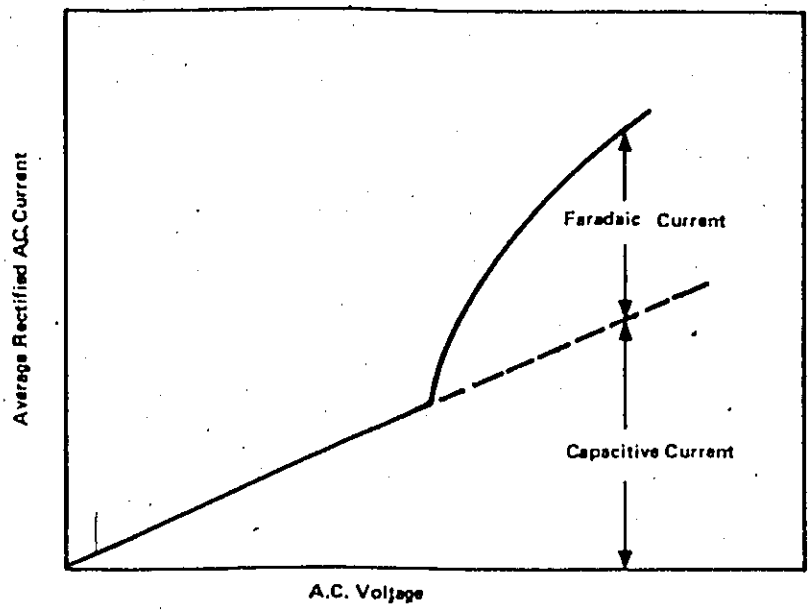

Fig. 4. Method for distinguishing Faradaic current from total current produced by a.c. voltage.

response of the solar cells, a correction factor was obtained for converting the measured photon current into the actual photon current.

A plot of the total corrected photon current *vs* the Faradaic current was then made. The slope of this plot yields twice the quantum efficiency of the EGCL because equal amounts of light were produced at each electrode and the total was measured and plotted against the Faradaic current. The EGCL efficiency is expressed in photons emitted out of the cell per sec per total Faradaic electron charge (in electrons) passed per sec. The symbol ϕ_{coul} will be employed to represent this quantity in accordance with the convention established by Bard *et al*[24].

The complete apparatus for measuring ϕ_{coul} is illustrated in schematic form in Fig. 5. It probably represents the most important experimental contribution from this work. By developing an independent method for measuring the quantum efficiency of EGCL, it became possible to establish more reliable quantum efficiency values. The reliability of these values is to be judged by the merits of the method itself and by virtue of the reasonable agreement of the results with some of the previously published results which had, however, been at variance with other published results.

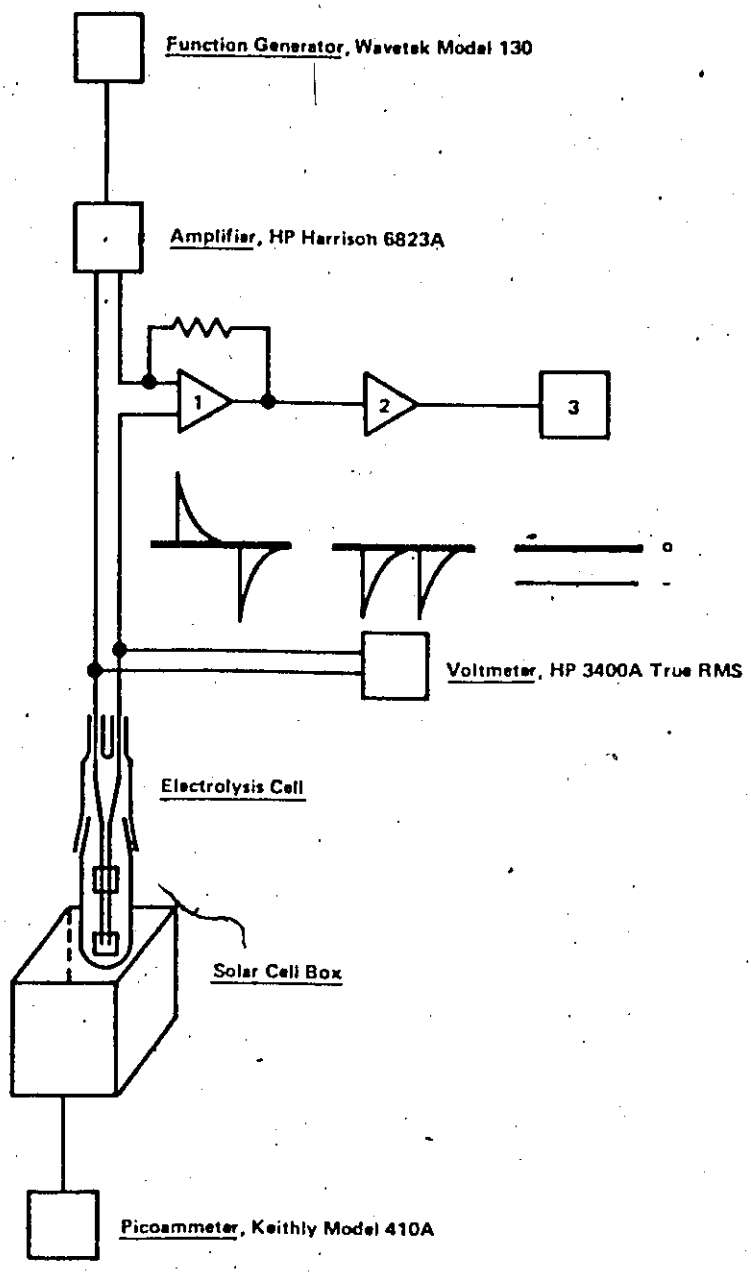

Fig. 5. Apparatus for measuring ϕ_{coul}.

6. EXPERIMENTAL

6.1 Chemicals and Their Purification

6.1.1 Acetonitrile

Acetonitrile is a very difficult solvent to purify. The impurities in it vary not only from supplier-to-supplier but also from batch-to-batch from the same source. The variable quality of commercial acetonitrile is probably indicated by the numerous reports for its purification[34,35]. The method used to purify acetonitrile for this work was derived from attempts to purify the acetonitrile by literature methods. Some of the impurities in the as-received acetonitrile could be removed by adsorption onto alumina while others could be separated by distillation. Fortunately, it was possible to obtain commercial acetonitrile which contained only those impurities that could be removed by the adsorption-distillation procedure.

The commercial acetonitrile was analyzed by vapour phase chromatography (VPC) on a Porapak Q column. A sample was then passed through a column packed with activated alumina and the eluant was analyzed by VPC to determine what impurities, if any, were removed by the alumina. The alumina was previously thermally activated by vacuum heating it at 350 °C for 2 days. The eluant from the alumina column was then distilled in Pyrex glassware. A packed distillation column was used to provide greater fractionation of the distillate. The distillate was periodically analyzed by VPC to determine its composition. The middle cut was normally the purest.

Each of the available samples of acetonitrile was, in turn, subjected to the adsorption-distillation procedure until a sample was found whose impurities were all removed by these purification methods. Some acetonitrile from MC&B and Aldrich could be purified to better than 99.99 % purity by the above procedure.

A new impurity was introduced by purifying the acetonitrile by the method described above. (This impurity was not detectable in the starting material but as much as 6 ppm was found in the purified acetonitrile.) One form of this impurity was produced by the alumina treatment but the distillation converted it into another form.

6.1.2 Benzene

In this investigation, benzene was added to other aprotic solvents to obtain solvent mixtures of varying polarity.

Samples of the purest commercial sources of benzene were purchased and then analyzed by VPC on an Apiezon L column to resolve non-polar impurities and on a Porapak Q column to resolve polar impurities. The VPC analysis indicated only ppm quantities of water, toluene and the three xylene isomers. Fisher B-414 (99.9 Mol %) benzene was consistently found to be purer than other brands. It typically contained less than 50 ppm total impurities. Only the water in the benzene was judged to be detrimental. It was removed by drying the benzene with two batches of pre-dried Linde type 5A molecular sieves, each for 24 hours. The dried benzene was decanted into a vacuum distillation apparatus and distilled at *ca.* 10 mm Hg.

The vacuum distillation was done inside a nitrogen-filled dry box. The glassware was vacuum heated just before it was used to dry it of adsorbed water.

6.1.3 Benzonitrile

Each of the commercially available, highest purity grades of this aprotic solvent contained a total of *ca.* 0.1 % of numerous impurities as indicated by VPC on an Apiezon L column. After drying the MC&B material (Spectroquality grade) with Linde type 5A molecular sieves, a conducting solution of rubrene was prepared with it and the electrochemical behaviour of the rubrene was studied via cyclic voltammetry. Both the oxidation and reduction products of rubrene were completely stable (constant $i_p/S^{1/2}$), even at very low scan rates down to 1 mV sec^{-1}. Further purification of this benzonitrile appeared unwarranted.

Mann[36] describes a method for the purification of benzonitrile.

6.1.4 Nitrogen

Nitrogen was used to purge the aqueous solutions from oxygen and to fill and flush the dry box. It was obtained from 99.99 % pure liquid N_2.

6.1.5 N,N-dimethylformamide (DMF)

Butler[37] and Mann[36] each have summarized the procedures required to purify this aprotic solvent. The methods involve chemical treatment followed by distillation. None of these methods was investigated because in their previous use, it has been reported that good ion-

radical stabilities could not be obtained.

Fisher D-133 (99.9 Mol %) was the purest of the available materials. It was analyzed by VPC on a Carbowax 20M-KOH column. The natural impurities in this solvent are formic acid, formaldehyde, dimethylamine, carbon monoxide and, of course, water[38]. All of these impurities are relatively small molecules. Attempts to adsorb them on Linde type 5A molecular sieves were successful. The dimethylamine was only partially removed but the other impurities were almost completely removed. The 5A dried product was vacuum distilled and stored in a nitrogen-filled dry box. A troublesome by-product resulted from prolonged drying, i.e. two months, with these sieves. The purified DMF was at least 99.999 % pure.

6.1.6 Potassium Chloride

This salt was used as one of the supporting electrolytes for the work on aqueous ferro-ferricyanide as the test system for validating the small-amplitude a.c. polarographic technique. Fisher P-217 (Certified ACS) KCl was used directly.

6.1.7 Potassium Ferricyanide

The Fisher product (P-232, Certified ACS) was used without further purification.

6.1.8 Potassium Ferrocyanide

This chemical was purchased from Fisher (P-236, Certified ACS) and used as received.

6.1.9 Propylene Carbonate

A literature report on the purification of this aprotic solvent is available[39]. The conclusion from this report was that vacuum distillation can yield a satisfactory product.

All of the purchased samples of propylene carbonate (e.g. Eastman #7050, MC&B PX 1705) were pale yellow. Upon vacuum distillation, the yellow substance became concentrated in the pot. The middle 60 % cut was collected and tested electrochemically. Its conducting solution contained electroactive impurities originating from the solvent. The vacuum distilled product was therefore further purified by pre-electrolyzing it. A potential difference of 4 V d.c. was applied between a pair of platinum electrodes (each 10 cm^2 in area and made from 0.020" dia. wire) in 25 ml of 0.1 M TBAP solution. The solution was stirred and electrolyzed for two days. The pre-electrolyzed solution was again vacuum distilled. This product, when used as a solvent for rubrene electrolysis, offered adequate ion-radical stability.

6.1.10 Rubrene

Rubrene was selected as the sole fluorescor to be used in this investigation. A complete literature survey on EGCL quickly revealed that rubrene was relatively the most stable electrochemiluminescent compound. Metal chelates and porphyrins were excluded from consideration because of insufficient background information. Furthermore, these two classes of compounds were not typical of classical EGCL. Some of the other, normal, electrochemiluminescent compounds that

were considered were 9,10-diphenylanthracene, pyrene, and 1,3,4,6-tetraphenylisobenzofuran. They were not selected because they either lacked sufficient ion-radical stabilities or produced too dim an EGCL, or both. Besides offering the overall best ion-radical stabilities, rubrene also required the lowest potential span for generation of its ions; also, its EGCL was the most intense.

It has been reported[40] that rubrene can be purified by vacuum sublimation. When this method was tried using rubrene from Aldrich (R-220-6), stratification of the products was observed but the process was accompanied by considerable thermal degradation of the starting material. The strata were not pure because their melting points had a range in excess of 50 C°.

A method reported for the purification of anthracene[41] was then applied to the purification of the rubrene. One gram of the starting material was dissolved in 60 ml of boiling xylene (Fisher, X-5). The resultant solution was then poured into twice its volume of cold (*ca.* 0 °C) methanol (Fisher, A-936). A red-orange precipitate immediately fell out of the mixed solution. It was given one hour to digest and then its mother liquor was decanted. The precipitate was then re-dissolved in hot xylene and the solution again poured into cold methanol. After again giving the precipitate time to become digested, its mother liquor was decanted and the residual solvents allowed to evaporate. The dry precipitate was then vacuum heated at 140-160 °C for at least two hours and stored in a dark desiccator. In order to avoid photo-oxidation of the rubrene[42], the

purification was carried out in a dark room and nitrogen was continuously passed over the solution containing the rubrene.

The original material began to melt at 255 °C and, on standing at 300 °C, it decomposed. The purified rubrene had a melting point of 335.5-337.0 °C, and was thermally stable. All of the extra fluorescence bands in the starting material were eliminated by this purification procedure.

6.1.11 Sodium Chloride

The sodium chloride was purchased from Baker (Analyzed Reagent, 3624) and used without further purification.

6.1.12 Sodium Perchlorate

This salt was acquired from Fisher (Purified, S-360). It was recrystallized from a hot, saturated aqueous solution once and then allowed to dry by evaporation. The evaporation was accelerated by allowing dry nitrogen to pass over the crystals.

6.1.13 Tetra-*n*-butylammonium Perchlorate (TBAP)

TBAP is the universal electrolyte material employed for work on EGCL. Consequently, no other electrolyte material was considered.

It has been reported that TBAP can be purified by either washing it with water until neutrality is reached[43] or by recrystallizing it from ethanol-water[44], followed by vacuum heating below 100 °C. In this work, it was found that 1 g of TBAP (from Southwestern Analytical Chemicals) could be dissolved in 3 ml of boiling absolute ethanol. On cooling this solution to 0 °C, over 80 %

of the material was recoverable. Water was therefore eliminated from the purification procedure. This was extremely desirable because water is very detrimental to the stability of the ion-radicals[28]: Two recrystallizations from ethanol were normally employed in the purification of TBAP. While the TBAP was dissolved in the first batch of ethanol, some activated carbon was added to this solution to remove the pale-yellow colour from it. The solution containing the carbon was separated from the carbon by filtering the hot solution.

The TBAP purified by the above method had a melting point of 214.5-217.0 °C.

6.1.14 Water

Since this work was carried out at Bell-Northern Research, their "electronic grade" water was used. Its purification begins with the treatment of the well water by means of sand and carbon filters. After being softened, it is again filtered through sand and carbon, and a 2 micron Millipore filter. It is then passed through a reverse osmosis unit which removes 90 % of dissolved ions. From there, it is pumped through separate cation- and then anion-exchange resin beds, and then a mixed ion-exchange bed. Following this treatment, it is irradiated with UV light and given a final filtering with another 2 micron Millipore filter.

The purified water had a conductivity of 18 Megohms.

6.2 Cleaning of Glassware

Glassware that had not been previously used was first scrubbed with cleansing powder, then rinsed thoroughly with water and finally vacuum dried. Glassware that had been used for aqueous solutions was similarly cleaned.

The procedure for cleaning glassware that had been used for non-aqueous solutions consisted of three rinses with benzene to wash away any fluorescor material and to dissolve the grease used to seal the ground glass joints, followed by three rinses with methanol to remove residual electrolyte and benzene. This glassware was then cleaned with cleansing powder, rinsed with water and vacuum heated to dryness.

6.3 Preparation of Solutions

6.3.1 Aqueous Solutions

The solutes were weighed directly into volumetric flasks and the solutions were prepared by first dissolving the solutes with a small amount of added water and then filling the flask to the mark with more water. Nitrogen was immediately bubbled through the solutions. After *ca.* 10 min., nitrogen bubbling was terminated and the volumetric flask was promptly stoppered. The stopper was taped to the flask using electrical tape.

When part of an aqueous solution was transferred from its volumetric flask to an electrochemical cell for experimentation, both vessels had nitrogen bubbled through them for *ca.* 10 min.

before being stoppered. Any solution that had been transferred to an electrochemical cell was used within five hours and then discarded.

6.3.2 Non-aqueous Solutions

Non-aqueous solutions were prepared inside a nitrogen-filled dry box in which were stored the already purified solvents. The solutes were weighed outside and transferred directly into the volumetric flask in which the solution would be prepared. The charged volumetric flask was then placed on a hot plate inside the antechamber to the dry box. The antechamber was evacuated to *ca.* 1 mm Hg using a mechanical pump and with the vacuum continuously on, the hot plate was heated to 140-160 °C. The vacuum line from the pump to the antechamber had a U-bend in it which was placed inside a Dewar flask filled with liquid nitrogen. After heating for two hours, the hot plate was turned off and the pressure brought to 1 atmosphere using nitrogen. The contents of the antechamber were then transferred to within the dry box. As soon as the volumetric flasks containing the dried solutes had cooled to below *ca.* 50 °C, the solvent(s) were added in parts first to dissolve the solutes and then to dilute the solution to the marks on the flask.

The solution in the flask was used to charge the cleaned electrochemical cell previously placed inside the dry box. Residual solution was stored inside the dry box while the cell was stoppered and brought out of the dry box for experimentation. The electrochemical cell was usually brought in with the volumetric flask con-

taining the solutes of the test solution. Only certain parts of the cells could be heated to bake off water adsorbed to the glass. Fortunately, it was possible to design all of the cells such that those parts which came in contact with the solution could be heated.

6.4 Electrochemical Cells

6.4.1 Aqueous Solutions

The cell used for the aqueous electrochemical work is illustrated in Fig. 6. The main body was constructed from a TS 55/50 Pyrex female joint while the side compartment for the reference electrode was made from a TS 24/40 Pyrex female joint. The two compartments were interconnected just above their bottoms with an 8 mm tube which extended into the centre of the main compartment and terminated with a vertical Luggin tip. In Fig. 6 are also shown details of the two types of working electrodes employed in this investigation. The working electrode was placed *ca.* 1 mm above the Luggin tip. Gold and platinum were used as electrode materials; consequently, soft glass tubing had to be used to imbed the electrodes with a hermetic seal. The counter electrode consisted of a 6 mm diameter platinum helix wound centrally and extensively around the Luggin tip-working electrode area.

The cell was suspended *ca.* 1" from the bottom of a thermostated water bath. The water bath was stood on top of a magnetic stirrer which rotated a stirring bar in the electrolysis cell. The liquid level of the water bath was kept just above the solution

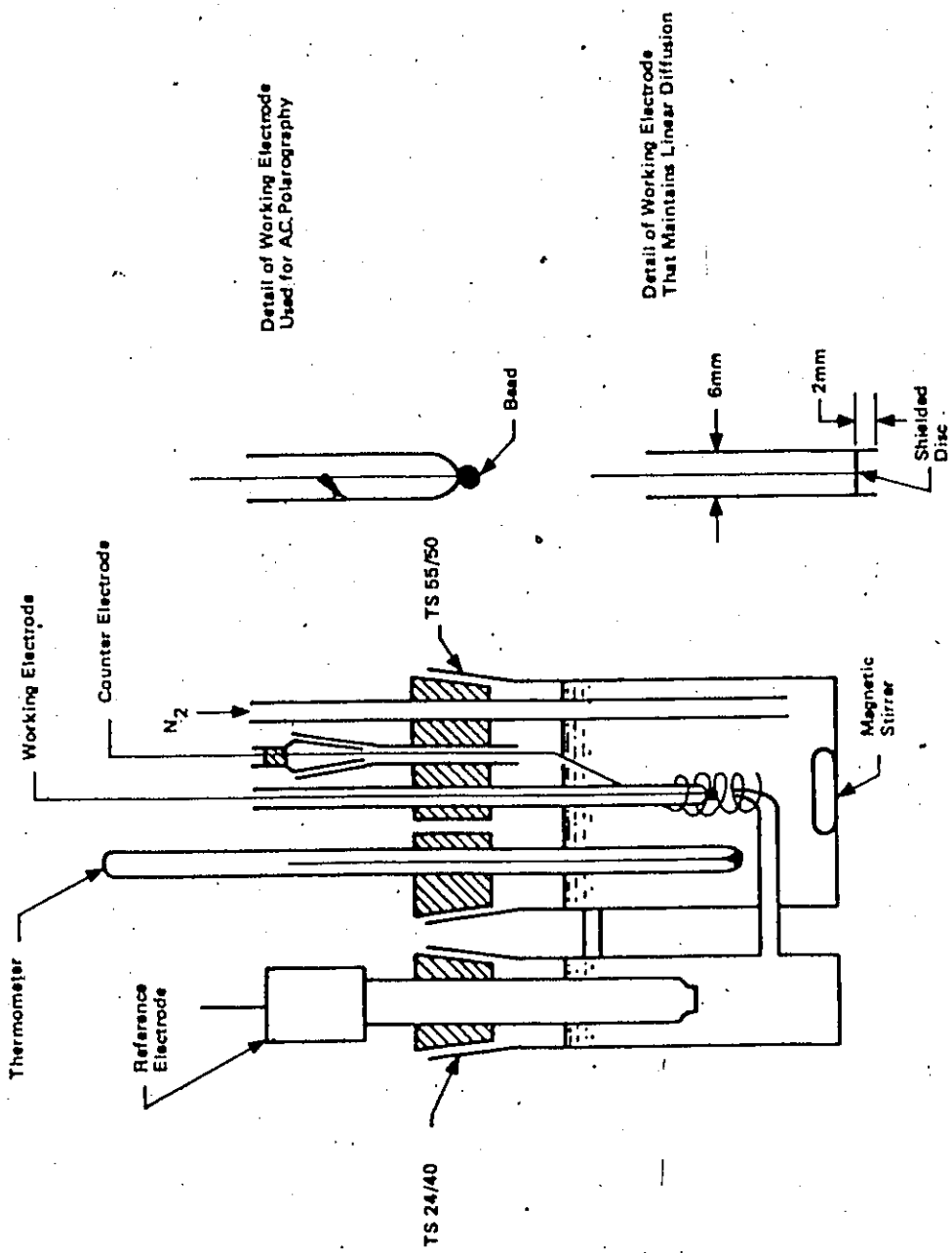

Fig. 6. Electrochemical cell for aqueous solutions.

level in the cell.

6.4.2 Non-aqueous Solutions

The cell for the non-aqueous electrochemical work had to be hermetic over its operating temperature range, 0 to 50 °C. This was accomplished with the design illustrated in Fig. 7. The lower section was built from a TS 55/50 Pyrex male joint. It was designed to contain 100 ml of solution below the side arm. The side arm was stoppered with a Rotaflo Pyrex-Teflon stopcock. It was used in outgassing the solution because oxygen diffused into the cell during prolonged experiments.

The cell top was built from a TS 55/50 Pyrex female joint and provided with receptacles for all three electrodes. The counter and reference electrodes were fitted into TS 10/30 Pyrex female joints. The male joints of these two electrodes served as their feedthroughs. The platinum-to-Pyrex seals were not initially hermetic but were made so by filling the glass cups above the seals with conductive silver epoxy (Epoxy Products Inc., E-solder 3021). The working electrode was positioned inside the larger diameter tubing on the cell top and a seal was made by means of a Teflon union. Details of the two types of working electrodes employed with this cell are shown in Fig. 6.

All ground-glass joints were lubricated with Corning high-vacuum grease to make these joints vacuum tight. Since benzene dissolves this grease, it was important to prevent the benzene from coming in contact with the grease.

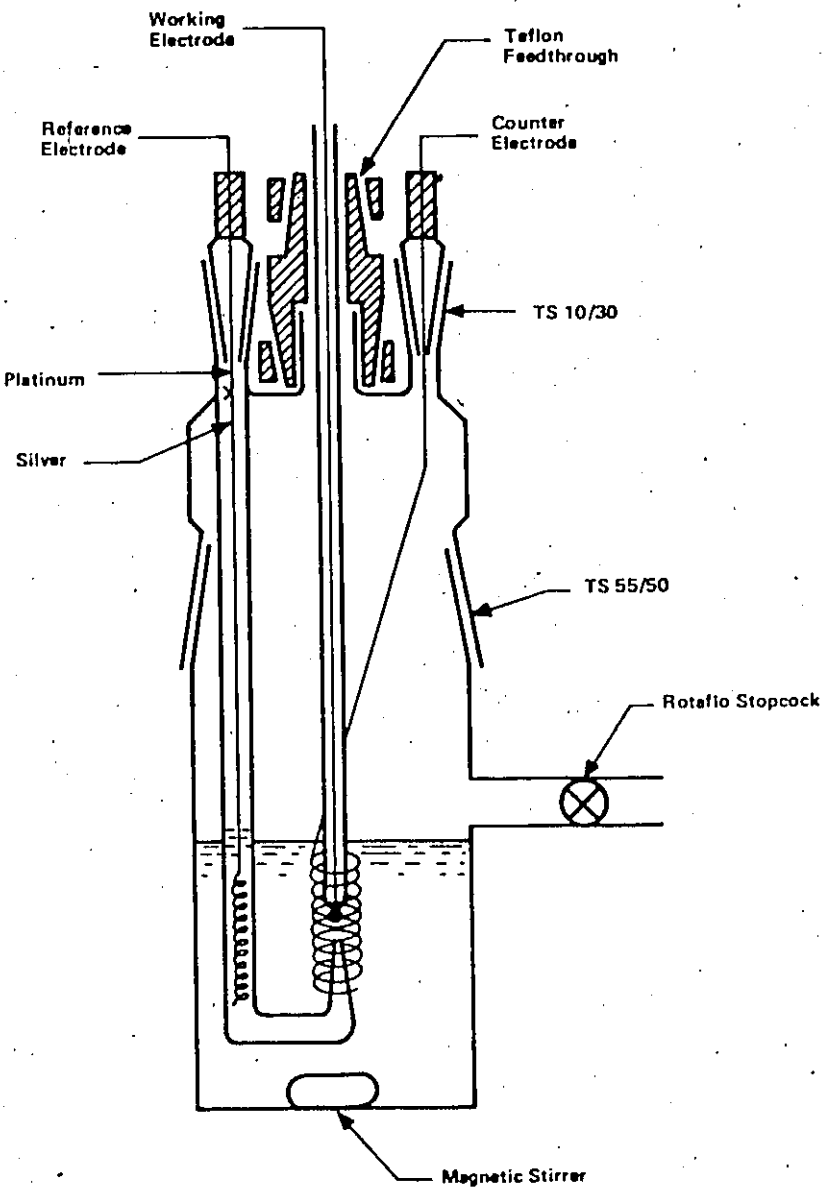

Fig. 7. Electrochemical cell for non-aqueous solutions.

The cell top had a Luggin tip attached to it to provide a compartment for the reference electrode which was fabricated from a silver wire connected to a platinum wire just below the feedthrough (Silver-to-Pyrex seals were found to be unreliable and so platinum was substituted at the feedthrough.) The use of a silver wire in a solution that nominally contains no silver ions has no apparent merit because the reference electrode cannot be associated with any definite thermodynamic equilibrium. Nevertheless, silver immersed in conducting aprotic solutions behaves well, giving a stable potential electrode[45]. It was necessary to employ the silver reference electrode; it is convenient to make and does not contaminate the test solution. If a conventional reference electrode had been employed, such as the SCE, it would have required addition of aqueous KCl to the solution, or an aqueous/non-aqueous junction.

6.4.3 Electron Spin Resonance (ESR)

The cell was made of non-magnetic materials and was shaped like a gun (Fig. 8). The "barrel" contained both electrodes and fitted inside the cavity of the ESR spectrometer. The tips of the electrodes were maintained *ca.* 4 cm apart. This permitted the independent observation of either the anode or the cathode.

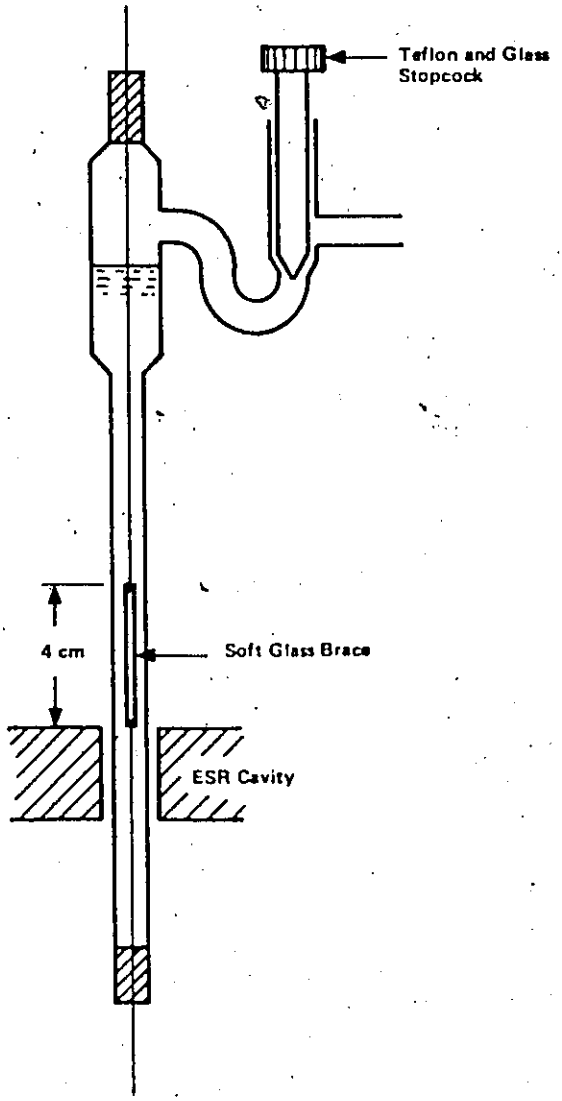

Fig. 8. Electrolysis cell for ESR spectroscopy.

6.4.4 Spectral Measurements of EGCL

A cell with which the EGCL spectra, with and without self-absorption, could be measured was constructed from a TS 24/40 Pyrex male and female joint (Fig. 9). When the a.c. potential was applied across the platinum wire and helix electrodes deep in the solution, the observed EGCL radiation had to travel through sufficient solution that it would be self-absorbed. The two electrodes were purposely made greatly different in area so that the EGCL would be produced at only one electrode, the smaller one. When the EGCL was produced at a strip of conductive transparent tin oxide on the window of the same cell, the observed emission was mostly unabsorbed. It is practically impossible to obtain completely unabsorbed EGCL spectra because the light produced radiates in all directions. The light which travels into the solution is absorbed and then re-emitted in all directions. Thus, some absorbed EGCL will always be detected.

6.4.5 Quantum Efficiency of EGCL

This cell (Fig. 10) was made from a TS 10/30 Pyrex joint. The cell was filled to the upper soft glass bracing. This bracing, together with the one at the end of the two electrodes, held the electrodes rigidly in place *ca.* 1 mm apart and fixed their area ratio near to unity. The working sections of the electrodes were located such that when the cell was placed in the solar cell box, the electrodes were automatically situated in the centre of the box. With the electrodes in this position, the solar cells collected *ca.* 5/6 of

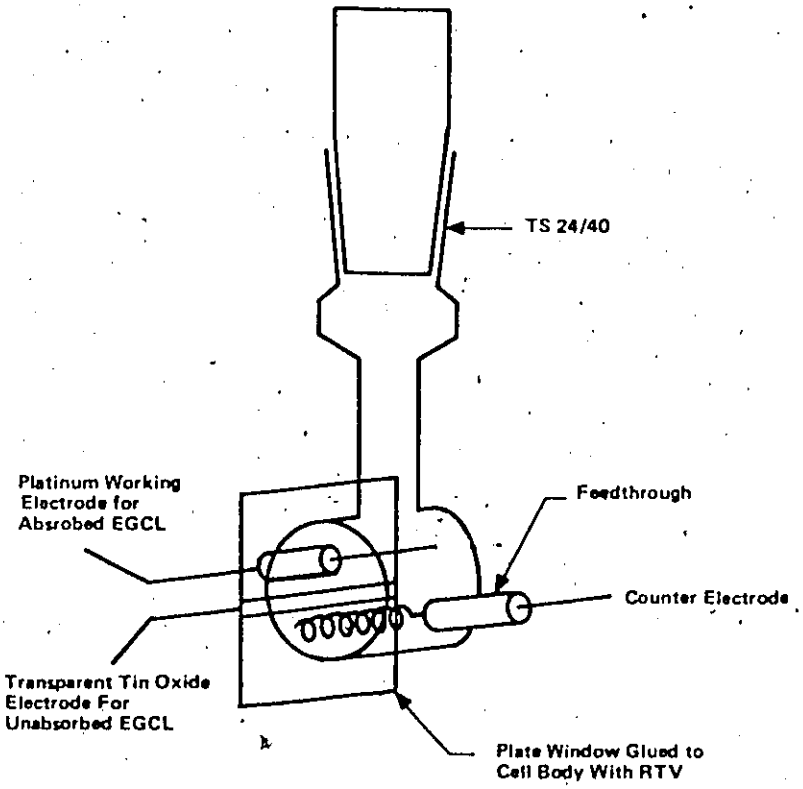

Fig. 9. Electrolysis cell for spectral measurements of EGCL.

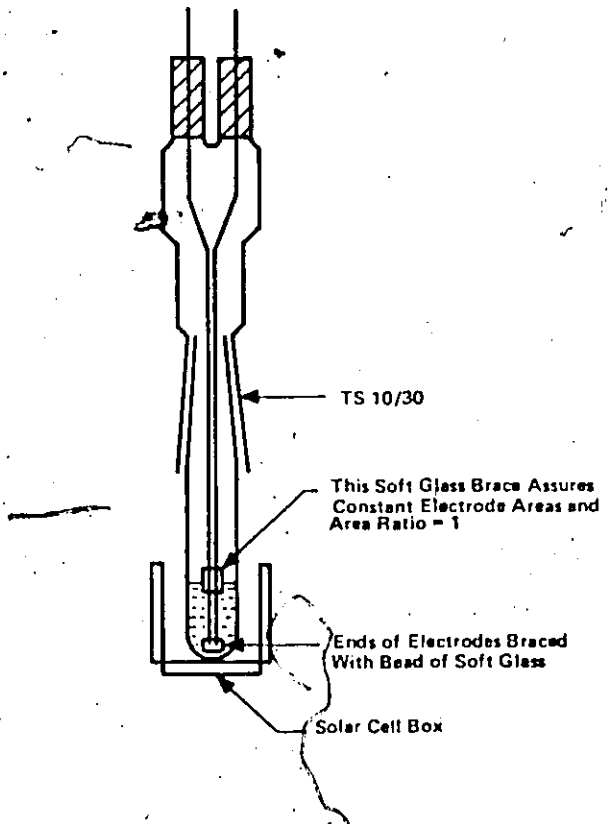

Fig. 10. Electrolysis cell for quantum efficiency measurements of EGCL.

of the total light emitted out of the electrolysis cell.

6.5 Instrumentation

All of the electrochemical measurements were made with a Princeton Applied Research PAR 170 Electrochemistry System. The X-Y recorder of the PAR 170 was used to record slow traces (below 500 mV sec^{-1}) while a Tektronix 564 Storage Oscilloscope was used for faster traces. The display on the oscilloscope was photographed with a Tektronix C-12 camera on Polaroid type 107 film.

The fluorescence spectra were recorded with a Farrand Mk 1 spectrofluorimeter provided with a 1P28 photomultiplier.

A Cary 14 spectrophotometer was used to record the absorption spectra.

The EGCL spectra were measured with a Spex 1702 monochrometer fitted with an RCA 7326 photomultiplier.

Vapour-phase chromatography was performed with a Hewlett-Packard HP 5754B Research Gas Chromatograph. A thermal conductivity detector was used to sense the non-combustible components and a flame-ionization detector was used to sense the combustible components.

The ESR spectra were taken with a Varian E-line instrument at the National Research Council of Canada.

Solutions were prepared in a Vacuum/Atmosphere Corp. Model HE-43-6 Dri-Lab or equivalent filled with nitrogen and fitted with a Panametrics Model 1000 hygrometer. Whenever the moisture in the dry box rose above 1 ppm, the dry box was flushed with fresh nitrogen.

7. RESULTS AND DISCUSSION

The main solvents employed in this investigation of rubrene EGCL were DMF and an equivolume benzene-DMF mixture. They were selected because they have nearly the same viscosities, their bulk dielectric constants are very different and because of the heteropolar nature of the mixed solvent.

7.1 Rubrene Ion-Radical Stability

7.1.1 Cyclic Voltammetry

Fig. 11 illustrates the reproducible form of a repetitive cyclic voltammogram of the oxidation and reduction of rubrene in 0.100 M TBAP in DMF established after a few cycles at 500 mV sec^{-1}. Inspection of this voltammogram indicates that both the cation- and anion-radicals of rubrene resulting from electrolysis are stable at 500 mV sec^{-1} since the conjugate pairs of anodic-cathodic current-voltage profiles are nearly identical.

A detailed study of the stability of the ion-radicals of rubrene in both solvents was made using cyclic voltammetry. It consisted of measuring the peak forward current, under linear diffusion control, of the first cycle of voltammograms for both the oxidation and reduction over a wide range of scan rates and at selected temperatures. A shielded platinum disc electrode was used to provide linear diffusion control. The results for DMF solutions are shown in Fig. 12 while those for benzene-DMF are shown in Fig. 13. The data are presented as plots of $i_{p,f}/S^{1/2}$ *vs* log S. Theory predicts that $i_{p,f}/S^{1/2}$

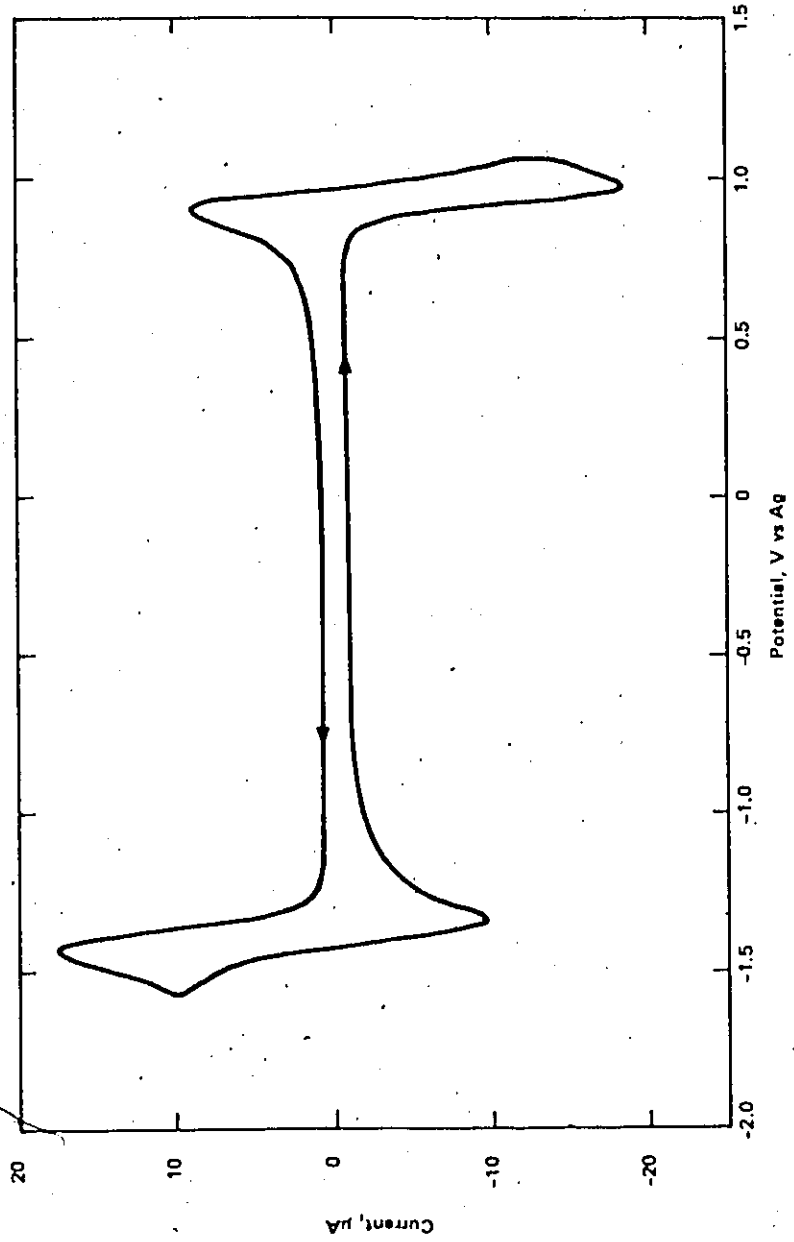

Fig. 11. Cyclic voltammogram of rubrene in a DMF solution.

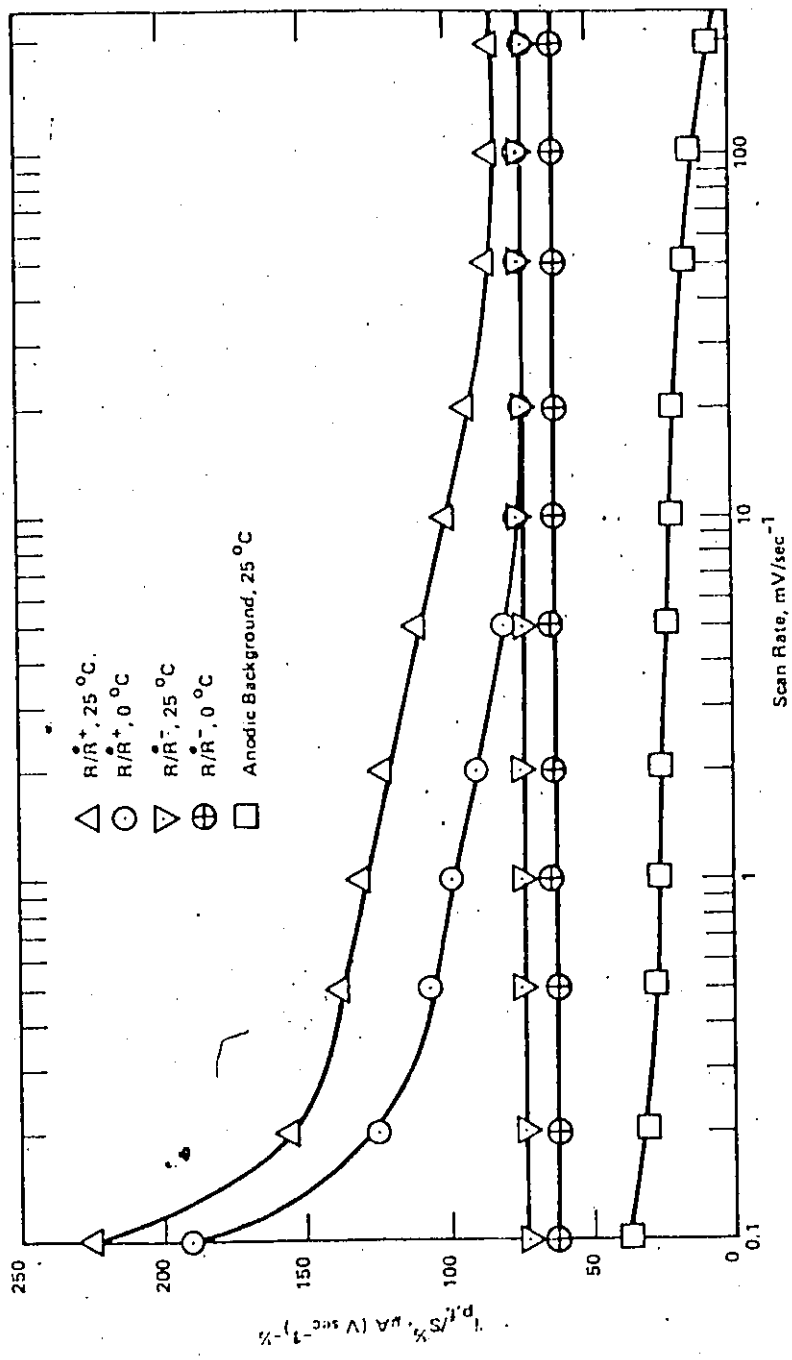

Fig. 12. Variation in the peak current with scan rate of cyclic voltammograms of rubrene in a DMF solution.

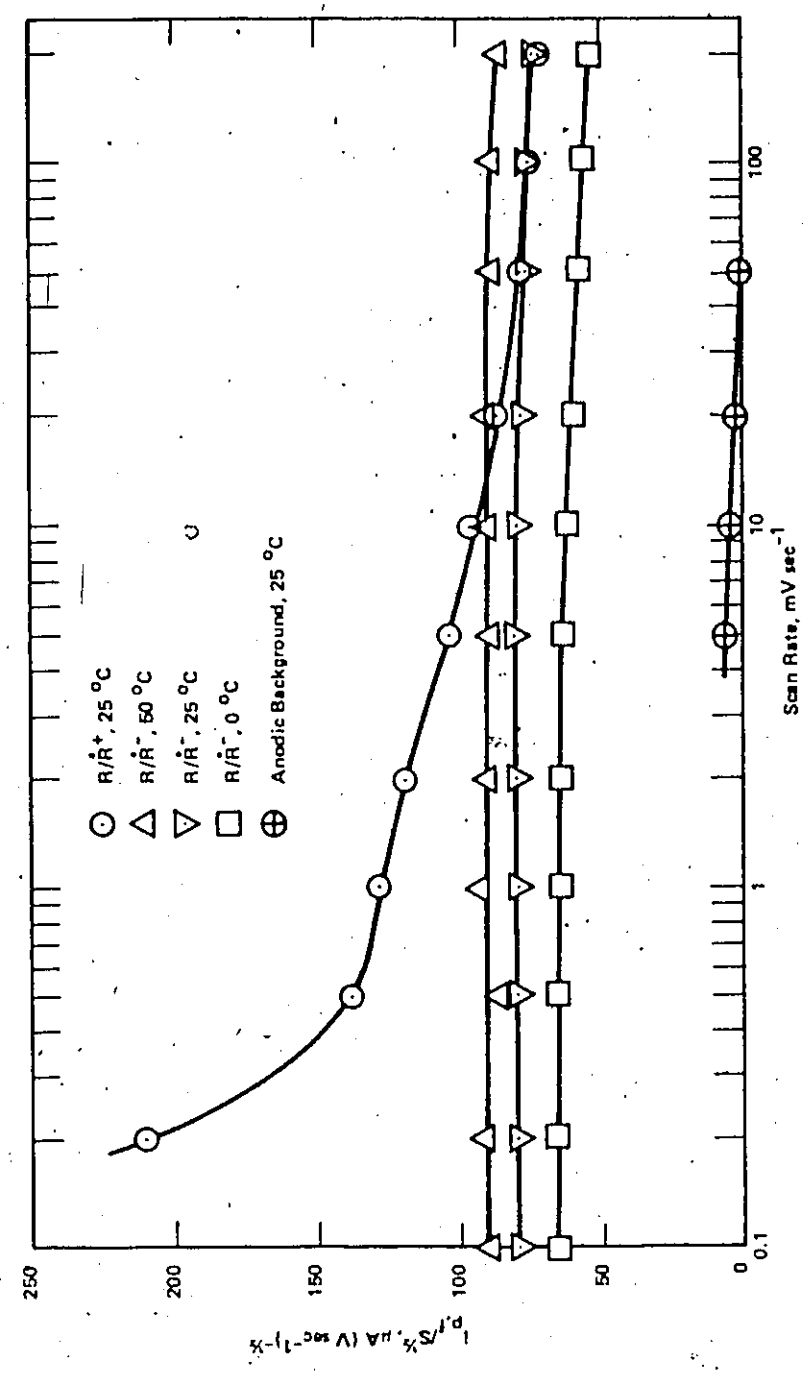

Fig. 13. Variation in the peak current with scan rate of cyclic voltammograms of rubrene in an equivolume benzene-DMF solution.

is constant for a stable system but increases in magnitude with increasing ion-radical instability as the scan rate decreases. The reduction of rubrene in both solutions exhibits constant $i_{p,f}/S^{1/2}$ down to S = 0.1 mV sec^{-1}. At this low scan rate, the ion-radicals were generated for an average of *ca.* half an hour. (The scan of potential was made to go *ca.* 100 mV past the peak potential and was then reversed.) In these plots, $i_{p,f}/S^{1/2}$ increases with increasing temperature because i_p is directly proportional to the square root of the diffusion coefficient of the electro-active species. The diffusion coefficient is inversely proportional to the solution viscosity which, of course, decreases with increasing temperature.

Figs. 12 and 13 indicate that the oxidized form of rubrene is unstable relative to a time scale of 10 sec V^{-1} in the potential scan, *viz.* for S less than 100 mV sec^{-1}, at 25 °C. By reducing the temperature to 0 °C, the rubrene cation-radical is stable down to a time scale of 100 sec V^{-1}. The temperature coefficient of the cation-radical instability is too great to correspond to a diffusion-controlled reaction process. A chemical side reaction with the solvent was therefore suspected. A conducting DMF solution without fluorescor was prepared, and its anodic background current profile examined. The solution exhibited a Faradaic current component corresponding to an oxidation at a potential almost overlapping that for rubrene itself. The variation of the current of this background Faradaic process with scan rate is also shown in Fig. 12. The background process was less pronounced in conducting benzene-DMF solution.

Therefore, the electroactive impurity was presumed to have originated from the DMF despite the fact that it had been purified. The presence of this impurity does not affect the cyclic voltammetric results at moderate or higher scan rates since its diffusion effects are then rendered relatively negligible.

The values of $i_{p,f}/i_{p,r}$ at various scan rates for the reduction of rubrene in the two main solvents are given in Table 2. These data imply that the rubrene anion-radical is completely stable in these solutions. The equivalent data for the oxidation of rubrene is not given because the irreversible background process discussed above would give misleading results.

TABLE 2

Constancy of $i_{p,f}/i_{p,r}$ with S for the Reduction of 1 mM Rubrene in 0.100 M TBAP Solutions at 25 °C

S	$i_{p,f}/i_{p,r}$	
mV sec^{-1}	DMF	equivolume benzene-DMF
1	0.98	1.00
2	0.97	1.00
5	0.96	1.02
10	1.00	1.00
20	0.97	1.02
50	0.99	1.00
100	1.00	1.00
200	0.99	1.00

Table 3 shows data of the difference between the forward and reverse peak potentials for the reduction of rubrene and re-oxidation of its anion-radical in 0.100 M TBAP solutions. The separations approach the expected theoretical value at 25 °C (58 mV) with

decreasing scan rate. These data were taken from cyclic voltammograms that were recorded without iR compensation. Therefore, it should be expected that the separation would increase with increasing scan rate because the current increases proportionally to $S^{1/2}$ for the linear diffusion controlled process, so that iR effects will tend to increase the separation with increasing scan rate.

TABLE 3

Variation in $(E_{p,f}-E_{p,r})$ with S for the Reduction of 1 mM Rubrene in 0.100 M TBAP Solutions at 25 °C

S	$(E_{p,f}-E_{p,r})$ mV	
mV sec^{-1}	DMF	equivolume benzene-DMF
1	62	60
2	65	70
5	75	70
10	72	80
20	80	90
50	90	100
100	100	120
200	115	150

All of the results from the preceding cyclic voltammetric data indicate clearly that both the reduction and oxidation of rubrene in 0.100 M TBAP solutions in either DMF or equivolume benzene-DMF yield ion-radicals which are practically stable within time scales corresponding to scan rates greater than 100 mV sec^{-1} at room temperature.

7.1.2 Chronoamperometry

The potential on a shielded platinum disc electrode immersed in a solution of rubrene in TBAP-DMF was taken in a step to, and maintained constant at, *ca.* 200 mV beyond the reduction potential of rubrene and the current was recorded *vs* time for 750 sec. A plot of $it^{1/2}$ *vs* t was then made (Fig. 14) and the product $it^{1/2}$ was found to be constant with time. This indicates that the anion-radicals did not engage in follow-up reactions as this would have produced a positive deviation (i.e. a current larger than expected) in the plot. It is assumed that linear diffusion was maintained at the electrode. Unless it were argued that the type of diffusion which prevailed at the electrode, by chance, completely compensated the effect of secondary reactions, then the electrode must, in fact, have maintained linear diffusion during this relatively long period of time.

Recording of a chronoamperogram of the oxidation of rubrene was not attempted because the oxidizable impurity in the DMF, referred to previously, would have contributed a current corresponding to an unstable species.

7.1.3 Electrogenerated Chemiluminescence

A solution composed of 1 mM rubrene in 0.100 M TBAP in DMF was continuously electrolyzed at room temperature at a platinum electrode with a ramp potential which scanned to 100 mV beyond the oxidation and reduction potentials at 500 mV sec^{-1}. The electrolysis was continued for 210 hours. A pulse of dim orange light was obtained at

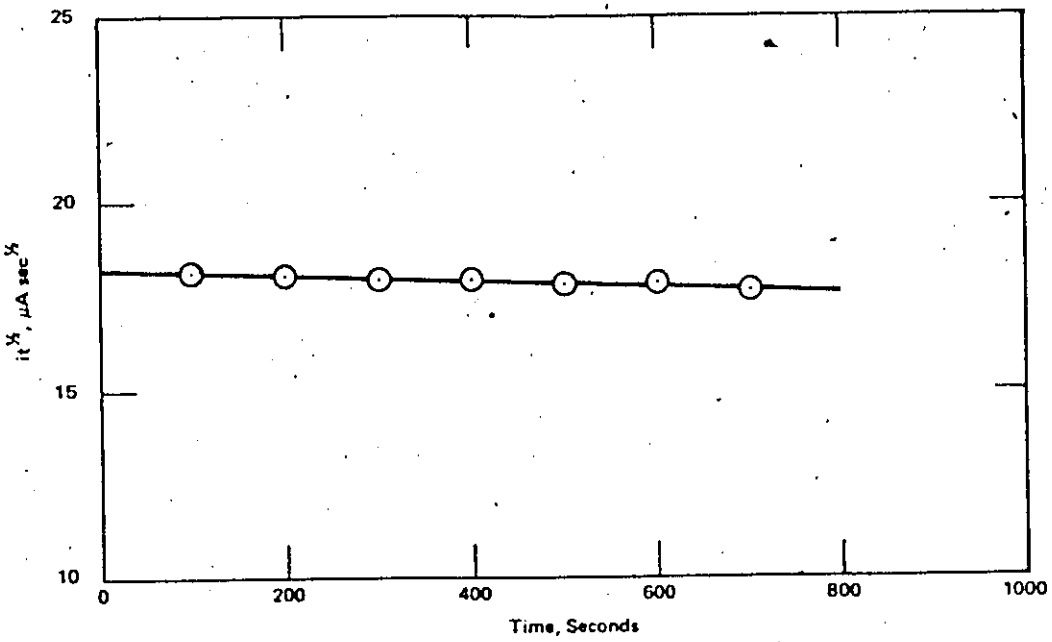

Fig. 14. Constancy in $it^{1/2}$ with t for the reduction of rubrene at a shielded platinum disc electrode in a DMF solution.

each potential limit for oxidation and reduction during the whole experiment. The peak current remained virtually unchanged throughout the experiment (Fig. 15). This experiment therefore clearly demonstrated the complete stability of rubrene EGCL, even when generated with a ramp potential corresponding to a time scale as long as 2 sec V^{-1} ($\equiv$ 500 mV sec^{-1}) in the periodic oxidation and reduction of rubrene. No significant consumption of rubrene occurred (as shown by the results in Fig. 15), nor were side reactions significant.

7.1.4 Electron Spin Resonance (ESR)

This aspect of the work consisted of producing rubrene ion-radicals in an ESR cavity and monitoring the strength of the observed signal. The ion-radicals were generated with a constant d.c. voltage. The solution surrounding the cathode turned deep green while that around the anode turned colourless. A good ESR spectrum could be generated from the anion-radicals in both DMF and equivolume benzene-DMF solutions but the cation-radicals did not generate an ESR signal in either solution. This is presumably due to the well-known greater stability of the anion- than the cation-radicals. The ESR spectrum of the rubrene anion-radical in DMF solution was qualitatively identical to the corresponding spectrum in equivolume benzene-DMF solution (Fig. 16).

With the anode region in the ESR cavity, the voltage was disconnected from the cell after a strong ESR signal had been developed and the spectrum was repeatedly scanned. The ESR signal from the

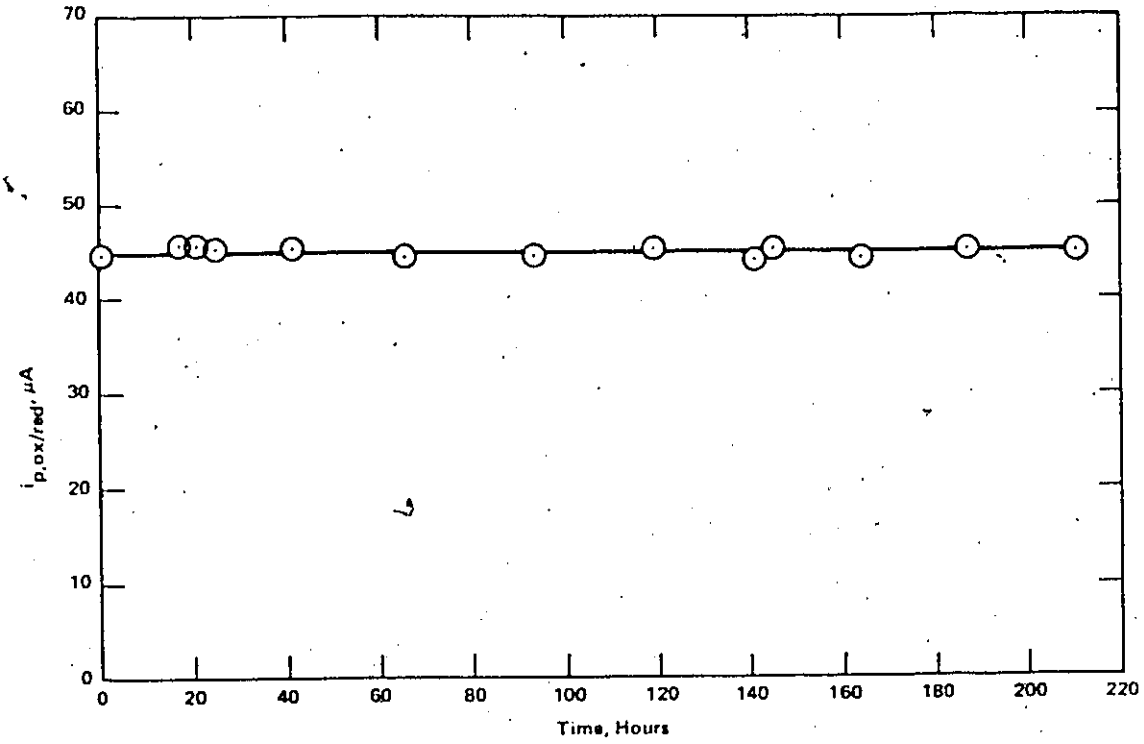

Fig. 15. Constancy in the electrolysis current with time on repeated electrolysis of rubrene in a DMF solution.

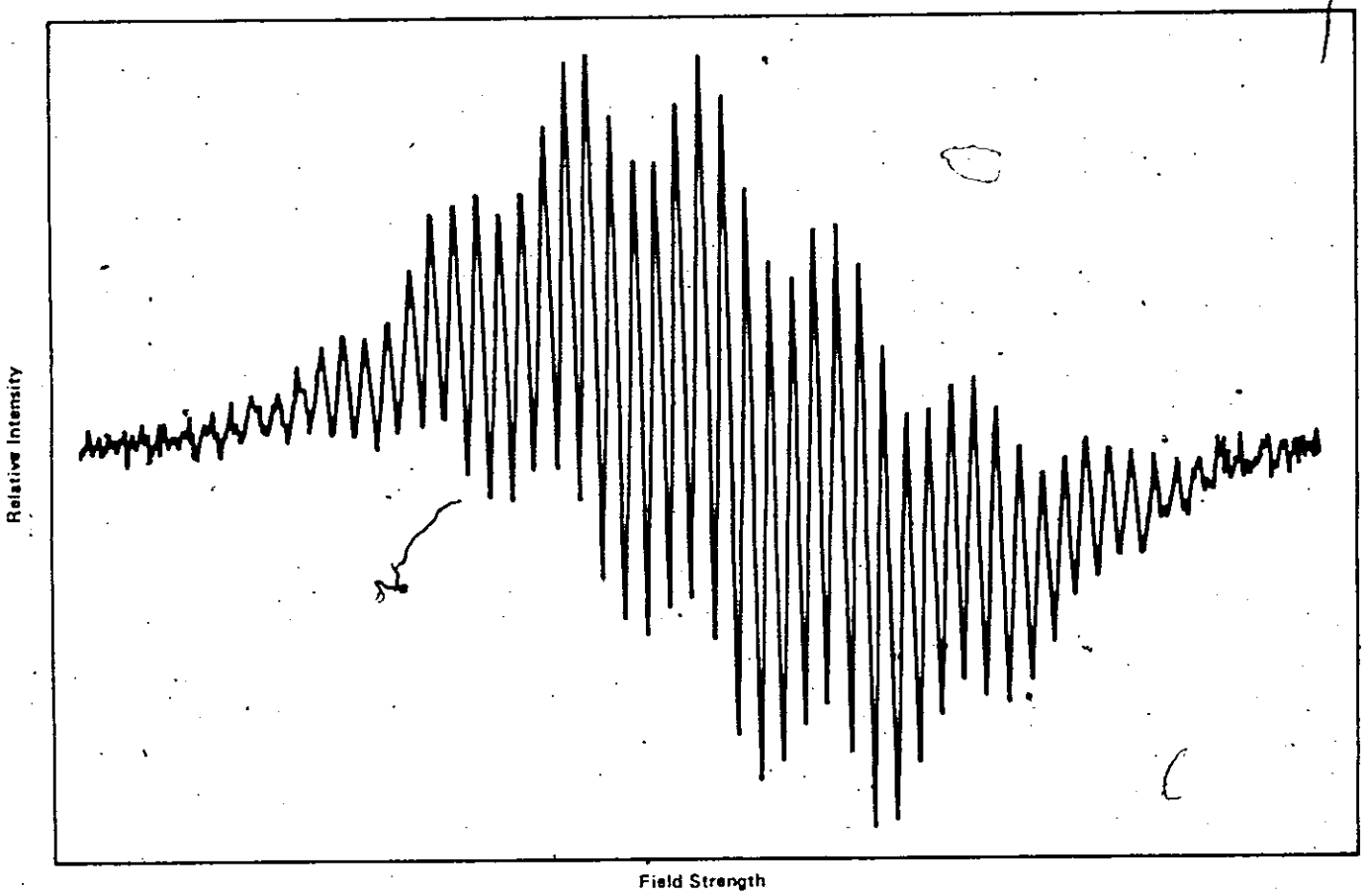

Fig. 16. ESR spectrum of the rubrene anion-radical in an equivolume benzene-DMF solution.

anion-radicals in both DMF and benzene-DMF decreased slightly during the first hour. The cells were removed from the cavity and allowed to stand disconnected from the voltage. It took six hours for the green colour around the anode of a rubrene-TBAP-benzene-DMF solution to fade away completely. Assuming that the green colour was from the anion-radicals of the rubrene, then from these results, it may be estimated that the half-life of the rubrene anion-radical in TBAP-benzene-DMF at room temperature, *ca.* 25 °C, is a few hours. The anion-radicals were slightly less stable in TBAP-DMF solution.

The ESR spectrum of the rubrene anion-radical has been reported and discussed qualitatively elsewhere[46] by Wheeler and Bard.

7.2 Reaction Kinetics

7.2.1 Diffusion Coefficients

The oxidation and reduction of rubrene is a diffusion-controlled process under the conditions employed in the present work on EGCL. Hence, first, the diffusion coefficients were determined from chronoamperograms of the electro-active species at an electrode of known area. The electrode area was determined from the chronoamperogram of a system of known diffusion coefficient. The oxidation of 4 mM potassium ferrocyanide in 1.00 M aqueous KCl at 25 °C with +0.400 V *vs.* SCE was used as the reference system. Its diffusion coefficient is 6.32×10^{-6} cm^2 sec^{-1} at 25 °C. The electrode potential was rested *ca.* 200 mV past the peak potential of the test system and the current recorded for the first 30 or more seconds. A plot of $it^{1/2}$

vs t was made and the diffusion coefficient calculated from the extrapolated value of $(it^{1/2})_{t=0}$ using Equation 14.

Fig. 17 illustrates a family of $it^{1/2}$ *vs* t curves for the oxidation of 4.00 mM potassium ferrocyanide in 1.00 M aqueous $NaClO_4$ at selected temperatures. The $it^{1/2}$ *vs* t plot for the reference system at the same electrode is also included in this Figure. All of the diffusion data are summarized in Table 4.

TABLE 4
Diffusion Coefficients at Selected Temperatures

		$D_T^{1/2}$ $(cm^2\ sec^{-1})^{1/2} \times 10^3$				
Compound	Solvent	0 °C	10 °C	25 °C	35 °C	50 °C
Rubrene	0.100 M TBAP in DMF	1.72	1.92	2.19	2.40	2.79
Rubrene	0.100 M TBAP in equivolume benzene-DMF	1.88	2.05	2.28	2.47	2.73
Potassum ferrocyanide	1.00 M aqueous KCl	1.76	2.06	2.51	2.79	3.22
Potassium ferrocyanide	1.00 M aqueous NaCl	1.55	1.84	2.25	2.57	3.09
Potassium ferrocyanide	1.00 M aqueous $NaClO_4$	1.67	1.93	2.32	2.73	3.09

The above data are the average of several determinations made with different solutions and electrodes. The reproducibility of $D^{1/2}$ was better than ±3 %. The entries in Table 4 have not been corrected for the temperature dependence of the concentration. (The volume of the solution varies with temperature by a relatively negligible amount.)

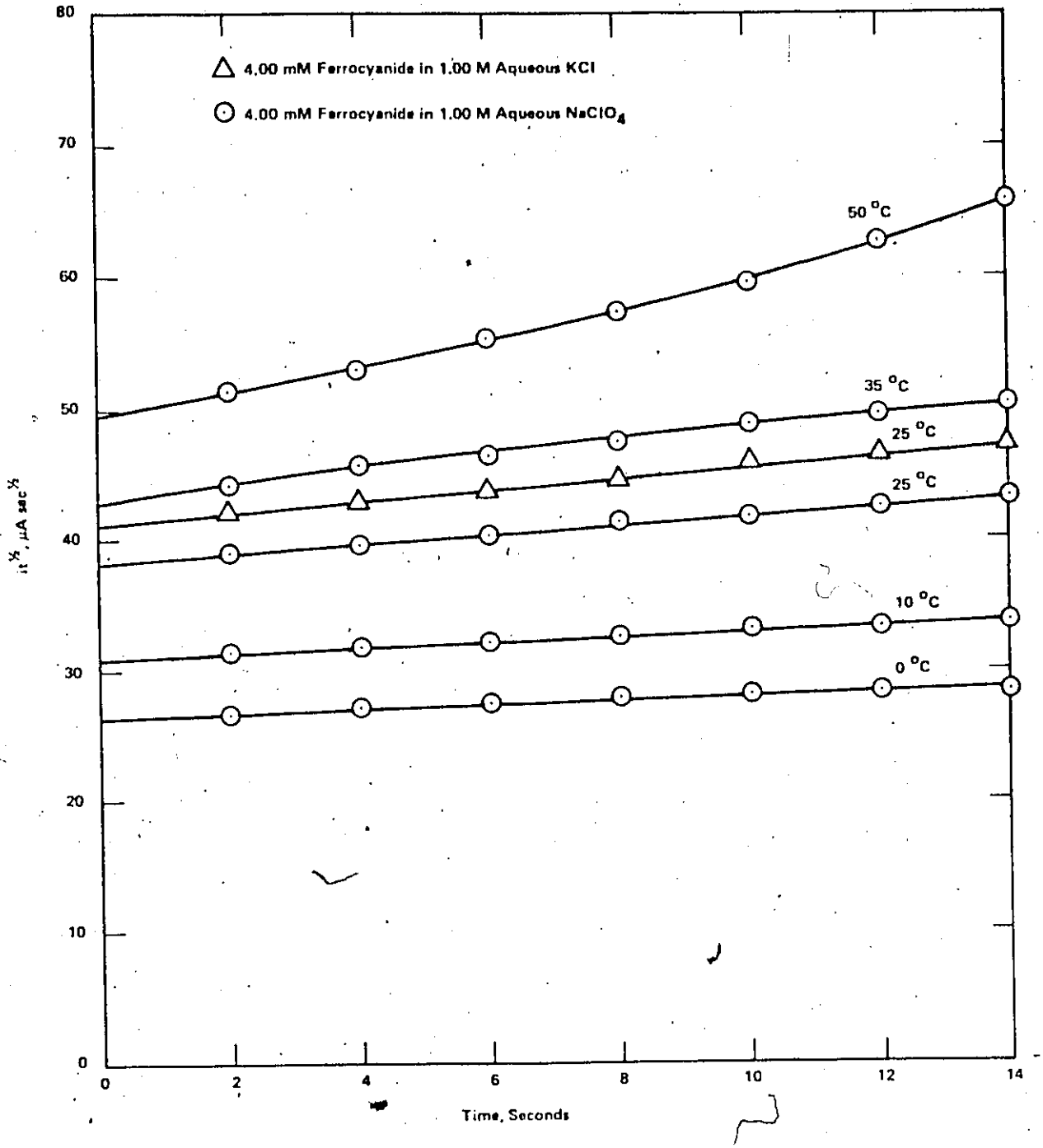

Fig. 17. A family of $it^{1/2}$ *vs* t plots used to determine the diffusion coefficients of potassium ferrocyanide in aqueous $NaClO_4$ solutions.

The viscosity of each solution at 25 °C was measured using an Ostwald viscometer previously calibrated with water. The results are entered in Table 5 together with the corresponding diffusion coefficients.

TABLE 5
Viscosity and Diffusion Data at 25 °C

Compound	Solvent	η cp	$D \times 10^6$ $cm^2\ sec^{-1}$	$D\eta$ $cm^2\ sec^{-1}\ cp$
Rubrene	0.100 M TBAP in DMF	0.89	4.8	4.27
Rubrene	0.100 M TBAP in equivolume benzene-DMF	0.81	5.2	4.21
Potassium ferrocyanide	1.00 M aqueous KCl	0.904	6.32	5.71
Potassium ferrocyanide	1.00 M aqueous NaCl	0.964	5.1	4.92
Potassium ferrocyanide	1.00 M aqueous $NaClO_4$	0.944	5.9	5.57

It is to be noted that the values of the product $D\eta$ are essentially constant for rubrene in the two solutions, a result consistent with the Stokes-Einstein equation[20]. The $D\eta$ values for the potassium ferrocyanide are, however, different because of differences in solvation. For example, the ferrocyanide arises from dissolved potassium ferrocyanide. In KCl solution, the ferrocyanide will be associated with potassium ions. However, in NaCl solution, there is such a large amount of Na^+ ions present compared with K^+ ions (1000:4), that

the ferrocyanide will tend to be associated most likely with Na^+ ions. The Na^+ ion has a radius smaller than that of K^+. Consequently, not only will Na^+ be bound more strongly with the $Fe(CN)_6^{-4}$ than K^+, but Na^+ is also more strongly solvated by water. Thus, it can be the greater solvation by water of the Na^+ ions associated with the ferrocyanide that may account for the reduction of the rate of diffusion of the ferrocyanide.

7.2.2 The Ferro-Ferricyanide Model System

The ferro-ferricyanide redox reaction in aqueous KCl was used as the model process for testing the validity of the small-amplitude a.c. polarographic method for determining heterogeneous electron transfer rate constants. Tanaka and Tamamushi[47] have made a tabulation of reported heterogeneous rate constants. Studies of the ferro-ferricyanide system at platinum in 1 M aqueous KCl at 20-25 °C have been frequently made in previous work. The reported apparent rate constants for this redox couple have ranged from 0.052 to 0.090 cm sec^{-1} with an energy of activation of *ca.* 4 Kcal $mole^{-1}$.

After having established (see below) the applicability of the small-amplitude a.c. method, the investigation of the model process was extended to evaluating the kinetics of this couple at gold electrodes in the same KCl solution and then in aqueous NaCl and $NaClO_4$ at both platinum and gold electrodes. A study of the kinetics at two electrode materials was made in order to examine the effect of work function on the energy of activation and to evaluate double-

layer effects on the magnitude of the rate constants. The electrolyte was changed from KCl to NaCl in order to indicate if there was any effect of ion-pairing on the rates and activation energy of the reaction. Finally, since the chloride ion is more strongly adsorbed on platinum than on gold, while the perchlorate is not strongly adsorbed on either, the change in electrolyte from NaCl to $NaClO_4$ enabled the effect of adsorbed anions on the rate and energy of activation of the reaction to be evaluated.

Using Equations 15 and 16, and the reported values of the rate constant for the ferro-ferricyanide redox couple, the phase angle at which the Faradaic current would be maximum was calculated. The maxima varied around 35° in the frequency range 20 to 100 Hz. Using a phase angle of 35° and a scan rate of 20 mV sec^{-1} for the oxidation of ferrocyanide in 1 M aqueous KCl at 25 °C, preliminary results at platinum were obtained. The amplitude of the a.c. voltage superimposed upon the ramp potential was 10 mV peak-to-peak. The working electrode was spherical in shape and a three-electrode electrochemical cell for aqueous solutions was employed.

The preliminary experiments with the model system gave linear plots of $i_{p,ac}/\omega^{1/2}$ vs $\omega^{1/2}$. However, the points were scattered and the reproducibility was poor. Therefore, the effect of electrode preconditioning on the measured rate constant was examined. For this purpose, the following procedures were tried:

a) using the electrode to evolve chlorine from aqueous KCl

b) using the electrode to evolve hydrogen from aqueous KCl

c) immersing the electrode in hot sulphuric acid; and

d) heating the electrode white hot in the outer part of a propane-oxygen flame.

The results obtained, some of which are illustrated in Fig. 18, clearly demonstrate the importance of electrode pre-conditioning. The Pt pre-conditioned by chlorine evolution yielded reproducible results which were in the range of the literature values, provided the electrode potential was kept above +0.05 V *vs* SCE. If the electrode was rested at a potential lower than +0.05 V *vs* SCE, its behaviour became increasingly irreproducible.

The results given in Fig. 18 for hydrogen pre-treatment were obtained soon after the conditioning. On standing, such electrodes gave continuously decreasing rate constants. The initial value of the rate constant was *ca.* 0.2 cm sec^{-1} but this decreased with time to as low as 0.04 cm sec^{-1}. The acid pre-treatment, method (c) above, did not stabilize the behaviour of the electrode during a.c. experiments. Heated electrodes gave results similar to those obtained with the chlorine-treated electrodes.

It was reported earlier that the rate constant of the model system, when studied at Pt pre-conditioned by chlorine evolution, was dependent on the rest potential of the potential scan for ferrocyanide oxidation. The rest potential had to be +0.05 V *vs* SCE or less ; otherwise, it would be great enough to cause oxidation of the ferrocyanide. With a rest potential of +0.05V *vs* SCE prior to

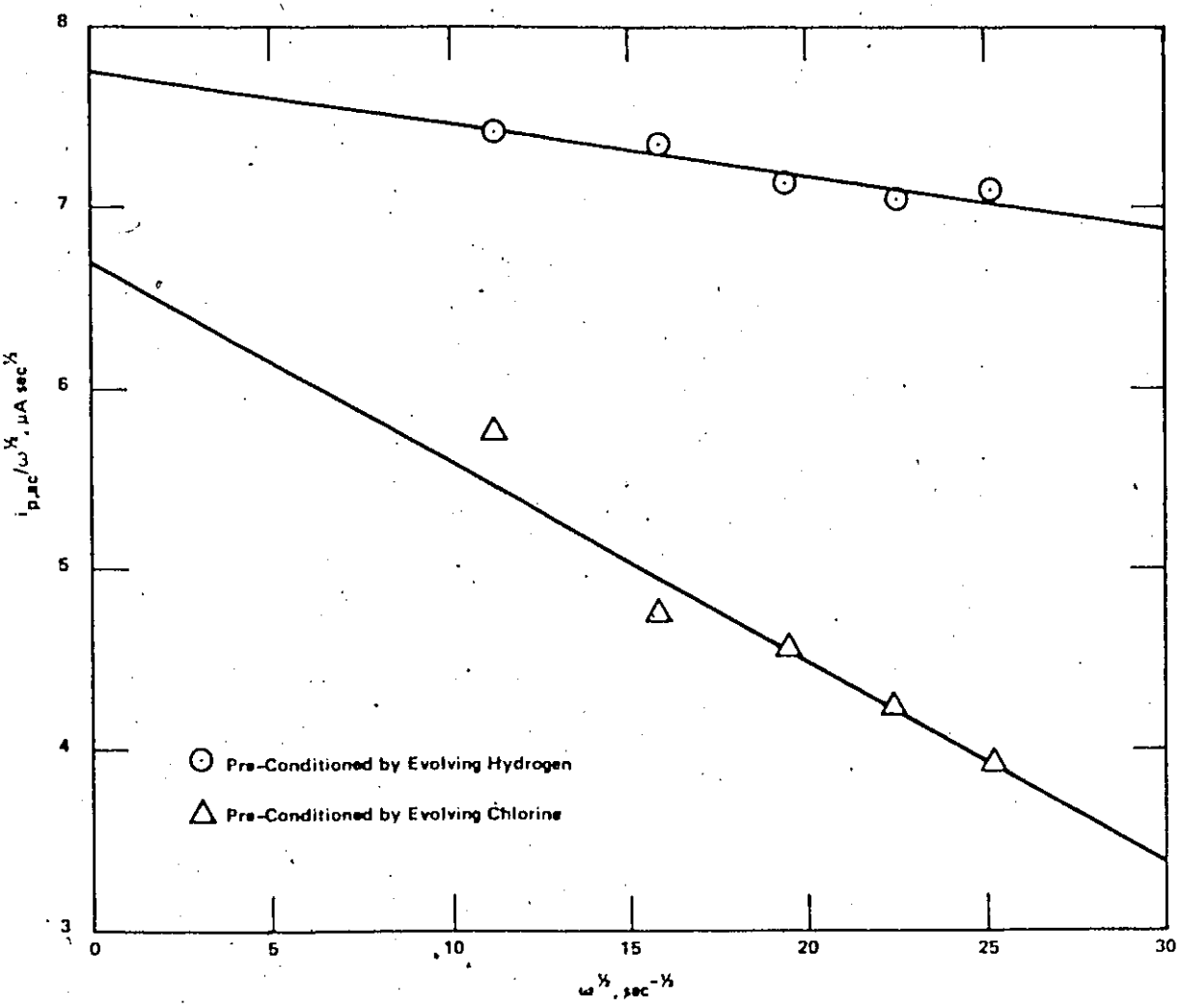

Fig. 18. Effect of platinum electrode pre-conditioning on the small-amplitude a.c. current of the ferro-ferricyanide redox couple in an aqueous KCl solution.

the commencement of the potential scan, the rate constants agreed with published values but at smaller (less positive) rest potentials, the rate constants were relatively smaller and more irreproducible. The behaviour could be explained by the ionization of hydrogen at the lower rest potentials[48]. If this were indeed the case, then the association of the proton(s) with the ferrocyanide ion near the electrode surface resulted in a decrease in the rate constant of the electrolysis of the ferrocyanide ion.

Platinum pre-conditioned by hydrogen evolution exhibited a larger extrapolated value of $(i_{p,ac}/\omega^{1/2})_{\omega=0}$ than Pt pre-conditioned by chlorine evolution (Fig. 18). It is likely that the latter method for pre-conditioning the electrode caused chloride to be adsorbed by the platinum. The adsorbed chloride can not only block the oxidation of the ferrocyanide but may also decrease the electron density on the metal surface[49]. Each of these adsorption effects tends to reduce the current for the oxidation of the ferrocyanide. Thus, this provides some account of the smaller $(i_{p,ac}/\omega^{1/2})_{\omega=0}$ exhibited by Pt electrodes pre-conditioned by chlorine evolution.

It should be noted in Fig. 18 that the frequency of the a.c. voltage was limited to 20-100 Hz. At lower frequencies, the diffusion-layer thickness could have become significant relative to the curvature of the electrode surface. If this occurred, non-linear diffusion would prevail and Equation 18, which is based on a process controlled by linear diffusion, could no longer be used to calculate the rate

constant. The frequency was kept below 100 Hz to maintain the capacitive current relatively small (the capacitive current is directly proportional to the frequency while the Faradaic current is directly proportional to $\omega^{1/2}$) and to avoid exceeding the RC constant of the cell.

The PAR 170 has both a.c. and d.c. iR compensation capability. However, it can only perform one or the other function at a given time. Consequently, since a.c. compensation was more important, the uncompensated d.c. resistance accounted for the decrease of the measured a.c. current with increasing scan rate (Fig. 19). Fortunately, this problem was not important if the scan rate was kept below 50 mV sec^{-1}. Below 50 mV sec^{-1}, the a.c. current was independent of scan rate in accordance with theory.

Although iR compensation of the a.c. signal was employed, the iR compensation in the concentrated solutions of strong electrolytes used here resulted in only a small increase in the measured current. This suggested that in the aqueous solutions employed, the electrolytic resistance between the reference and working electrodes was quite small.

By this time, sufficient experience had been acquired with the a.c. technique for reliable experiments to be performed. The electrodes (both platinum and gold) were conditioned prior to each experiment by heating them white hot in a propane-oxygen flame. In order to avoid the possible problems discussed earlier when ferrocyanide solutions were employed (the initial ramp potential could

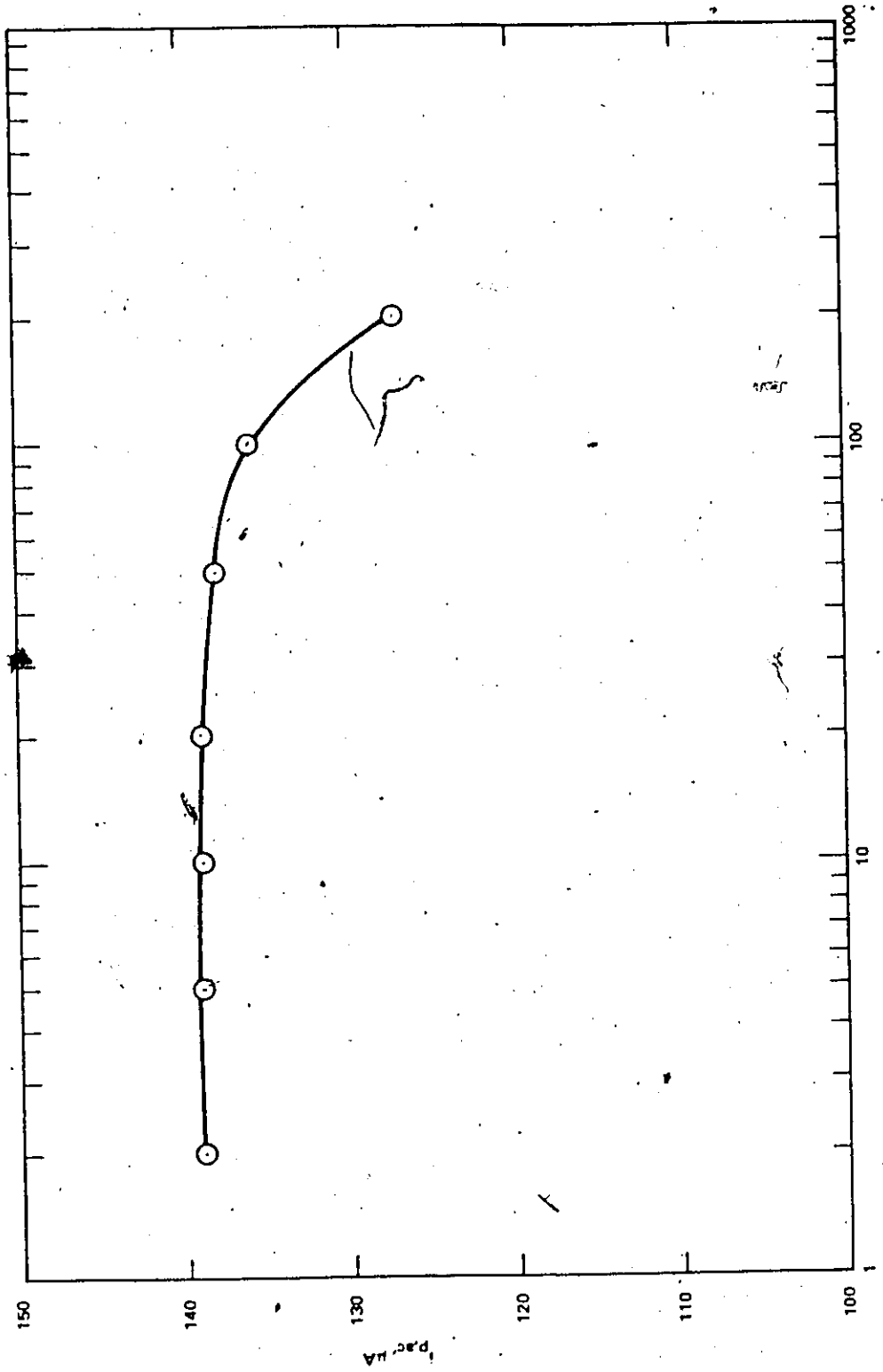

Fig. 19. Variation in $i_{p,ac}$ with scan rate for the redox of ferro-ferricyanide in an aqueous KCl solution.

cause ionization of hydrogen), ferricyanide solutions were employed. The ramp potential was varied from +0.600 to +0.050 V *vs* SCE at a rate of 20 mV sec^{-1}. The a.c. voltage superimposed on the ramp potential was 10 mV peak-to-peak. IR compensation was employed and the current was recorded at 35° out of phase with the a.c. voltage. The electrode was rested at the initial potential for a few minutes prior to each ferricyanide reduction run. The cell was immersed in a thermostated water bath which was regulated to ±0.2 C° and the solution in the cell stirred for *ca.* half an hour to ensure that it was at the same temperature as the water bath. The order of frequencies studied in each experiment was 100, 20, 80, 40 and 60 Hz while the temperature order was 25, 0, 10, 35, and 50 °C. These orders ensured randomization of any systematic effects.

A family of $i_{p,ac}/\omega^{1/2}$ *vs* $\omega^{1/2}$ plots at the selected temperatures is shown in Fig. 20. It is to be noted how well the points fall in line and how properly spaced the lines are (the extrapolated values of $(i_{p,ac}/\omega^{1/2})_{\omega=0}$ are directly proportional to $D^{1/2}$). The slope of each line was calculated using linear regression analysis and was equal to $K(D/2)^{1/2}/2$. The diffusion coefficients are known. Thus, once the slopes were evaluated, calculation of the rate constants was rudimentary. With this a.c. method for measuring the rate constants, the measured rate is the apparent rate constant at the half-wave potentials. The results were not corrected for double-layer effects[15], which are only important in dilute electrolyte solutions.

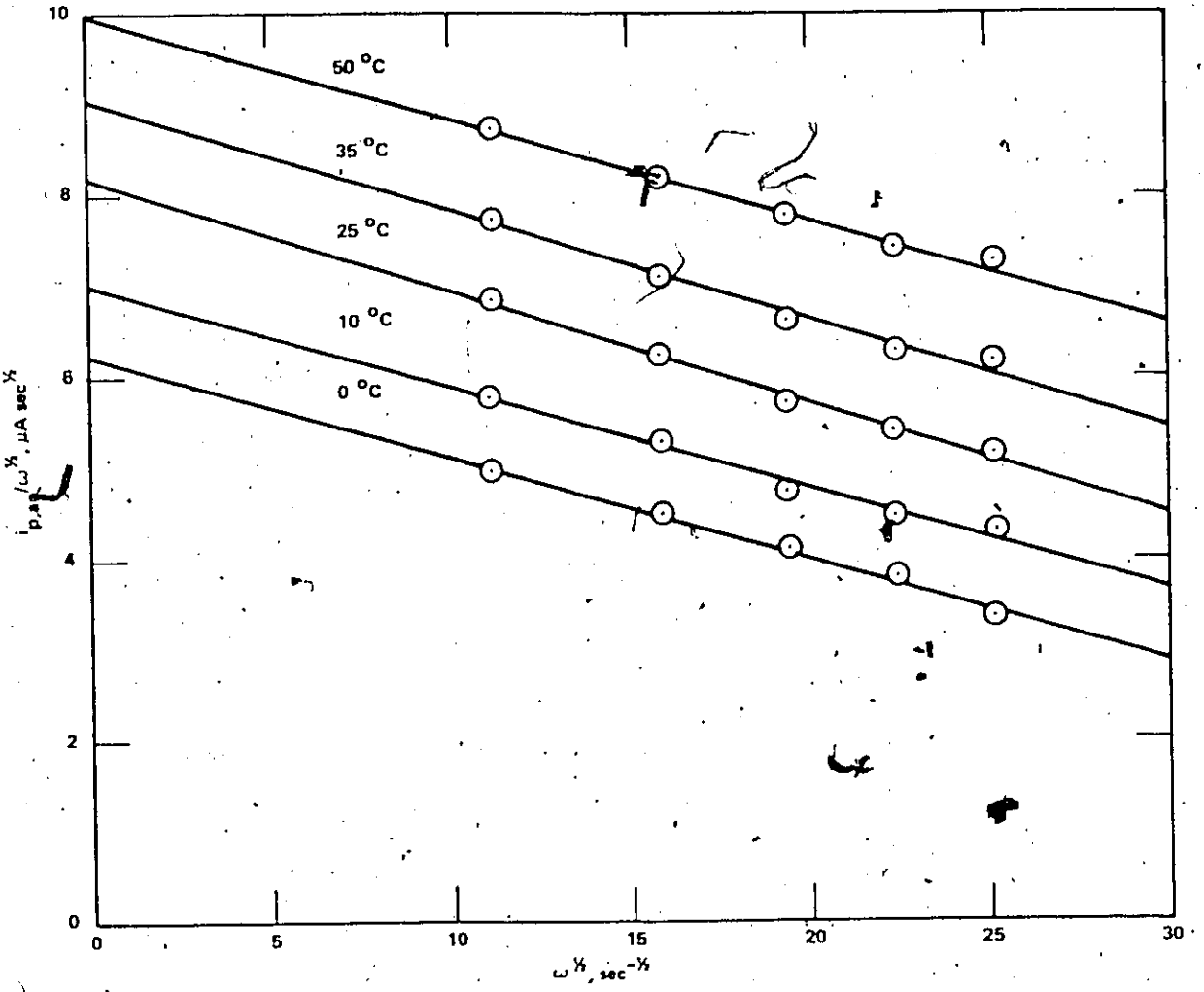

Fig. 20. A family of $i_{p,ac}/\omega^{1/2}$ *vs* $\omega^{1/2}$ plots used to determine the heterogeneous rate constants of the ferro-ferricyanide redox reaction at a platinum electrode in an aqueous NaCl solution.

The ferrocyanide ion normally has a smaller diffusion coefficient than the ferricyanide ion in the same medium and at the same temperature because of differences in solvation shells. For example, in 1 M KCl at 25 °C, the diffusion coefficient of 4.0 mM ferrocyanide is 6.32×10^{-6} cm^2 sec^{-1} while for 4.0 mM ferricyanide it is[26] 7.63×10^{-6} cm^2 sec^{-1}. Consequently, the diffusion coefficient employed in calculating rate constants was the average of the two species, e.g. $(6.32+7.63) \times 10^{-6}/2 = 6.98 \times 10^{-6}$ cm^2 sec^{-1} in 1M KCl at 25 °C. Note that the average value of the diffusion coefficient is, in this case, 6.98/6.32 = 1.10 that of the ferrocyanide. Only the diffusion coefficients of the ferrocyanide ion were measured and it was assumed that the average values of the diffusion coefficients were always 1.10 that of the ferrocyanide ion in the same solution.

The rate constants for each system were measured at five well-spaced temperatures and Arrhenius plots were made from which energies of activation could be calculated. Again, linear regression analysis was used to calculate the slopes of the Arrhenius plots which are shown in Figs. 21, 22 and 23. The values of these slopes are given in Table 6.

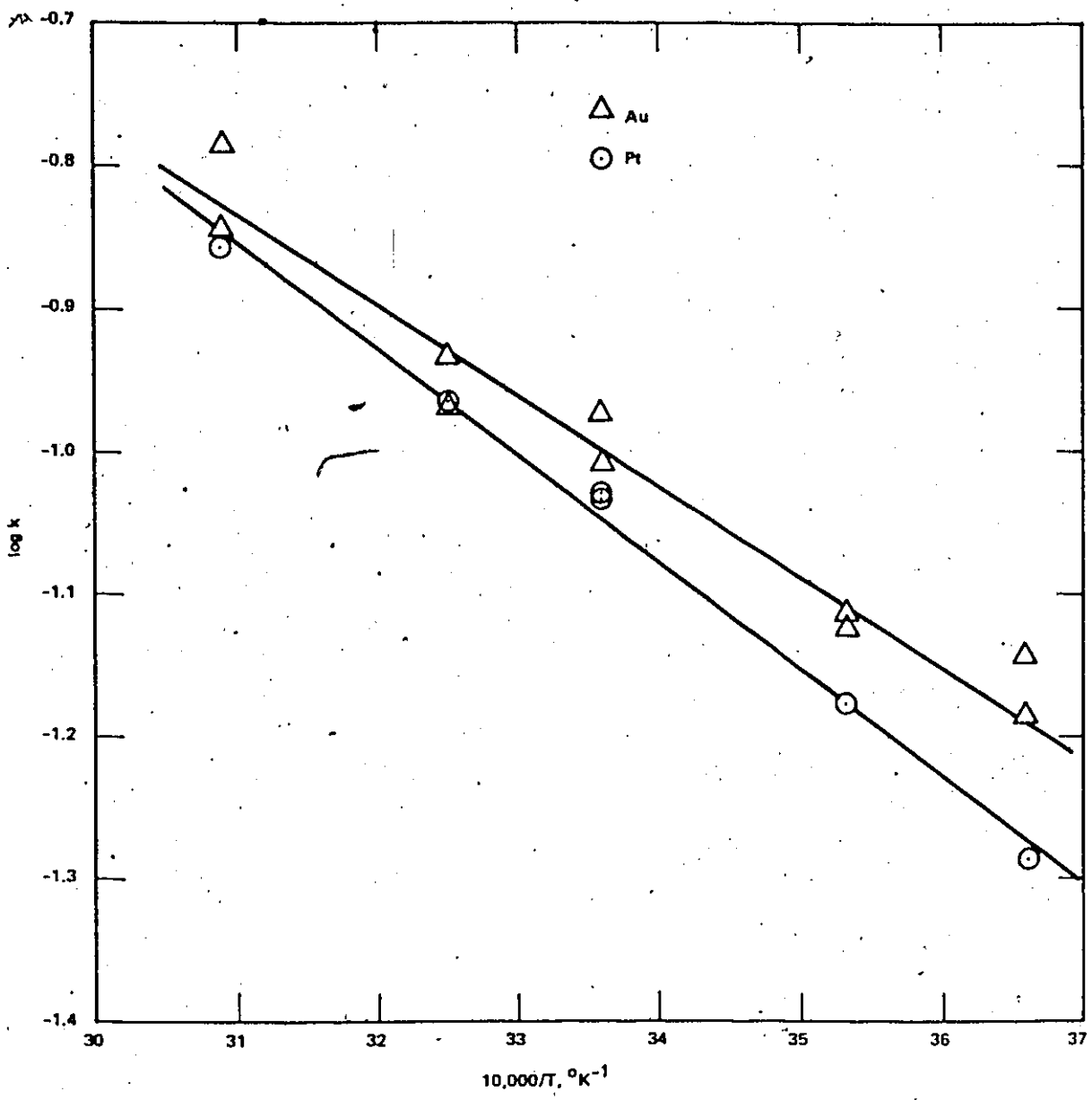

Fig. 21. Arrhenius plots of the ferro-ferricyanide redox reaction in an aqueous KCl solution.

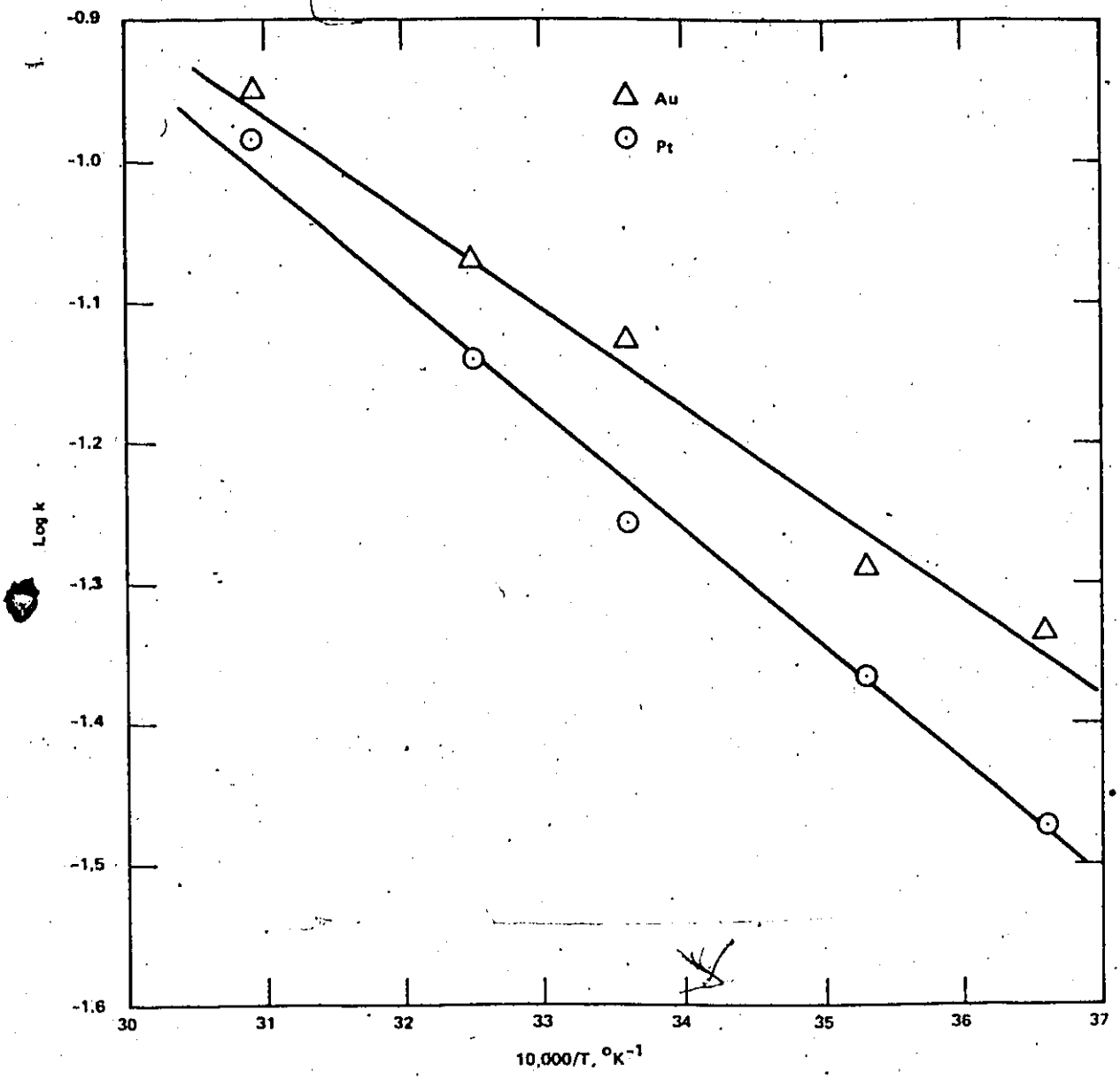

Fig. 22. Arrhenius plots of the ferro-ferricyanide redox reaction in an aqueous NaCl solution.

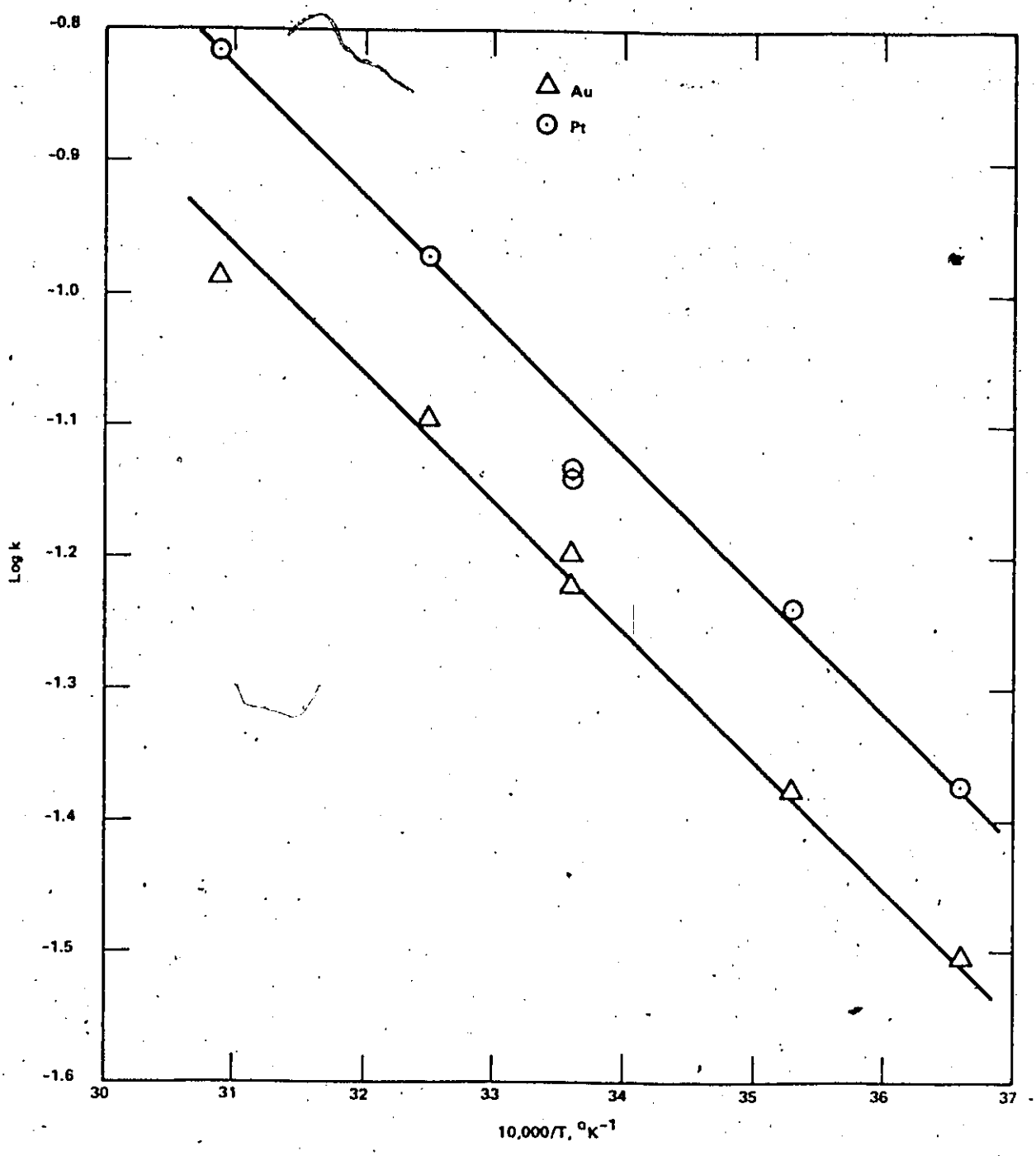

Fig. 23. Arrhenius plots of the ferro-ferricyanide redox reaction in an aqueous $NaClO_4$ solution.

TABLE 6

Energies of Activation of the Ferro-Ferricyanide Redox Couple at Platinum and Gold Electrodes in Aqueous KCl, NaCl and $NaClO_4$ Solutions

	ΔE^* / Kcal mole^{-1}	
Solvent	Platinum	Gold
1.00 M aqueous KCl	3.49	2.79
1.00 M aqueous NaCl	3.85	3.21
1.00 M aqueous $NaClO_4$	4.39	4.24

Electroactive species: 4.00 mM potassium ferricyanide

The uncertainty in each measured energy of activation is *ca.* ±0.2 Kcal mole^{-1}. Thus, a difference of more than 0.4 Kcal mole^{-1} between a pair of results is significant.

The magnitudes of the rate constants and energies of activation for the ferro-ferricyanide couple at platinum in 1.00 M aqueous KCl agree very well with the published values[47]. Therefore, the small amplitude a.c. method for measuring heterogeneous rate constants of fast processes may be accepted as a reliable procedure suitable for use with the rubrene system. In fact, this method offers better precision than other methods.

Several important conclusions can usefully be drawn from the data in Table 6:

1. The energy of activation increases with increasing tendency for ion-pair formation. This is illustrated by comparison of the data for KCl with that for NaCl. The Na^+ ions form stronger ion-pairs with ferro-ferricyanide ions than do K^+ ions.
2. The energy of activation increases with adsorption of Cl^-. At gold, consistently smaller energies of activation are exhibited in chloride solutions, while in perchlorate solution, the same energy of activation is found at gold as at platinum. This is because the chloride ion is adsorbed by platinum while neither electrode material adsorbs perchlorate ions appreciably. This influence of Cl^- adsorption may originate from a bridging effect in electron-transfer similar to that known in homogeneous electron-transfer processes[50].
3. The double-layer effect increases the energy of activation with increasing radius of the supporting electrolyte anion. In changing the electrolyte anion from chloride to perchlorate, both electrode materials exhibited an increase in the energy of activation for ferro-ferricyanide electron-transfer.
4. There is no work-function effect on the energy of activation. In aqueous $NaClO_4$, both electrodes gave the same energy of activation. Neither electrode material adsorbs any species from this solution.

7.2.3 The Rubrene System

It has been shown above how the reliability of the small-amplitude a.c. polarographic method for studying the kinetics of heterogeneous electron-transfer reactions was verified by using it to study a known system, the ferro-ferricyanide redox couple. In applying the same technique to the rubrene system, an important difference between the two systems should be noted. The work on the ferro-ferricyanide redox couple was performed in aqueous solutions containing 1 M concentration of a strong electrolyte while work on the rubrene system was carried out in aprotic solutions containing only 0.1 M TBAP supporting electrolyte. The TBAP concentration was limited by the low solubility of this salt in the aprotic solvents employed.

The specific conductance of one of the aqueous solutions studied, 1.00 M KCl in water, is[11] 0.112 ohm^{-1} cm^{-1} at 25 °C while for one of the aprotic solutions, 0.100 M TBAP in equivolume benzene-DMF, it is 0.00234 ohm^{-1} cm^{-1} at 25 °C. The conductance of the aprotic solution was measured with an a.c. impedance bridge at 50 mV rms. The cell constant of the conductivity cell was determined using a 0.100 M KCl solution in water at 25 °C and the known[11] specific conductance of the KCl solution. It is seen that the test solution is almost 50 times more resistive than the solution for the model system. Uncompensated cell resistance effects will tend to decrease the measured rate constants. It was therefore necessary to estimate the effect of the greater cell resistance on the results for rubrene.

The importance of employing iR compensated a.c. in non-aqueous solutions is clearly evident from Fig. 24. In this case, the measured apparent rate constant is almost doubled by the iR compensation (the rate constant is inversely proportional to the slope of this plot). The electrolytic resistance between the Luggin tip and working electrode can be estimated from an equation developed by Němec[51] for this purpose, i.e.

$$R = \frac{1}{4 \pi r K} \left(1 - \frac{1}{d/r}\right) \qquad (20)$$

where r is the radius of the electrode, K is the specific conductance of the solution and d is the distance between the Luggin tip and working electrode. The solution used to obtain the data in Fig. 24 had a specific conductance of 0.00391 ohm^{-1} cm^{-1} (at 25 °C), the radius of the working electrode was 0.05 cm and it was positioned *ca.* 0.1 cm from the Luggin tip. Therefore,

$$R = \frac{1}{4 \pi (0.1)(0.00391)} \left(1 - \frac{1}{0.1/0.05}\right)$$

$$= 102 \text{ ohms}$$

Assuming 95 % iR compensation[52], the residual, uncompensated resistance for the "iR compensated" plot in Fig. 24 was *ca.* 5 ohms.

From the slope of the iR compensated plot in Fig. 24, a rate constant of *ca.* 0.1 cm sec^{-1} is obtained. Using this measured rate constant and Equation 15, it is now possible to calculate the Faradaic resistance R_F of this system. The R_F will be calculated for

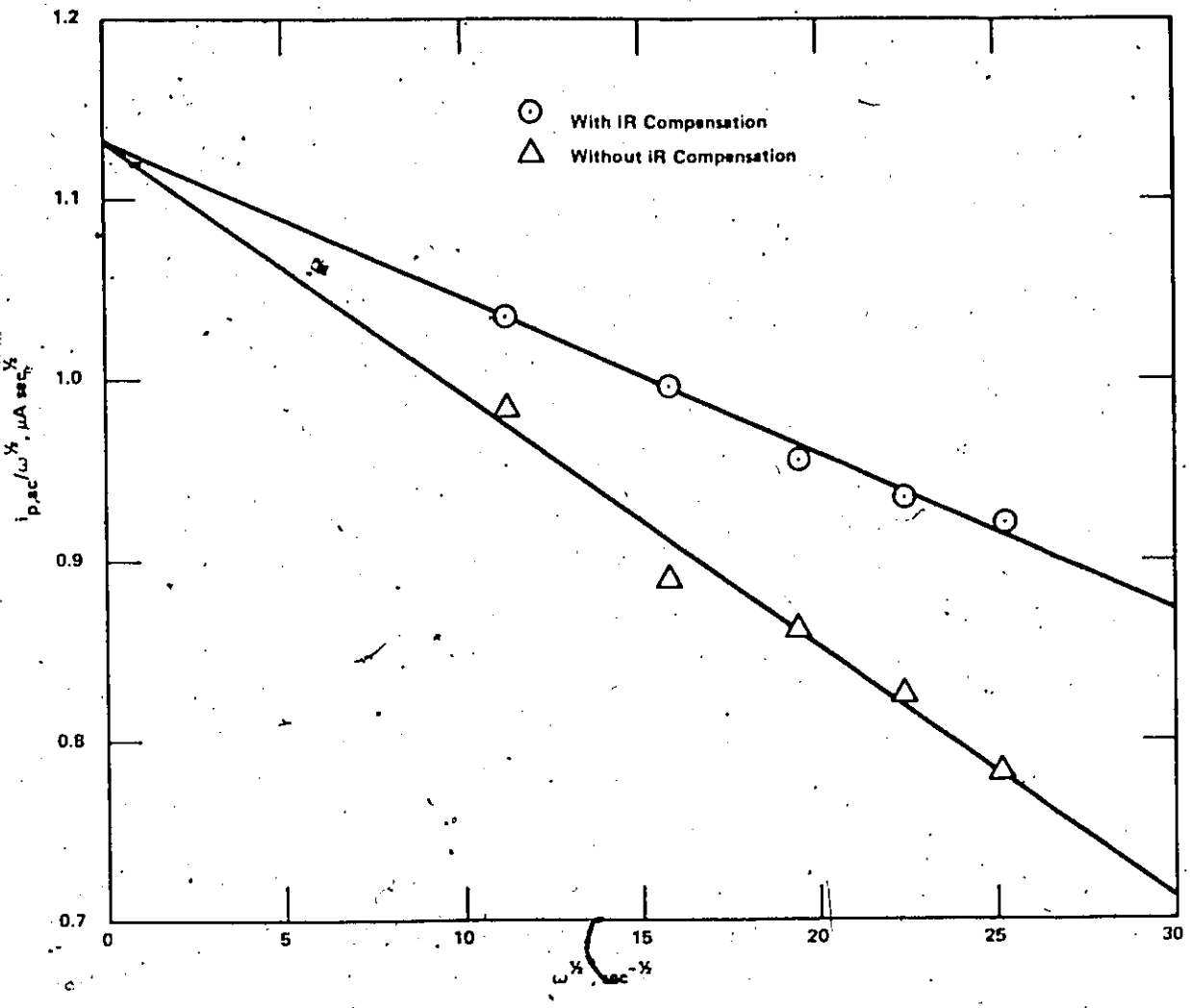

Fig. 24. Importance of iR compensated a.c. voltage in the small-amplitude a.c. polarographic determination of the heterogeneous rate constants of rubrene in aprotic (DMF) solutions.

ω = 628 radians sec^{-1} (100 Hz).

$$R_F = \frac{(8.31)(298)}{(1)^2(96500)^2(0.001)(0.1)} \left[\left(\frac{2}{(628)(4.8\times10^{-6})} \right)^{1/2} + \frac{1}{0.1} \right]$$

$$= 95 \text{ ohms}$$

If k is very large, then $1/k \approx 0$ and R_F = 68 ohms. Therefore, the resistance which caused $i_{p,ac}/\omega^{1/2}$ to decrease linearly with increasing $\omega^{1/2}$ is (95-68) = 27 ohms. Of these 27 ohms, 5 can be attributed to residual, uncompensated resistance. Thus, the rate constant only adds (27-5) = 22 ohms to the apparent Faradaic resistance. This corresponds to a rate constant of *ca.* 0.12 cm sec^{-1}. Apparently, although iR compensation was employed, the measured rate constants were still *ca.* 20 % less than the actual values due to residual, uncompensated resistance effects.

The feedback circuit which provided the iR compensation probably becomes unstable below a certain minimum resistance. Consequently, the residual, uncompensated resistance probably remained constant regardless of the amount of compensation. Experimentally, the rate constant increased with temperature so that its "resistance" decreased with temperature. With a constant, residual uncompensated resistance the measured (apparent) rate constants hence had a smaller apparent temperature coefficient than the actual rate constants. Thus, the measured rate constants will all be low, typically 20 % less than the true

values, while the energies of activation are low, *ca.* 120 % of the actual values. It should be noted that despite these inherent errors in the measurements, the comparison of values of different systems will be largely unaffected by these errors.

Fig. 25. shows a plot of the peak a.c. current *vs* the amplitude of the a.c. voltage at constant phase angle and frequency for the oxidation of rubrene at a Pt electrode in a TBAP-DMF solution. This plot indicates that $i_{p,ac}$ is directly proportional to V_{ac} in accordance with theory. The point to be noted is that with this technique the iR effects cannot be diminished by passing smaller currents with smaller a.c. voltages. If the voltage were to be, say, reduced by half, the current would also be halved, i.e. the resistance is constant. Thus, half the current will cause half the iR drop. However, the ratio $iR:V_{ac}$ would remain the same.

The variation in a.c. current with phase angle at constant a.c. voltage and frequency is shown in Fig. 26. It is clear from these plots that a phase angle of 35° in the experimental measurements will be acceptable for all frequencies employed (20-100 Hz) without incurring significant errors.

The kinetics of the oxidation and reduction of rubrene were investigated in two solvents, 0.100 M TBAP in DMF and 0.100 M TBAP in equivolume benzene-DMF mixture, at both platinum and gold electrodes. The results are presented in the form of Arrhenius plots in Figs. 27 and 28. From these plots, energies of activation of the processes were obtained. The values are given in Table 7. The

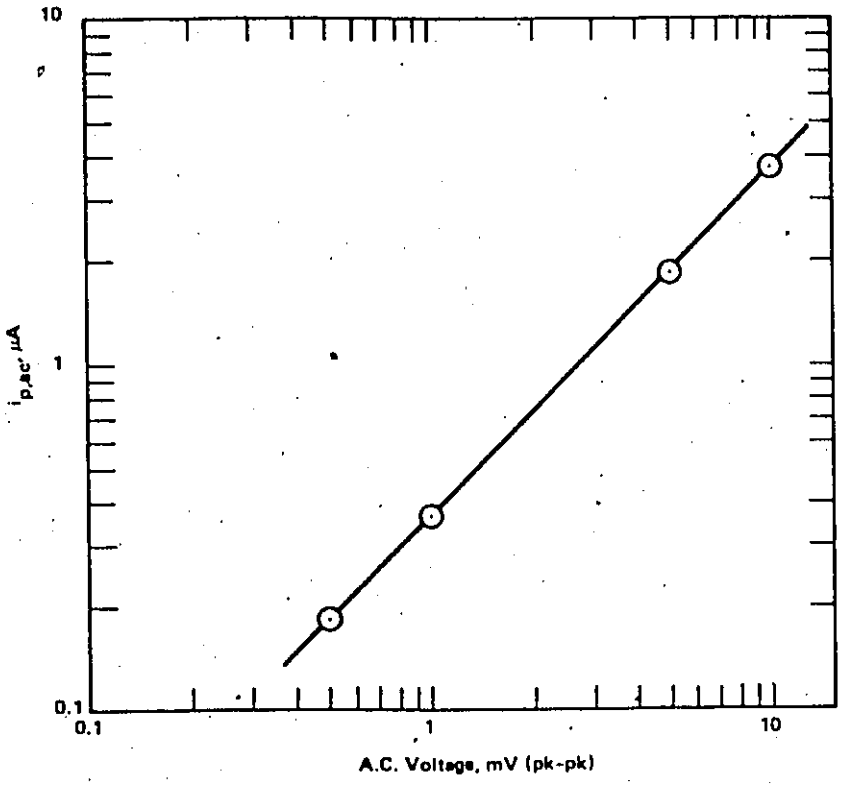

Fig. 25. The a.c. current is directly proportional to the a.c. voltage

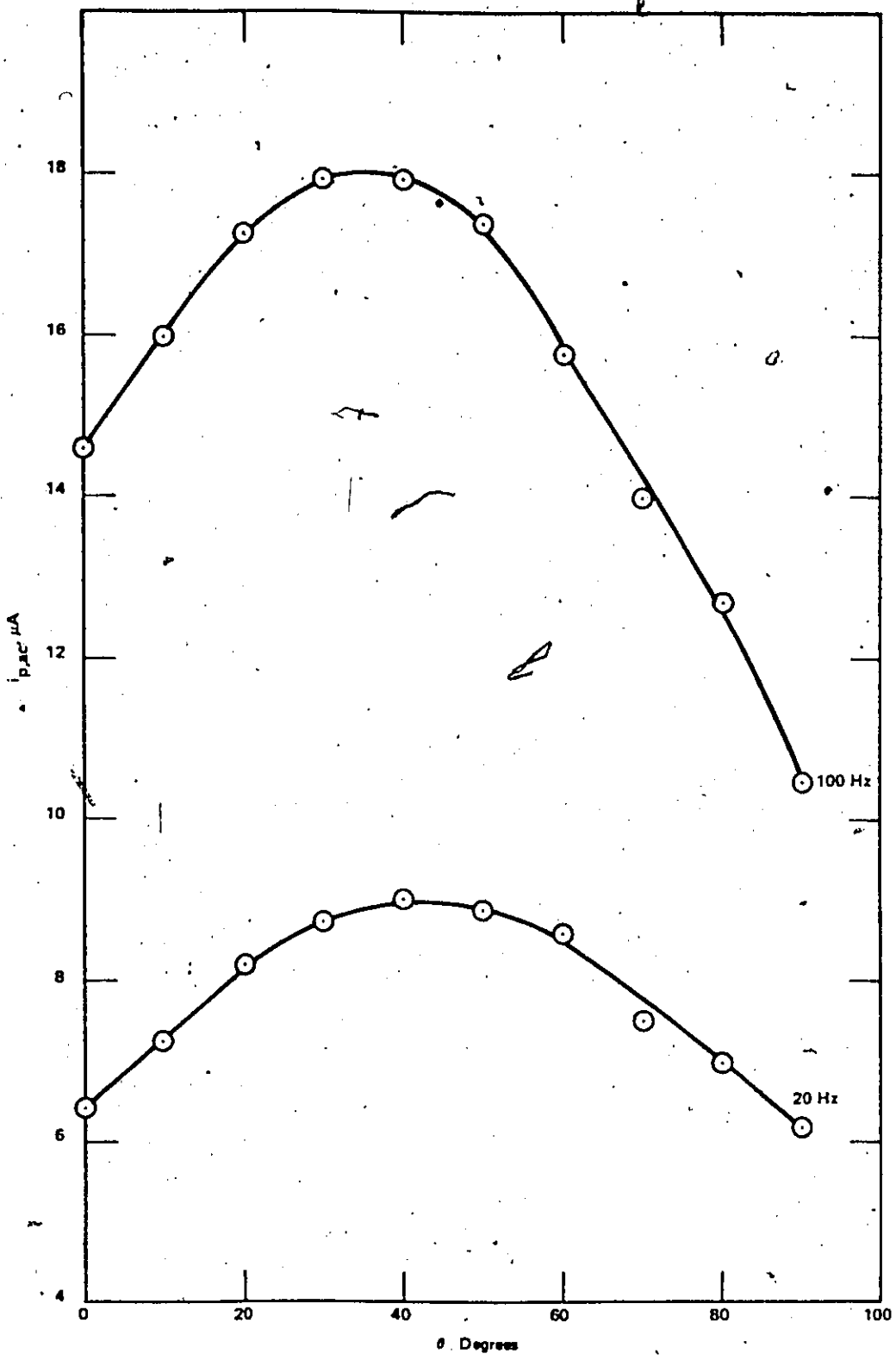

Fig. 26. Variation in $i_{p,ac}$ with phase angle for the rubrene system in a DMF solution.

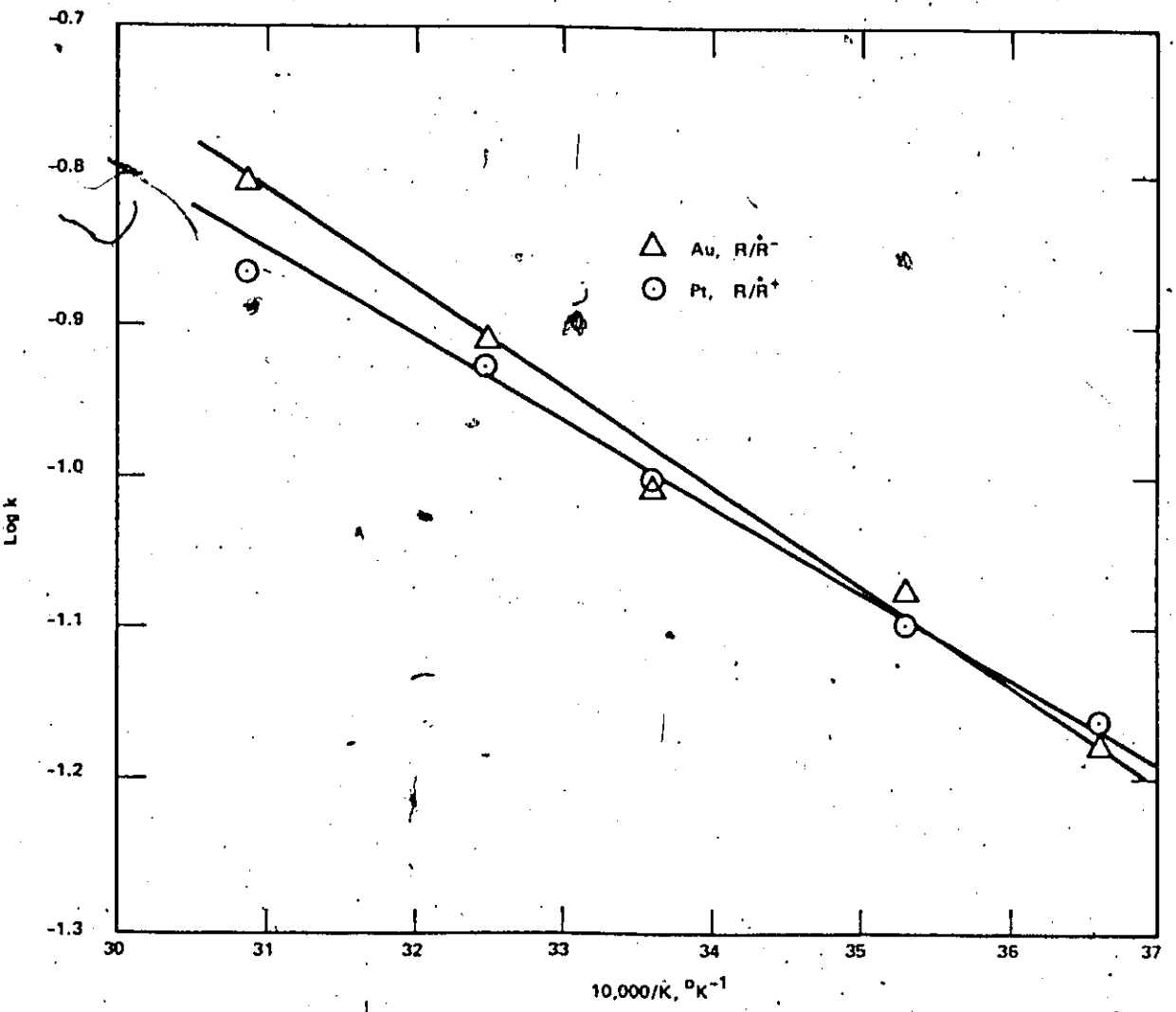

Fig. 27. Arrhenius plots for the rubrene redox processes in a DMF solution.

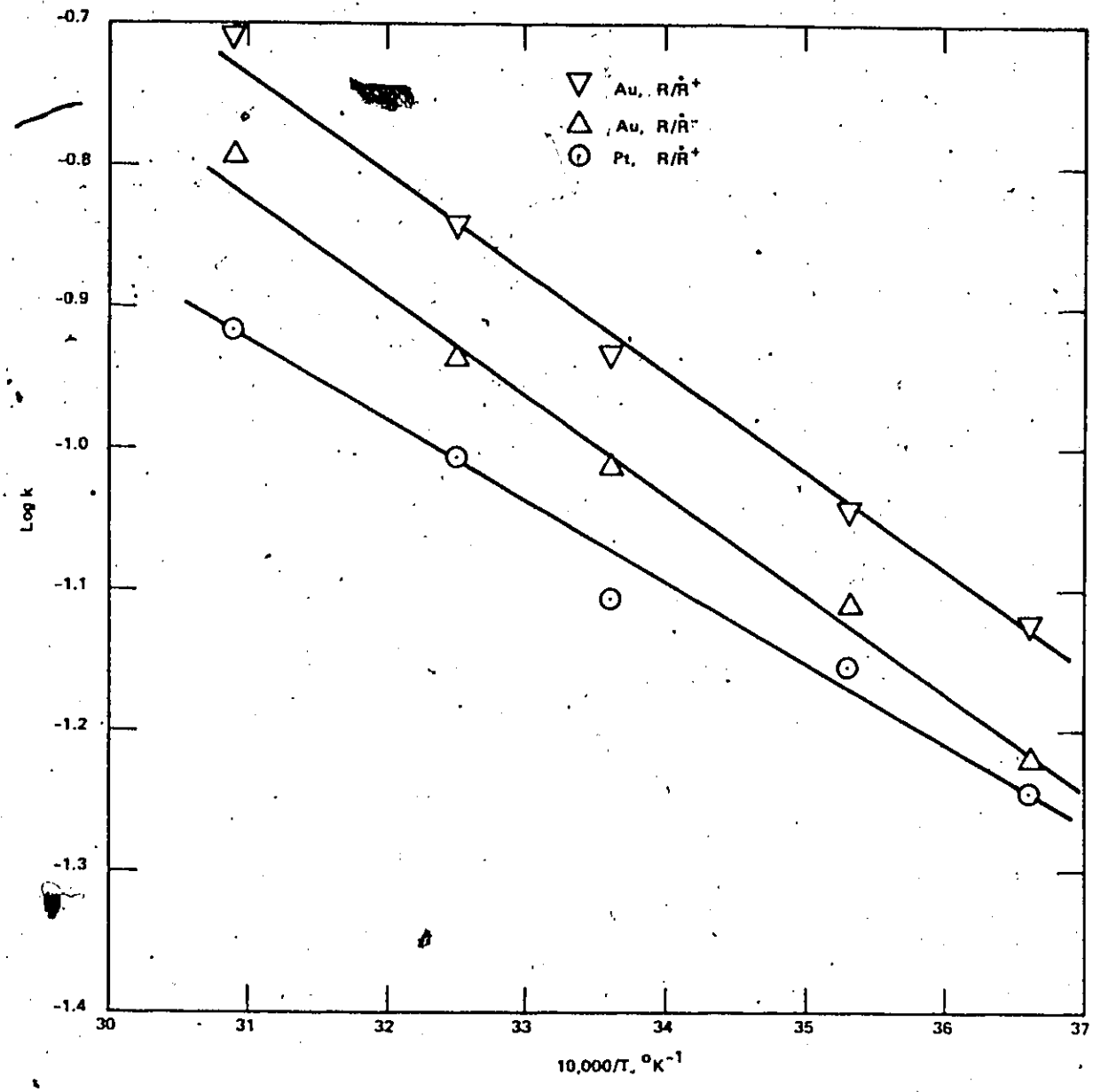

Fig. 28. Arrhenius plots for the rubrene redox processes in an equivolume benzene-DMF solution.

results in Figs. 27 and 28, and Table 7, are the directly measured values and thus have not been corrected, e.g., for residual, uncompensated iR effects.

TABLE 7

Energies of Activation for the Oxidation and Reduction of Rubrene at Platinum and Gold Electrodes in 0.100 M TBAP in DMF and Equivolume Benzene-DMF Solutions

	ΔE^* Kcal mole^{-1}			
Solvent	Platinum		Gold	
	$R/\dot{R}^+$	$R/\dot{R}^-$	$R/\dot{R}^+$	$R/\dot{R}^-$
DMF	2.46	-	2.81	2.97
equivolume benzene-DMF	2.50	-	3.32	3.32

The reduction of rubrene at platinum electrodes in both solutions gave a.c. currents that were only *ca.* 1/3 of the normal values, compared to the oxidation at Pt and both the oxidation and reduction at Au electrodes. It has been shown[53] that the adsorption of aromatic hydrocarbons and their radical-anions does not occur to an appreciable extent for low concentrations in aprotic solvents. It thus appears that the anomalously small a.c. currents for the reduction of rubrene at platinum electrodes in both aprotic solutions cannot be explained by invoking adsorption effects.

The addition of 100 ppm of water or formic acid to the aprotic solutions did not affect the reduction behaviour of the rubrene system at platinum electrodes but the addition of 100 ppm of formaldehyde normalized its behaviour at this electrode material. (All three additives are natural impurities of DMF.) The reproducibility of the small reduction a.c. waves was poor while that for the processes which exhibited normal currents it was good (±5 %). The small a.c. reduction waves could be accounted for by suggesting that the rubrene and/or its anion-radicals were indeed adsorbed by the platinum (in contradiction to the literature reports). The adsorbate, being very large, could exhibit a blocking action against further electrolysis of the rubrene from the polarized interphase and this would account for the smaller-than-expected experimental currents. The addition of formaldehyde to the solutions restored normal reduction currents probably because it was preferentially adsorbed by the platinum. This preferential adsorption of the formaldehyde would diminish adsorption of rubrene. The formaldehyde molecule is relatively much smaller in size than rubrene so that adsorbed formaldehyde might be expected to exhibit a smaller blocking action to rubrene reduction than adsorbed rubrene itself.

The energies of activation at gold electrodes are the same whether the rubrene was reduced or oxidized in both solutions. This is to be expected for a structure such as that of rubrene with a large delocalized electron system. However, gold shows an increase in energy of activation for the redox process in going from TBAP in

DMF to TBAP in equivolume benzene-DMF mixture while platinum does not. Furthermore, the energies of activation for the oxidation at platinum in both solutions are significantly less than for the same process at gold in both solutions. Despite the greater energies of activation at gold, the rate constants for the redox processes are greater at gold. Apparently, relatively higher activation energies at gold are more than compensated for by greater frequency or exp $\Delta S^*/R$ factors. Perhaps adsorption or double-layer effects cause an orientation of rubrene at the electrode favourable to electron-transfer.

7.3 Thermodynamics of the Rubrene Redox System

Fig. 29 shows the variation with temperature of the difference between the peak oxidation and reduction potentials for rubrene in the two solvents studied. These data were derived from cyclic voltammograms of both the oxidation and reduction at a scan rate of 100 mV sec^{-1} with iR compensated d.c. It has been previously noted (Section 7.1.1) that at this scan rate both the cation- and the anion-radicals of rubrene are practically stable in both of these solutions.

The absolute value of the peak potential is 1.109RT/nF volts greater than the absolute value of the half-wave potential[27]. Thus, 2(1.109RT/nF) volts were subtracted from each potential difference shown in Fig. 29 to express the potential differences in terms of half-wave potentials. These data are entered in Table 8.

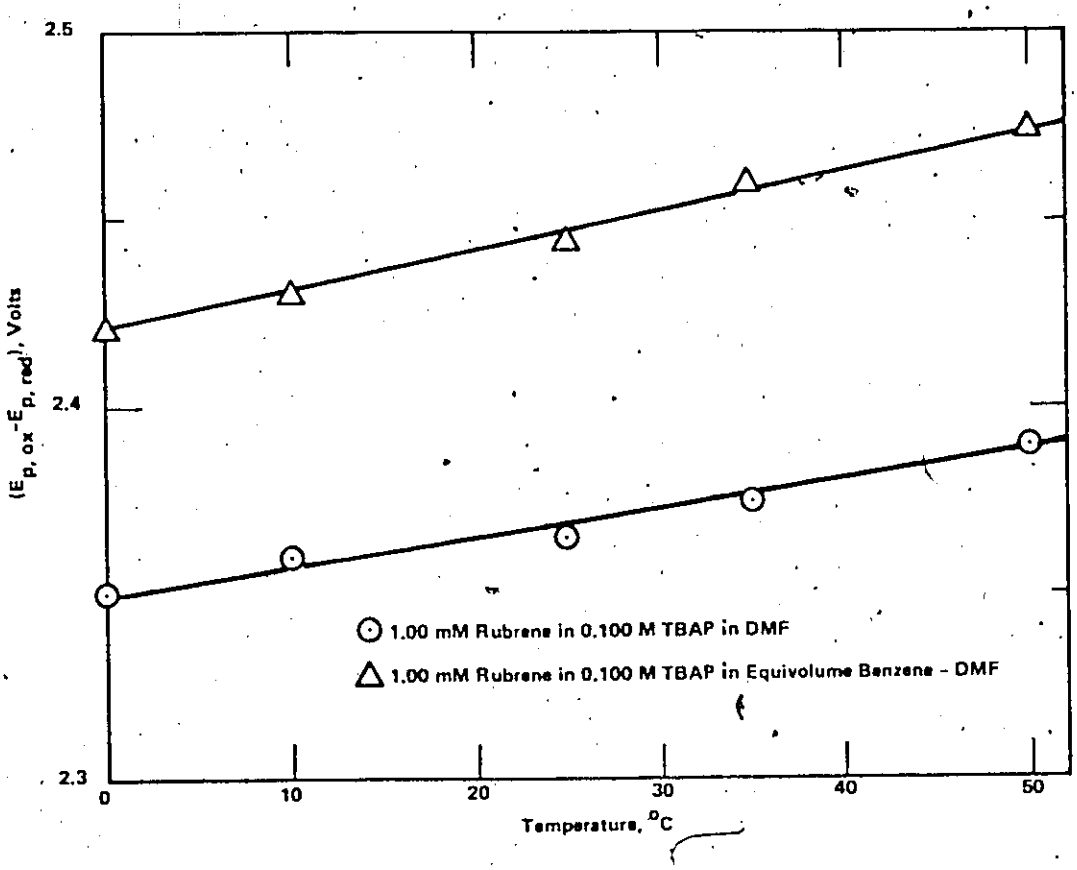

Fig. 29. Variation of $(E_{p,ox}-E_{p,red})$ with temperature for rubrene.

TABLE 8

Variation in the Difference Between the Half-Wave Oxidation and Reduction Potentials of Rubrene with Temperature

Temperature °C	$E_{1/2,ox}-E_{1/2,red}$, volts: 0.100 M TBAP in DMF	$E_{1/2,ox}-E_{1/2,red}$, volts: 0.100 M TBAP in equivolume benzene-DMF
0	2.355	2.425
10	2.365	2.435
25	2.365	2.445
35	2.375	2.460
50	2.385	2.470

The iR drops in the recordings of the cyclic voltammograms were estimated to determine the accuracy of the potential difference measurements. A platinum bead working electrode was used in the cyclic voltammetry. Consequently, the electrolytic resistance between the Luggin tip and the working electrode can be calculated using Equation 20. For the DMF solution, the cell resistance was calculated earlier (p. 89) to be 102 ohms at 25 °C. The peak currents of the cyclic voltammograms were *ca.* 20 μA at 25 °C. Thus, in the absence of iR compensation, the iR drops in the DMF solutions made the peak oxidation potential ($20\times10^{-6}\times102$) = 2 mV more positive than the true value and the peak reduction potential was also made more negative by 2 mV. In calculating ($E_{p,ox}-E_{p,red}$), the iR losses become additive, i.e. 2 + 2 mV = 4 mV. Assuming that the iR compensation was 95 % effective, it is seen that the residual, uncompensated iR is less than 1 mV - a negligible amount. The benzene-DMF solution

is approximately twice as resistive as the DMF solution but even in the more resistive mixed solvent solution the iR effects are negligibly small when iR compensation is employed. The temperature coefficient of the conductance is negative and greater in magnitude than the positive temperature coefficient of the peak current. Consequently, iR effects, if they were important, would increase in magnitude with decreasing temperature.

From the temperature coefficient of the difference between the half-wave oxidation and reduction potentials (Table 8), the standard change in entropy of the homogeneous electron-transfer reaction in each solution was calculated using Equation 12. The temperature coefficient was assumed to be constant over the temperature range covered and the slopes were calculated using linear regression analysis. The results of these calculations are listed in Table 9, together with other relevant thermodynamic and spectroscopic data of rubrene in both solvents.

TABLE 9
Thermodynamic and Spectroscopic Data of Rubrene

Solvent	$\Delta S°$ cal mole^{-1} °K^{-1}	$\Delta H_{25\ °C}$ Kcal mole^{-1}	$E_{1_{R^*}}$ Kcal mole^{-1}	Relative Fluorescence Efficiency
0.100 M TBAP in DMF	13	50.6	52.9	1.0
0.100 M TBAP in equivolume benzene-DMF	21	50.0	52.9	1.0

The changes in enthalpies in Table 9 are for the homogeneous electron-transfer reactions between the monoanion- and monocation-radicals of rubrene and were calculated using Equation 11a.

The energy of the lowest excited singlet state of rubrene was determined from the crossover point (Fig. 30) between the absorption and fluorescence spectra of rubrene in each type of conducting solution. The absorption and fluorescence spectra were each the same in both solutions and are shown in Fig. 30. The solutions had to be diluted to 10^{-5} M in rubrene in order to completely eliminate self-absorption effects. The spectra of rubrene EGCL with and without self-absorption are shown in Fig. 31. These spectra were the same whether the EGCL was generated in DMF, benzonitrile and mixtures of DMF, benzonitrile, acetonitrile and propylene carbonate with benzene, i.e. the emission spectrum was independent of solvent.

The fluorescence and EGCL spectra were recorded with different photomultiplier tubes and the spectra have not been corrected for any specific spectral responses of the detectors. Nevertheless, it is possible to see the similarity between the unabsorbed rubrene EGCL spectrum and the fluorescence spectrum of rubrene. Thus, the only species which emits light in rubrene EGCL is the lowest excited singlet state.

The relative fluorescence efficiencies were obtained by comparing the intensities of the fluorescences of 10^{-5} M rubrene in each conducting solution. The fluorescences were excited with 4500 Å radiation. Neither solvent absorbs at this wavelength, so that the

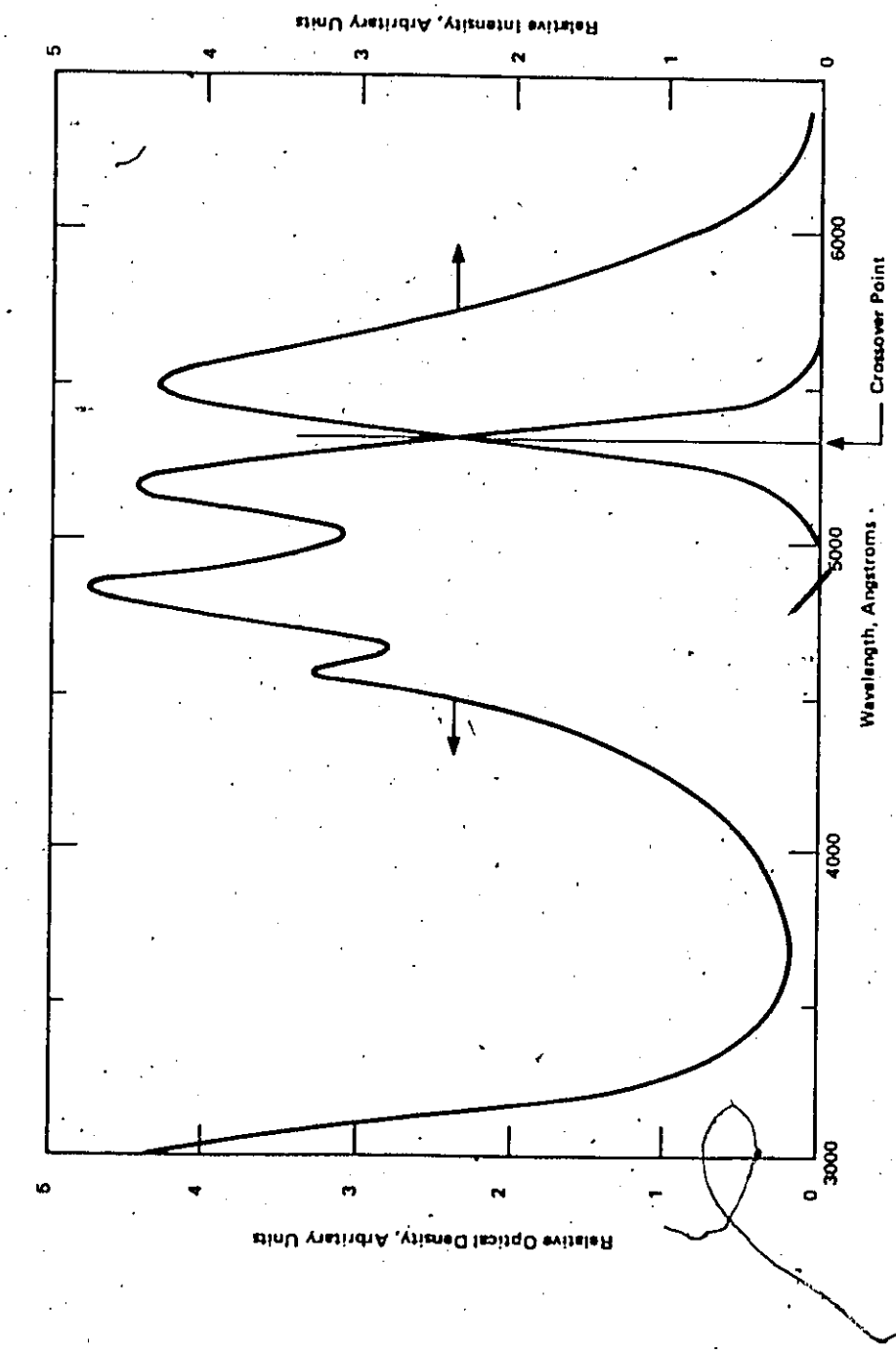

Fig. 30. Uncorrected absorption and fluorescence spectra of rubrene in a DMF solution.

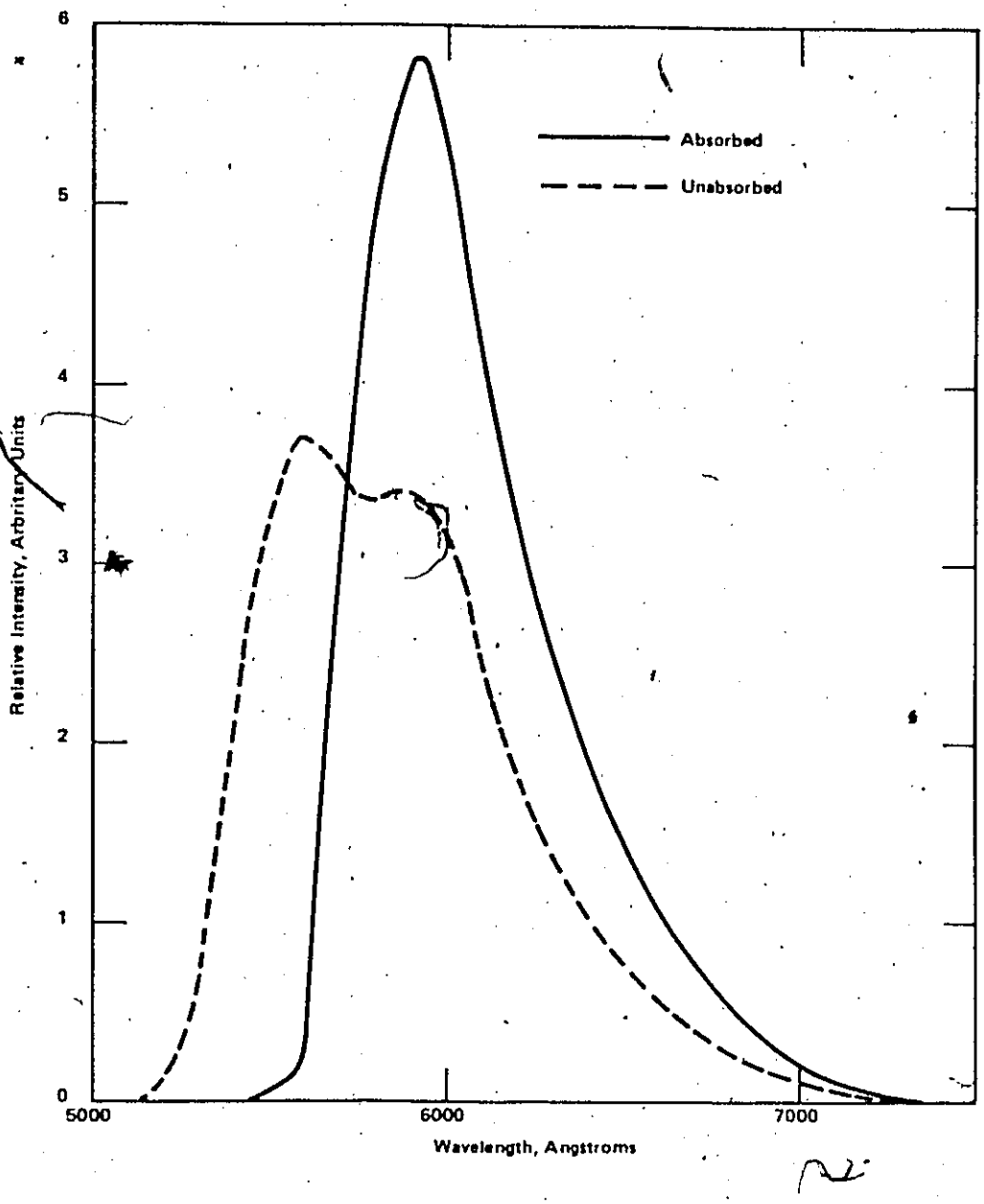

Fig. 31. Uncorrected spectra of rubrene EGCL.

fluorescence intensities did not have to be corrected for differences in absorption, but only for the ratio of the squares of the refractive indices of their solutions[54].

A most important conclusion can now be drawn from the data in Table 9. The change in enthalpy of the homogeneous electron-transfer reaction in both solutions is clearly less than the energy of the emitting singlet state. Thus, there is no doubt that rubrene EGCL is "energy deficient" and is hence produced via the "triplet route". The mechanism for rubrene EGCL is therefore as given in Table 1 but with the following important modification: the singlet state is not directly produced; it is only produced via triplet-triplet annihilation. Therefore, Equation 3 for the rubrene energy deficient EGCL must be written as follows:

$$\dot{R}^+ + \dot{R}^- \rightarrow 3/4\ {}^{3}R^* + 5/4\ R \qquad (3a)$$

7.4. Quantum Efficiency of Rubrene EGCL

The experimental set-up for measuring the coulombic efficiency, ϕ_{coul}, of EGCL was illustrated in Fig. 5. The method consisted of measuring the average rectified a.c. current and average photon current *vs* applied voltage.

The reproducibility of the ϕ_{coul} data was such that the results for the same system, using solutions prepared nine months apart, were within 10 % of each other. A number of equivalent solutions prepared simultaneously yielded ϕ_{coul} values which had a standard

deviation of *ca.* 5 %.

Fig. 32 shows a typical current-voltage curve for processes occurring in the electrolysis cell. Prior to the appearance of EGCL, the current increases linearly with applied voltage and at constant voltage this current was almost directly proportional to the frequency. Since this behaviour is characteristic of a capacitive current, then this current must be the current that is used to polarize the electrode-solution interphase and charge (or discharge) the double-layer capacitance. The abrupt rise in current at *ca.* 2.3 V (peak) coincides with the appearance of detectable EGCL. If it is assumed that the iR drop between the two electrodes is negligibly small, then the "critical" potential for onset of EGCL approximately corresponds to the free energy change of the ion-radical charge neutralization reaction.

In Fig. 32, the capacitive current line has been extrapolated into the potential region where EGCL occurs. For this extrapolation, the usual assumption was made that the Faradaic processes do not alter the double-layer capacity and that the double-layer capacity is constant with potential. The effect of iR drop on the extrapolation was evaluated and found to be insignificant.

Subtracting the capacitive current from the total at the same voltage then yields the Faradaic current at that voltage. This is an important quantity to evaluate, since the total current at high frequencies is dominated by the double-layer charging current which thus obscures the Faradaic current corresponding to EGCL. It is

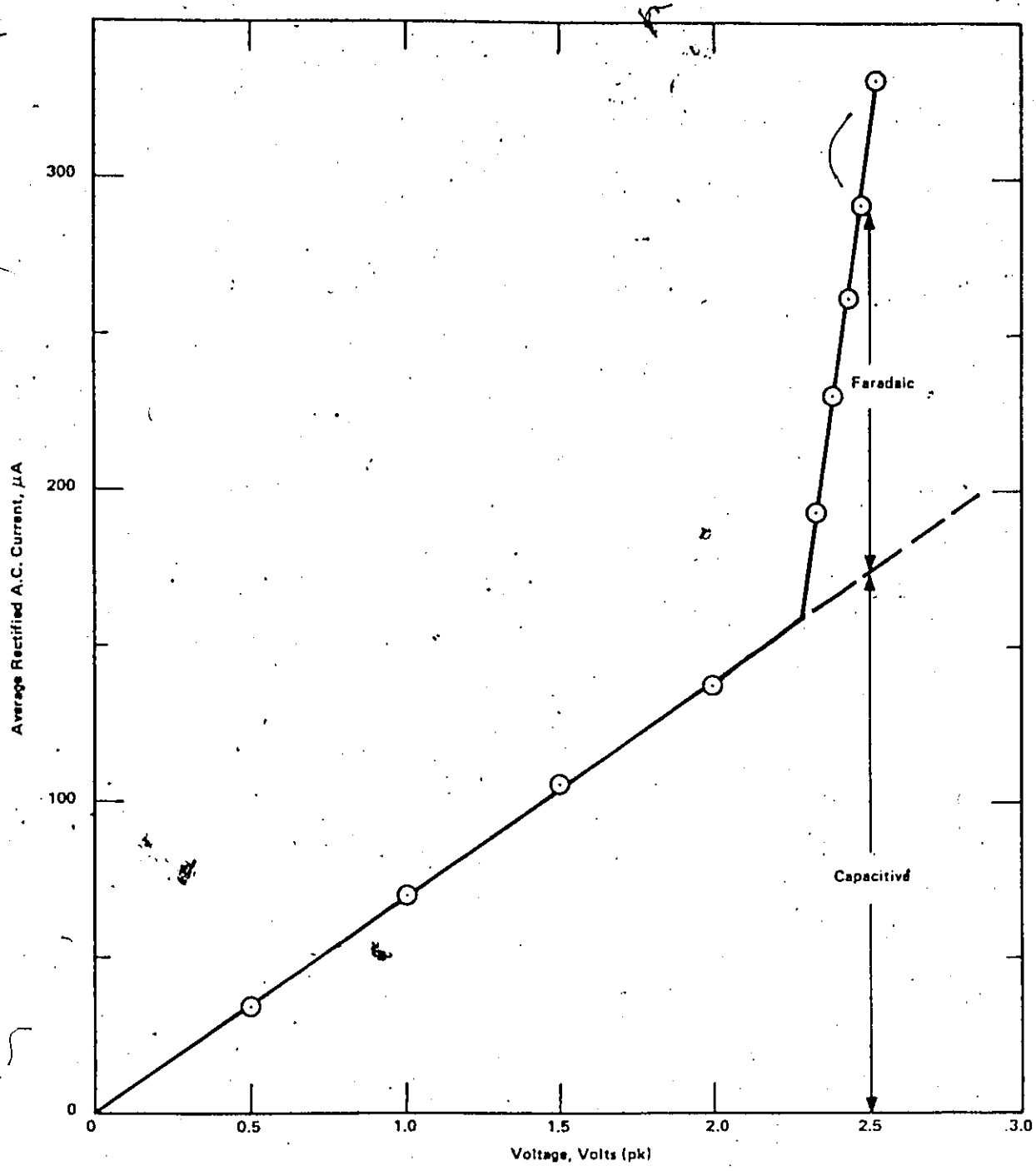

Fig. 32. Typical current-voltage plot used to calculate the Faradiac component of the total electrolysis current. Solution: 1.00 mM rubrene in 0.100 M TBAP in equivolume benzene-DMF.

this Faradaic current, however, that is required for evaluation of the EGCL quantum efficiency ϕ_{coul}.

The measured photon current had to be corrected for the collection efficiency (5/6) of the solar cell box and the spectral response of the solar cells with respect to the rubrene EGCL spectrum (0.7 e/photon). The correction factor employed was therefore the reciprocal of (5/6 x 0.7), i.e. 1.7. The measured photon currents were consequently multiplied by 1.7 to obtain the correct(ed) photon currents.

Fig. 33 illustrates a typical plot of corrected photon current *vs* Faradaic current.. This and all similar plots were linear. The slope of this plot yields twice ϕ_{coul} because equal intensities of EGCL were produced at both electrodes and the <u>total</u> light output was the quantity measured. The electrodes are, of course, connected in series and thus the measured electrolysis current was the same as that exchanged at each electrode.

The linearity of the plots of photon current *vs* Faradaic current indicates that the loss of triplets via triplet decay (Equation 21)

$$^3R^* \rightarrow R \qquad (21)$$

is insignificant. This conclusion is arrived at from studying the equation for the triplet concentration[55]:

$$d[^3R^*]/dt = G - k_1[^3R^*] - k_2[^3R^*]^2 \qquad (22)$$

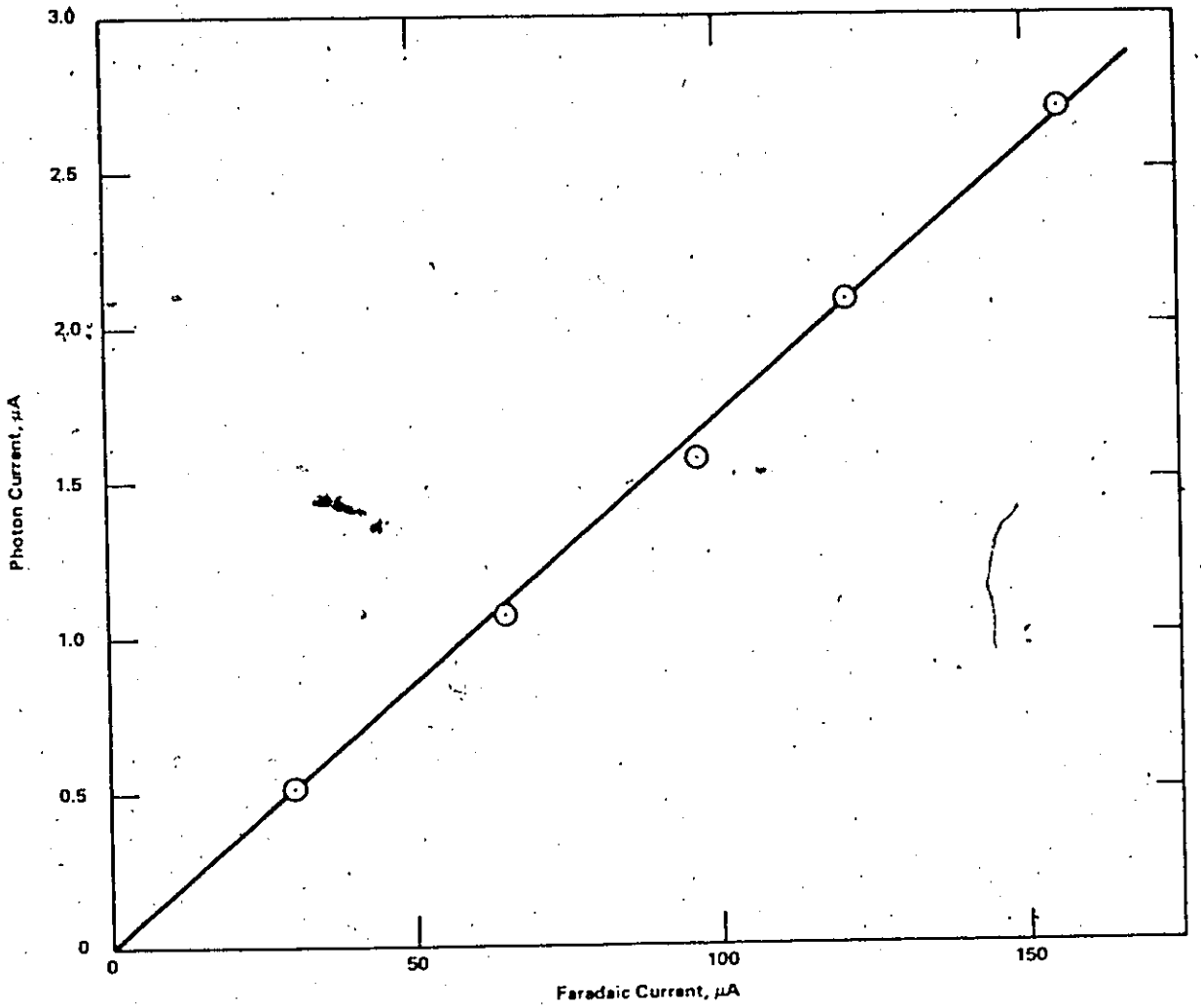

Fig. 33. Typical plot of photon current *vs* Faradaic current from whose slope ϕ_{coul} can be calculated. Solution: 1.05 mM rubrene in 0.100 M TBAP in equivolume benzene-acetonitrile.

where G is the triplet generation rate (directly proportional to the Faradaic current), the second term is the rate of triplet decay and the last term is the rate of triplet-triplet annihilation. The intensity of the EGCL is directly proportional to the rate of triplet-triplet annihilation. Under steady state conditions, $d[^3R^*]/dt = 0$ so that the EGCL intensity is given by

$$I \alpha k_2[^3R^*]^2 = G - k_1[^3R^*] \tag{23}$$

At low intensities

$$I \alpha k_2\left(\frac{G}{k_1}\right)^2 \tag{24}$$

i.e. the intensity is directly proportional to the square of the Faradaic current, while at high intensities, the linear result

$$I \alpha G \tag{25}$$

follows, i.e. the intensity is directly proportional to the Faradaic current because the loss of triplets via triplet decay is relatively small.

Although Fig. 33 indicates that the quantum efficiency is independent of the intensity, when the intensity was increased by increasing the fluorescor concentration, the quantum efficiency decreased (Fig. 34). This observation can be explained by assuming that not all of the emitted light which is absorbed by the rubrene is re-emitted. Under these conditions, Beer's law would predict that the apparent ϕ_{coul} should decrease linearly with increasing log

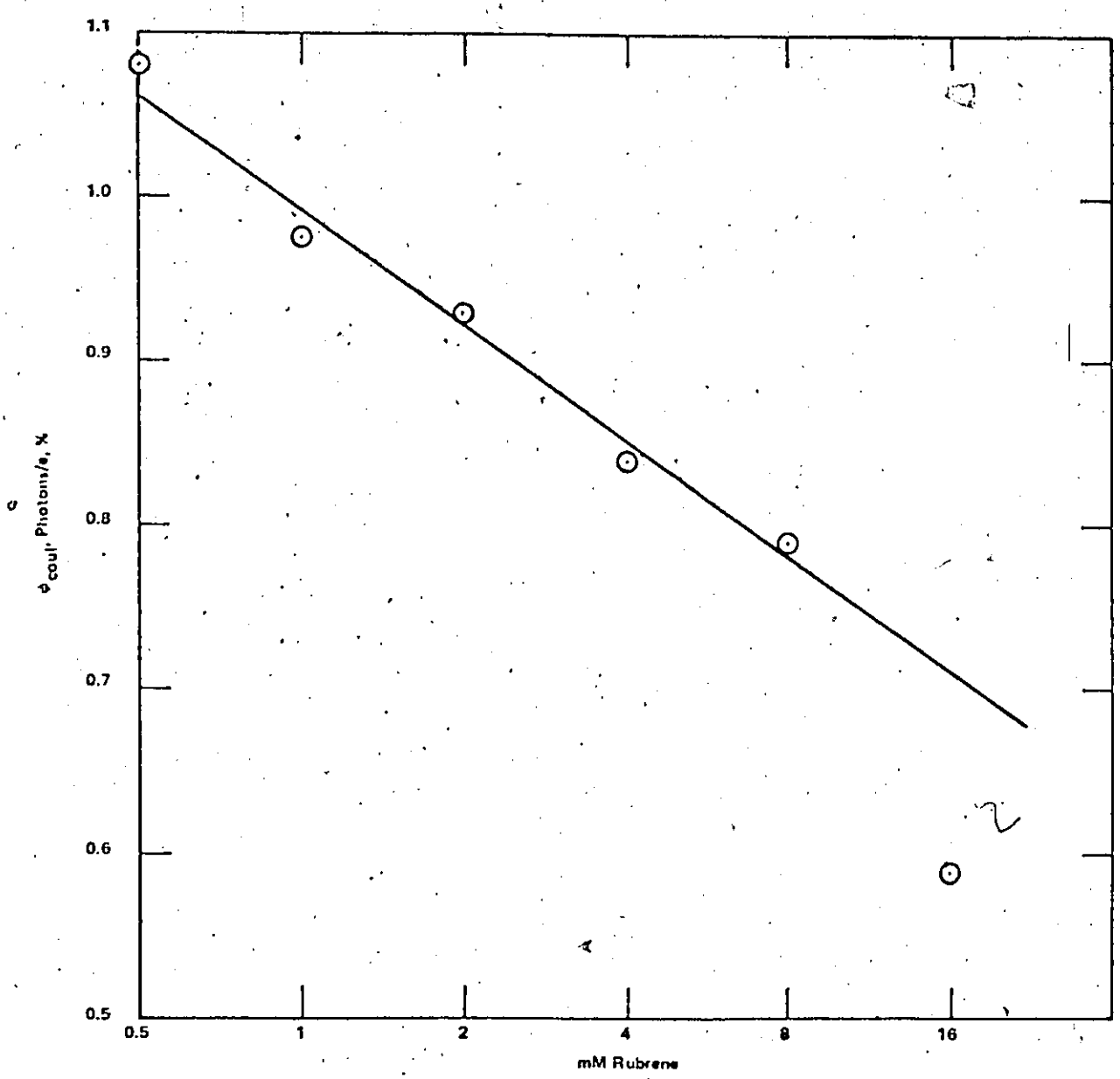

Fig. 34. Decrease in ϕ_{coul} with increasing rubrene concentration in 0.100 M TBAP in equivolume benzene-DMF (For the 16 mM rubrene solution, a 2:1 benzene:DMF solvent containing 0.200 M TBAP was used.).

[rubrene concentration]. This trend is apparent in Fig. 34.

The frequency dependence of ϕ_{coul} is illustrated in Fig. 35. The ϕ_{coul} for all three solutions decreases with increasing frequency. If a quencher were present in the bulk of these solutions, the fractional probability of quenching would decrease with increasing frequency because the triplet concentration would increase within a steadily more compact reaction zone. With a bulk quencher present, ϕ_{coul} would increase with increasing frequency. It is possible to account for the measured trend by suggesting that the electrode itself can quench the triplets. As the frequency is increased, the reaction layer becomes more compact and moves closer to the electrode. The increasing proximity of the triplets to the electrode tends to allow the degree of triplet quenching by the electrode to increase.

In discussing the concentration and frequency dependence of ϕ_{coul}, it was assumed that the fraction of ion-radicals neutralized by the reversal of the polarity of the electrode was constant. This fraction has been calculated to be 8 % by Bezman and Faulkner[32] and 17 % by Schwartz, Blekely and Robinson[33]. Both of their mathematical simulations of the a.c. electrolysis were consistent with respect to the independence of the fraction on concentration and frequency.

When the TBAP concentration in DMF was reduced from 0.100 M to 0.020 M, it was found that ϕ_{coul} was not affected (Fig. 35). It appears, therefore, that ion-pairing is not important in rubrene EGCL. Such a conclusion is not surprising because rubrene is a

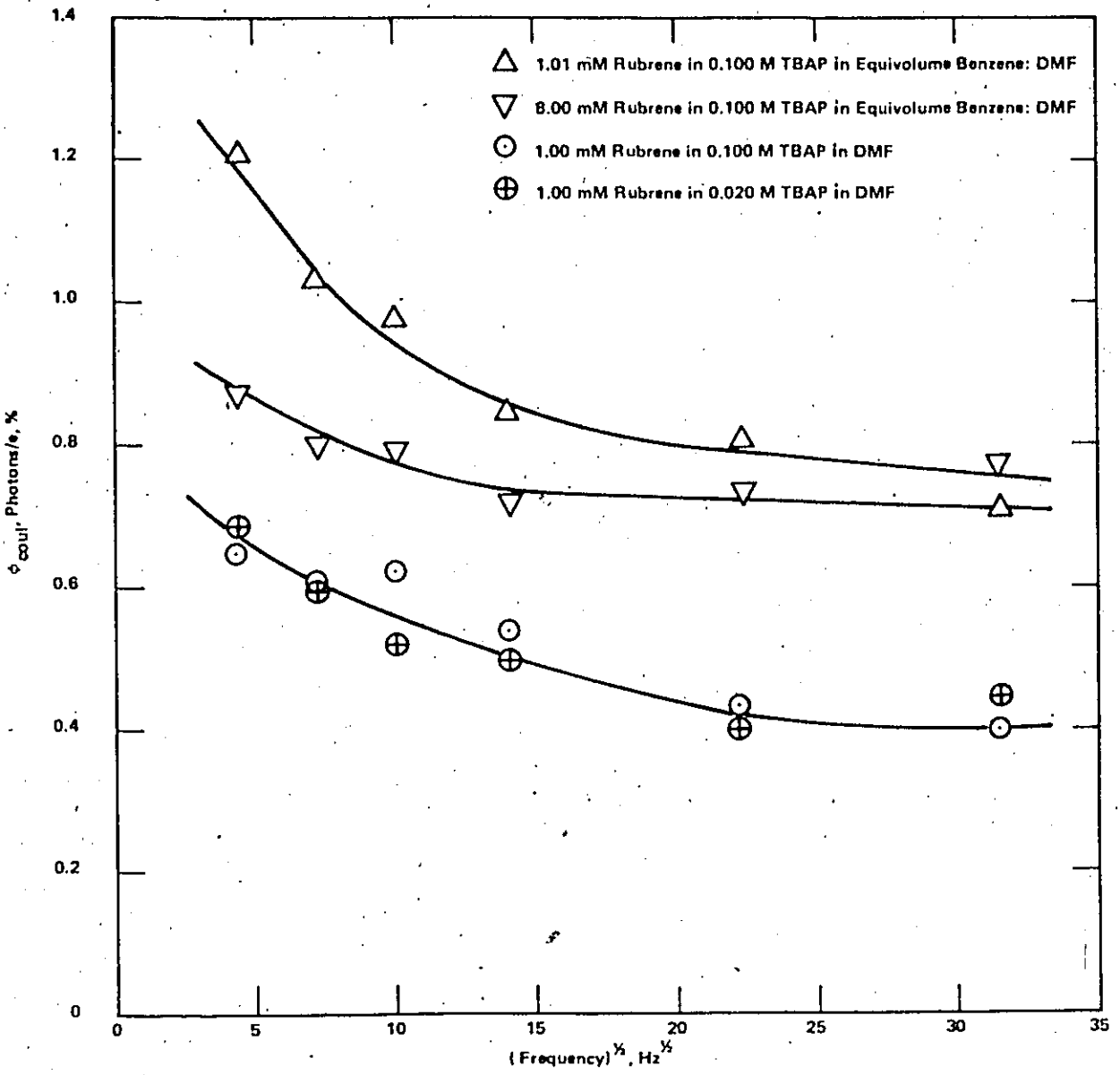

Fig. 35. Decrease in ϕ_{coul} with increasing frequency of the a.c. voltage used to generate the EGCL.

large molecule whose active centres for electron-transfer are blocked by phenyl groups. For 9,10-dimethylanthracene-tri-*p*-tolylamminium perchlorate EGCL, it has been reported that an increase in ϕ_{coul} occurred with decreasing electrolyte (TBAP) concentration[24]. The solvent used for that system was tetrahydrofuran (THF), a medium that has a much lower dielectric constant than DMF (ϵ = 7.4[56] *vs* 37[38]). Thus, ion-pairing tends to be more important in THF than in DMF.

In Table 10 are shown the values of ϕ_{coul} of rubrene EGCL in the various solvents studied. These results are the average of several determinations using the same and equivalent solutions. The Faradaic current used to calculate ϕ_{coul} was not corrected for

TABLE 10

ϕ_{coul} of 1 mM Rubrene EGCL in the 0.100 M TBAP Solutions Studied at 25 °C

Solvent	ϕ_{coul}, %
1:1* benzene:ACN	0.91
PhCN	0.90
1:1 benzene:PhCN	1.02
DMF	0.65
1:99 benzene:DMF	0.70
1:19 benzene:DMF	0.69
1:4 benzene:DMF	0.80
1:1 benzene:DMF	0.96
3:1 benzene:DMF	1.01
1:1 benzene:PC	0.68
DMF (0.020 M TBAP)	0.64

* For the mixed solvents, volume ratios are shown.

the fraction of ion-radicals which were neutralized at the electrode surface by the alternating potential. Since these data have a precision of ±5 %, it is clearly evident from the data in Table 10 that ϕ_{coul} of rubrene EGCL is dependent on the solvent. Various attempts were made to correlate the data in Table 10 with some property of the solution and the procedures used are reported below.

It is already known from earlier work that the changes in enthalpy of the anion-cation-radical charge neutralization reactions in DMF and equivolume benzene-DMF are nearly the same and are significantly less than the energy of the emitting state, i.e. the lowest excited singlet state of rubrene. The emitting state has the same energy in both of these solutions and the fluorescence efficiencies are also the same in both solutions. Despite the similar thermodynamic and spectroscopic properties of rubrene in these solutions, the ϕ_{coul} of rubrene in the mixed solvent solution is, however, nearly 50 % greater than that in the purely polar solvent. Therefore, the solvent dependence of ϕ_{coul} of rubrene EGCL cannot be explained by significant solvent effects on either the type of EGCL mechanism or on the fluorescence efficiency of the rubrene.

The triplet-triplet annihilation reaction and both the homo- and heterogeneous electron-transfer reactions are essentially diffusion-controlled. Addition of benzene (η = 0.61 cp[56]) to DMF (η = 0.80 cp[38]) decreased the solution viscosity and, in this case, ϕ_{coul} increased with decreasing solution viscosity. However, the

viscosity of benzonitrile (η = 1.24 cp[56]) is much greater than that of DMF and yet ϕ_{coul} is much greater in the more viscous solution. Thus, the ϕ_{coul} data in Table 10 do not show a consistent trend with solution viscosity.

Although the exact dielectric constants of the solutions used in the ϕ_{coul} study are not known, it is nevertheless possible to conclude that ϕ_{coul} increases with decreasing dielectric constant of the solution. As the fraction of benzene (ε = 2[56]) added to DMF (ε = 37[38]) is increased, ϕ_{coul} increases. Similarly, addition of benzene to benzonitrile also results in an increase in ϕ_{coul}. Hoytink[9] has shown from theoretical considerations that the rate of transfer of an electron from an anion- to a cation-radical should increase with decreasing dielectric constant of the solution. A larger homogeneous rate constant in a medium of lower dielectric constant could affect the extent of quenching of the excited triplets by the parent ion-radicals. However, the effective dielectric constant at a molecular level about the rubrene molecule in solution can be significantly different from the bulk dielectric constant so that the former should preferably be employed in establishing a correlation with ϕ_{coul}. Since, however, the significance of the term dielectric constant at the molecular level is difficult to define, it was hence decided to attempt to correlate ϕ_{coul} with a more readily determinable property of the solution, the change of solvation energy, which was related to this dielectric constant and will be discussed below.

It was not possible to dissolve the rubrene in either conducting ACN or PC to the extent of 1 mM and only slightly more than 1 mM

rubrene could be dissolved in conducting DMF. The solubility of rubrene in conducting benzonitrile solution was *ca.* 2mM. By adding benzene to all of the polar, aprotic solvents, the solubility of rubrene in the resultant mixed solvent solutions was, in each case, much greater than in the polar solvent alone. For example, 8 mM rubrene could be dissolved in conducting equivolume benzene-DMF.

Inspection of the ϕ_{coul} data in Table 10 reveals that addition of benzene to both PhCN and DMF caused an increase in ϕ_{coul}. Furthermore, with reference to the DMF data, it is noted that ϕ_{coul} increases as the benzene fraction of the mixed solvent solution is increased. Thus, the addition of an aromatic solvent to the polar solvents not only increased the solubility of the fluorescor but it also increased ϕ_{coul}.

The solvation of rubrene must follow its saturation solubility in the various solvents. It therefore became apparent that ϕ_{coul} increases with increasing solvation of the neutral rubrene. In order to establish this correlation, it was necessary to determine differences in the solvation energy of rubrene in the various solutions.

The half-wave potential of a redox process is given by the following equation in which the symbols have the usual significance[57]:

$$E_{1/2} = E^{\circ} - \frac{RT}{nF} \ln \frac{f_{red}}{f_{ox}} + \frac{RT}{F} \ln \left(\frac{D_{red}}{D_{ox}} \right)^{1/2} \qquad (7)$$

For an oxidation

$$E^{\circ}_{ox} = I + \Delta G^{\circ}_{sol,\dot{R}^+} - \Delta G^{\circ}_{sol,R} + C \qquad (8)$$

and for a reduction

$$E^{\circ}_{red} = A + \Delta G^{\circ}_{sol,R} - \Delta G^{\circ}_{sol,\dot{R}^-} + C \qquad (9)$$

where I and A are the gas phase ionization potential and electron affinity respectively, of the substance being electrolyzed, ΔG°_{sol} are free energies of solvation, and C is a constant. Since the solvation terms are the only contributions to the electrochemical potentials which are dependent on the solvent, then the electrochemical potentials of rubrene in the various solutions can be used as a measure of the relative energies of solvation of the rubrene.

It is known from the rubrene solubility data in these solutions that the solvation of rubrene increases with increasing benzene fraction in all mixed solvent solutions. The solutions actually studied each contained *ca.* 1 mM of rubrene. Since benzene is a non-polar solvent while the aprotic solvents are all polar, then the addition of benzene to the aprotic solvent lowers the dielectric constant of the resulting solution. The Born theory[57] predicts that the solvation of the ion-radicals would become more difficult (less negative) with decreasing dielectric constant. Thus, the addition of benzene to an aprotic solvent would normally tend to increase $\Delta G^{\circ}_{sol,R}$ and decrease both $\Delta G^{\circ}_{sol,\dot{R}^+}$ and $\Delta G^{\circ}_{sol,\dot{R}^-}$. Consequently, since the changes in solvation energies of the neutral

and charged species of the redox couple are reinforcing, $E^{\bullet}_{ox}$ will become more positive and E°_{red} more negative.

When benzene was added to an aprotic solvent, there always remained a large excess of polar component in the solvent relative to the rubrene concentration. Hence, the probability that the radical-ions are, in fact, preferentially solvated by the polar component of the mixed solvent must be recognized; then, the solvation energy of the ion-radicals would not be expected to significantly change relative to the change in solvation energy of the neutral rubrene, when benzene was added to the aprotic solvent. This leaves changes of $\Delta G^{\circ}_{sol,R}$ as the main contribution to changes of E° which are found to be solvent dependent (i.e. for a given polar solvent with various amounts of benzene), as shown by the abscissae values for the points in Fig. 36.

The peak oxidation and reduction potentials ($E_{p,ox}$ and $E_{p,red}$, respectively) of rubrene in varous solutions were determined by means of cyclic voltammetry. Fig. 36 shows the plot of ϕ_{coul} *vs* the corresponding value of $(E_{p,ox}-E_{p,red})$. The variation in the difference between the redox potentials of rubrene with change in solvent is twice the magnitude of the change in solvation energy of the neutral rubrene for reasons previously discussed. A clear correlation between ϕ_{coul} and $(E_{p,ox}-E_{p,red})$ is obtained, ϕ_{coul} being found to increase with increasing $(E_{p,ox}-E_{p,red})$. Since the increases in $(E_{p,ox}-E_{p,red})$ result from relatively greater solvation

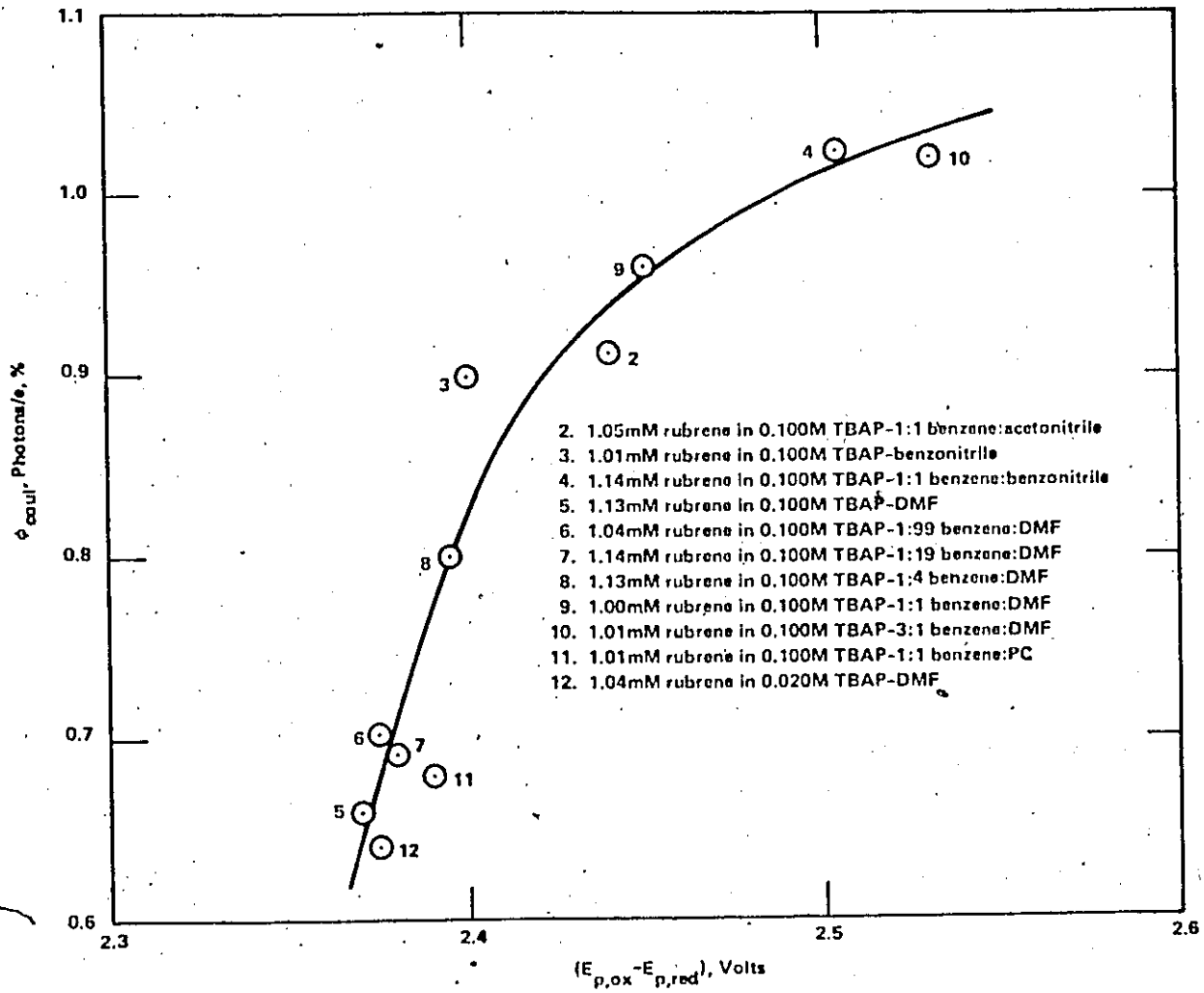

Fig. 36 Correlation between ϕ_{coul} of EGCL and $(E_{p,ox}-E_{p,red})$ of rubrene in various solvents.

of the neutral rubrene than of the conjugate ion-radicals, then the correlation between ϕ_{coul} and $(E_{p,ox}-E_{p,red})$ can be interpreted as an indication that the increase of ϕ_{coul} is mainly due to increasing solvation of the neutral rubrene.

The excited triplets which lead to the emission of light are also neutral species of rubrene. It is thus reasonable to assume that the solvation of the excited triplets also increases with increasing $(E_{p,ox}-E_{p,red})$. The excited triplets are susceptible to quenching by the parent ion-radicals[42]. A more strongly solvated triplet is, however, less likely to be quenched by the rubrene ion-radicals because the solvation cage will tend to shield (kinetically) the triplets from energy exchange with the radical-ions. In a solvent of mixed polarity, it is assumed that the triplets will be preferentially solvated by the less polar component, i.e. benzene, and the ion-radicals by the more polar component, the aprotic solvent, thereby further reducing the efficiency of the quenching mechanism.

The rate of increase in ϕ_{coul} with increasing $(E_{p,ox}-E_{p,red})$ decreases with increasing $(E_{p,ox}-E_{p,red})$. This is to be expected because solvents with relatively high $(E_{p,ox}-E_{p,red})$ will also tend to solvate the radical-ions. When both the rubrene in its excited triplet state and the ion-radicals are similarly solvated, the identical solvation shells will tend to offer less resistance to the quenching process than if they were different.

The four aprotic solvents employed, *viz.* DMF, PhCN, ACN and PC, are physically very different and yet ϕ_{coul} of rubrene EGCL in their solutions correlates very well with $(E_{p,ox}-E_{p,red})$. It is therefore concluded that the degree of solvation of the neutral rubrene is the dominant factor in determining the ϕ_{coul} of its EGCL.

8. CLAIMS TO ORIGINAL RESEARCH

This work has produced the following original contributions to the field:

1. A method for measuring the quantum efficiency of EGCL

Known methods for measuring the quantum efficiency of EGCL lacked both precision and accuracy. A unique method for this measurement was developed which offered significantly better reproducibility and the values are believed to be also more correct. The key feature of this method is its ability to distinquish the Faradaic current from the double-layer charging current produced by high-frequency, square-wave electrolysis voltages. The high frequencies of the driving voltage used to generate the EGCL ensured that the fluorescor ion-radicals would produce constant EGCL with time and without the build-up of by-products.

2. The quantum efficiency of rubrene EGCL increases with increasing solvation of the neutral rubrene.

Previous EGCL quantum efficienty data contained indications that the efficiency varied with the solvent employed for the EGCL. The apparent coulombic efficiency, ϕ_{coul}, of rubrene EGCL was measured in various solutions. It was observed that ϕ_{coul}: (A) varied with solvent, (B) was independent of electrolyte concentration, (C) decreased with increasing fluorescor concentration and (D) also decreased with increasing frequency of the driving voltage. From these results, it was concluded that: (A) ϕ_{coul} increases with

increasing solvation of the neutral rubrene because this results in less quenching of the excited triplet intermediates by the ion-radicals, (B) ion-pairing was unimportant to ϕ_{coul}, in the solutions studied, (C) self-absorption of the EGCL decreased ϕ_{coul} because only a fraction of the absorbed photons are re-emitted as lower energy photons and the balance is lost as heat, (D) the electrode is a quencher of excited rubrene triplets.

3. Rubrene EGCL is produced exclusively via the triplet route.

The mechanism for rubrene EGCL was not known previously with certainty. Careful measurements of the redox potentials over a wide temperature range permitted the calculation of accurate entropy and enthalpy data. It was found that in both solutions studied, the change in enthalpy of the cation-anion-radical charge neutralization reaction was significantly less than the energy of the emitting species, the lowest excited singlet state. It was therefore concluded that the excited singlet state was being produced exclusively via triplet-triplet annihilation.

4. The small amplitude a.c. polarographic method is a valid method for measuring heterogeneous electron transfer rate constants.

The instrumentation for this method became available recently, but only at a high cost. The applicability of this technique was verified by using this method to study a previously investigated

system, the ferro-ferricyanide redox reaction in aqueous KCl at platinum electrodes. The work in aqueous solution was extended to include gold electrodes and NaCl and $NaClO_4$ as electrolyte materials. From the results of this work, it was concluded: (a) that the energy of activation increases with increasing tendency for ion-pair formation, (b) that adsorption increases the energy of activation , (c) that increase of the radius of the supporting electrolyte anion increases the energy of activation and (d) that there is no work-function effect on the energy of activation.

5. The heterogeneous rate constant for the redox reaction of rubrene is *ca.* 0.1 cm sec^{-1}.

Theoretical considerations of the rubrene redox processes predict rate constants of the order of 10^4 cm sec^{-1}. The rate constants measured were found to be *ca.* 0.1 cm sec^{-1} at 25 °C and the energies of activation were *ca.* 3 Kcal $mole^{-1}$. In pure DMF solutions, the rubrene was adsorbed on platinum at negative potentials. This adsorption drastically decreased the exchange current of the reduction process at platinum electrodes.

9. LITERATURE CITED

1. D.M. Hercules, Science, 145, 808 (1964).
2. N.E. Tokel, R.E. Hemingway and A.J. Bard, J. Am. Chem. Soc., 95, 6582 (1973).
3. N.E. Tokel, C.P. Keszthelyi and A.J. Bard, J. Am. Chem. Soc., 94, 4872 (1972).
4. S.A. Cruser and A.J. Bard, J. Am. Chem. Soc., 91, 267 (1969).
5. A. Zweig, G. Metzler, A. Maurer and B.G. Roberts, J. Am. Chem. Soc., 88, 2864 (1966).
6. E.W. Grabner and E. Brauer, Ber. Bunserges physik. Chem., 76, 111 (1972).
7. M.A. Kabayama, A. Pighin and W.M. Coderre. Paper presented at Conf. Soc. Info. Displays, New York, N.Y. May, 1973.
8. G.J. Hoytink, Disc. Faraday Soc., 45, 14 (1968).
9. G.J. Hoytink. In *Chemiluminescence and Bioluminescence*. Edited by M.J. Cormier, D.M. Hercules and J. Lee. Plenum Press, New York, N.Y: 1973. p. 147.
10. R.A. Marcus, Can. J. Chem., 37, 155 (1959).
11. G.M. Barrow, *Physical Chemistry*, 2nd ed. McGraw-Hill, New York, N.Y. 1966.
12. R.A. Marcus, J. Phys. Chem., 67, 853 (1963).
13. A.C. Aten, J. Dieleman and G.J. Hoytink, Disc. Faraday Soc., 29, 182 (1960).
14. R. Dietz and M.E. Peover, Disc. Faraday Soc., 45, 154 (1968).

15. B.B. Damaskin, *The Principles of Current Methods for the Study of Electrochemical Reactions*. McGraw-Hill, New York, N.Y. 1967. p. 61.

16. A.C. Aten, C. Büthker and G.J. Hoytink, Trans. Faraday Soc., 55, 324 (1959).

17. B.A. Kowert, L. Marcoux and A.J. Bard, J. Am. Chem. Soc., 94, 5538 (1972).

18. K. Suga and S. Aoyagui, Bull. Chem. Soc. Japan, 45, 1375 (1972).

19. N. Winograd and T. Kuwana, J. Am. Chem. Soc., 93, 4343 (1971).

20. C.A. Parker, *Photoluminescence of Solutions*. Elsevier, Amsterdam. 1968.

21. R.E. Visco and E.A. Chandross, Electrochim. Acta, 13, 1187 (1968).

22. S.W. Feldberg, J. Phys. Chem., 70, 3928 (1966).

23. L.R. Faulkner, J. Tachikawa and A.J. Bard, J. Am. Chem. Soc., 94, 691 (1972).

24. A.J. Bard, C.P. Keszthelyi, H. Tachkawa and N.E. Tokel. In *Chemiluminescence and Bioluminescence*. Edited by M.J. Cormier, D.M. Hercules and J. Lee. Plenum Press, New York, N.Y. 1972. p. 193.

25. A. Pighin, Can. J. Chem., 51, 3467 (1973).

26. R.N. Adams, *Electrochemistry at Solid Electrodes*. Marcel Dekker, New York, N.Y. 1969.

27. R.S. Nicholson, Anal. Chem., 37, 1351 (1965).

28. J.R. Jesorek and H.R. Mark, Abstract 14, Mtng. Electrochem. Soc. Am., Sept. 1969.

29. D.J. Pastro and C.R. Johnson, *Organic Structure Determination*. Prentice-Hall, Englewood Cliffs, N.J. 1969. p. 217.

30. D.E. Smith. In *Electroanalytical Chemistry*, Vol. 1. Edited by A.J. Bard. Marcel Dekker, New York, N.Y. 1966. p. 1.

31. J.E.B. Randles, Disc. Faraday Soc., 1, 11 (1947).

32. R. Bezman and L.R. Faulkner, J. Am. Chem. Soc., 94, 6324 (1971); 95, 3083 (1973).

33. P.M. Schwartz, R.A. Blekeley and B.B. Robinson, J. Phys. Chem., 76, 1868 (1972).

34. G.A. Forcier and J.W. Olver, Anal. Chem., 37, 1447 (1965).

35. J.F. Coetzee, G.P. Cunningham, D.K. McGuire and G.R. Padmanabhan, Anal. Chem., 34, 1139 (1962).

36. C.K. Mann. In *Electroanalytical Chemistry*, Vol. 3. Edited by A.J. Bard. Marcel Dekker, New York, N.Y. 1969. p. 57.

37. J.N. Butler. In *Advances in Electrochemistry and Electrochemical Engineering*, Vol. 7. Edited by P. Delahay and C.W. Tobias. Interscience, New York, N.Y. 1970. p.77.

38. DuPont DMF, Technical Information Bulletin. E.I. DuPont de Nemours and Co., Wilmington, Del.

39. R.J. Jasinski and S. Kirkland, Anal. Chem., 39, 1663 (1967).

40. D.M. Hercules, R.C. Lansbury and D.K. Roe, J. Am. Chem. Soc., 88, 4578 (1966).

41. Chem. Abstracts, 63, 4060e (1965).

42. G.J. Hoytink. In *Advances in Electrochemistry and Electroanalytical Engineering*, Vol. 7. Edited by P. Delahay and C.W. Tobias. Interscience, New York, N.Y. 1970. p. 221.

43. C.A. Parker and G.D. Short, Trans. Faraday Soc., 63, 2618 (1967).

44. B. Fleet, G.F. Kirkbright and C. Pickford, Lab. Practice, 19, 804 (1970).

45. D.J. Fisher, W.L. Belew and M.T. Kelley. In *Polarography 1964*, Vol. 2. Edited by G.J. Hills. Interscience, New York, N.Y. 1966. p. 1043.

46. L.O. Wheeler and A.J. Bard, J. Phys. Chem., 71, 4513 (1967).

47. N. Tanaka and R. Tamamushi, Electrochim. Acta, 9, 963 (1964).

48. H. Angerstein-Kozlowska, B.E. Conway and W.B.A. Sharp, J. Electroanal. Chem., 43, 9 (1973).

49. Y.M. Povarov and P.D. Lukovstev, Electrochim. Acta, 18, 13 (1973).

50. R.K. Murmann, H. Taube and F.A. Posey, J. Am. Chem. Soc., 79, 262 (1957).

51. L. Němec, J. Electroanal. Chem., 8, 166 (1964).

52. Dr. Frank Ekker, Princeton Applied Research. Private communications.

53. M.J. Hazelrigg, Jr. and A.J. Bard, J. Electroanal. Chem. and Interfacial Electrochem., 46, 1414 (1973).

54. J.N. Demas and G.A. Crosby, J. Phys. Chem., 75, 991 (1971).

55. Dr. D.F. Williams, National Research Council of Canada. Private communications.

56. *Handbook of Chem. and Phys.*, 49th ed. Edited by R.C. Weast. The Chemical Rubber Co., Cleveland, Ohio. 1968-69.

57. M.E. Peover. In *Electroanalytical Chemistry*, Vol. 2. Edited by A.J. Bard. Marcel Dekker, New York, N.Y. 1967. p. 1.

APPENDIX I

Derivation of Equation 18 (peak current of a.c. polarogram)

A vector diagram of the Faradaic impedance is shown below.

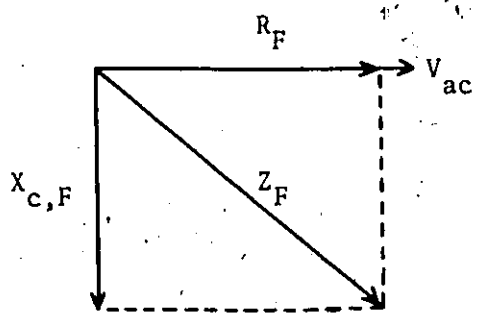

When a voltage V_{ac} is applied across Z_F, the resulting current I_{ac} is given by the following basic electrical equation:

$$I_{ac} = \frac{V_{ac}}{X_{c,F}} \sin\theta \qquad \text{(i)}$$

where $X_{c,F}$ is defined by Equation 16 in the text and

$$\sin\theta = \frac{X_{c,F}}{(X_{c,F}^2 + R_F^2)^{1/2}} \qquad \text{(ii)}$$

$$= \frac{\left[\frac{RT}{n^2F^2AC_o}\left(\frac{2}{\omega D}\right)^{1/2}\right]}{\left(\left[\frac{RT}{n^2F^2AC_o}\left(\frac{2}{\omega D}\right)^{1/2}\right]^2 + \left[\frac{RT}{n^2F^2AC_o}\left(\frac{2}{\omega D}\right)^{1/2} + \frac{1}{k}\right]^2\right)^{1/2}}$$

The expression for $\sin\theta$ can be simplified by squaring the above equation, inverting it and then dividing the numerator by the

denominator. The result is:

$$\sin\Theta = \frac{1}{\left(\left[1 + \frac{1}{k}\left(\frac{\omega D}{2}\right)^{1/2}\right]^2 + 1\right)^{1/2}} \qquad \text{(iii)}$$

This equation for $\sin\theta$ can be simplified further. Typical values for k, ω and D are 0.1 cm sec^{-1}, 377 rad sec^{-1} (60 Hz) and 5×10^{-6} cm^2 sec^{-1} respectively. Employing these values,

$$\frac{1}{k}\left(\frac{\omega D}{2}\right)^{1/2} = \frac{1}{0.1}\left(\frac{377(5\times10^{-6})}{2}\right)^{1/2} = 0.307$$

i.e. under the prevailing experimental conditions, $\frac{1}{k}\left(\frac{\omega D}{2}\right)^{1/2}$ is significantly smaller than 1. Recalling that

$$[(1+\Delta)^2+1]^{1/2} = [1+2\Delta+\Delta^2+1]^{1/2} \qquad \text{(iv)}$$

$$\approx [2+2\Delta]^{1/2} = [2\{1+\Delta\}]^{1/2} = 2^{1/2}(1+\Delta)^{1/2}$$

and

$$(1+\Delta)^{1/2} \approx 1 + \frac{\Delta}{2} \qquad \text{(v)}$$

also

$$\frac{1}{1+\frac{\Delta}{2}} \approx 1 - \frac{\Delta}{2} \qquad \text{(vi)}$$

Then,

$$\sin\theta = \frac{1 - \frac{1}{2k}\left(\frac{\omega D}{2}\right)^{1/2}}{2^{1/2}} \qquad \text{(vii)}$$

Substituting Equation vii into Equation i yields

$$i_{ac} = \frac{V_{ac}}{X_{c,F}} \left[\frac{1 - \frac{1}{2k}\left(\frac{\omega D}{2}\right)^{1/2}}{2^{1/2}} \right] \qquad \text{(viii)}$$

$$= \frac{V_{ac} n^2 F^2 A C_o \left(\frac{\omega D}{2}\right)^{1/2}}{RT} \left[\frac{1 - \frac{1}{2k}\left(\frac{\omega D}{2}\right)^{1/2}}{2^{1/2}} \right]$$

$$= \frac{V_{ac} n^2 F^2 A C_o (\omega D)}{2RT} \left[1 - \frac{1}{2k}\left(\frac{\omega D}{2}\right)^{1/2} \right]$$

At $E_{1/2}$, $C_o = 1/2\ C_b$ and i_{ac} will be at its maximum. Therefore,

$$i_{p,ac} = \frac{V_{ac} n^2 F^2 A C_b (\omega D)^{1/2}}{4RT} \left[1 - \frac{1}{2k}\left(\frac{\omega D}{2}\right)^{1/2} \right] \qquad (18)$$

The above equation is valid provided $k > (\omega D)^{1/2}$. This was the only assumption made in deriving the equation. Experimentally, k was measured to be *ca.* 0.1 cm sec^{-1} using frequencies in the range 20 to 100 Hz. For rubrene in the solutions studied, D is *ca.* 5×10^{-6} cm^2 sec^{-1}. Therefore, for ω = 377 rad sec^{-1} (60 Hz)

$$0.1 \overset{?}{>} [377(5 \times 10^{-6})]^{1/2} = 0.043$$

Since k is significantly larger than ωD, then Equation 18 can be applied to measure rate constants in the order of 0.1 cm sec^{-1} or greater.

UNIVERSITÉ D'OTTAWA
UNIVERSITY OF OTTAWA